Centro de Investigación en Matemáticas, A.C.

CIMAT

BONE METASTASIS TREATMENTS BASED ON OPTIMAL CONTROL

José Ariel Camacho Gutiérrez

Directora: Dra. Silvia Jerez Galiano

Tesis sometida en cumplimiento parcial de los requisitos para el grado de
Doctor en Ciencias con Orientación en Matemáticas Aplicadas.
Guanajuato, México, 2019

Alles ist einfacher, als man denken kann, zugleich verschränkter, als zu begreifen ist.
Maxim 1209, trans. Stopp, Johann Wolfgang von Goethe

We are only what we know, and I wished to be so much more than I was, sorely.
Cloud Atlas, David Mitchel

A Claudia

Agradecimientos

Hay muchas personas e instituciones a las cuales agradecer. Primero, quiero expresar mi profundo agradecimiento a la Dra. Silvia Jerez por darme la oportunidad de trabajar bajo su dirección. Su tenacidad, su liderazgo y su apoyo constante son un ejemplo a seguir y una fuente de motivación y admiración. De igual forma, agradezco a mis sinodales por haber aceptado la tarea de revisar este trabajo y haberme otorgado observaciones muy valiosas; gracias a la Dra. María Lourdes, al Dr. Ignacio, al Dr. Jorge y al Dr. Juan Carlos. En este tenor, quiero agradecer también las enseñanzas de todos mis profesores que, a lo largo de este extenso camino, me ayudaron a llegar a este punto. De manera especial, le doy un caluroso agradecimiento a mis profesores Janet y Sigfrido por su amistad, su confianza y sus enseñanzas.

Les doy las gracias también a mis familiares y a mis amigos: dos pilares fundamentales en mi vida. Les doy las gracias a mi madre, a mi padre, a mi hermana y a mi hermano por el inconmensurable apoyo que me brindaron y por el constante calor con el que me recibieron. Le doy un agradecimiento lleno de amor a Claudia, por su amor recíproco, por su paciencia, por alumbrarme con esa luz tan resplandeciente de su alma, por ser la persona más especial. $+2$.

La lista de amigos es muy extensa, pero cada uno de ellos ha dejado una huella brillante en mi vida. Con los que compartí cubículo (*¡arriba el D306, el D610!*), con los que compartí clases, con los que compartí seminarios, congresos y talleres, con los que compartí un café, con los que compartí hospedaje, con los que compartí juegos de mesa o de video, con los que compartí películas, con los que compartí reuniones, con los que compartí caminatas, con los que compartí risas, con los que compartí memorias: muchas gracias.

Finalmente, agradezco al CONACYT por el apoyo de la beca con número 412803, y el apoyo parcial del proyecto CB2016-286437. También agradezco al CIMAT por los apoyos con números 12806, 13017, 13529, y 13669. Agradezco enormemente al Mathematical Biosciences Institute-Ohio State University y a la Casa Matemática Oaxaca-Branff International Research Station por las becas para asistir a los talleres Control of Cellular and Molecular Systems y Mathematical Challenges in the Analysis of Continuum Models for Cancer Growth, Evolution and Therapy, respectivamente. Le doy las gracias también a la Sociedad Matemática Mexicana y a la Sociedad Mexicana de Computación Científica y sus Aplicaciones por las becas asignadas para presentar ponencias en sus respectivos congresos y escuelas nacionales. Por último, agradezco el apoyo de los organizadores del Seminario de Estudiantes por las oportunidades que me dieron para exponer tanto dentro como fuera del CIMAT.

Abstract

Metastatic disease is a lethal stage of cancer progression, characterized by the spread of aberrant cells from a primary tumor to distant tissues in the body. In recent years, there has been a multidisciplinary effort by the scientific community to understand the mechanisms of bone metastasis. Several treatments are used to deal with bone metastases formation. Unfortunately, they are mainly palliative as the disease is considered incurable. We devote this Thesis to the mathematical modeling of bone metastasis with the objective of gaining more insight about this biological process while exploring the optimization of treatments.

In this Thesis, we first propose a nonlinear differential model to describe the dynamics between tumor cells and bone cells, osteoclasts and osteoblasts. The model is based on a power law functional that represents and simplify the paracrine signaling between the BMU cells along with a logistic growth for cancer cells. This model allows us to explore different metastatic scenarios and to identify potential factors that may aid cancer cells in the colonization of bone. We then explore the effects of TGFβ and Wnt on bone dynamics with an extended mathematical model, and thereby study different disease control strategies. For these models, we present the corresponding stability analysis, deduce biological implications of these theoretical results, and show numerical simulations. This allows us to gain biological information regarding the success or failure of the invasion of bone metastasis, as well as to acknowledge a crucial interplay between TGFβ and Wnt in the bone remodeling process, both in health and in disease.

As a second step, in this Thesis we present an optimal control approach to explore treatment strategies for bone diseases with a main focus on bone metastasis. We first focus on denosumab and radiotherapy treatments through optimal control problems with L^2 cost functionals, obtaining continuous optimal control solutions. We provide proofs of existence and uniqueness of solutions to the corresponding optimal control problems for each treatment and present numerical simulations to analyze the effectiveness of both treatments under different metastatic invasion scenarios. We next focus on employing optimal control for the TGFβ/Wnt model. Clinically, optimal solutions may be more relevant if they only present 'off' and 'on' states, and that is why we propose in this case a L^1 cost functional to potentially obtain piecewise constant solutions. With this approach, first explore optimal treatments for osteoporosis while considering bisphosphonates, TGFβ and Wnt as treatment strategies, and then we focus on bone metastasis optimal treatments that includes chemotherapy, TGFβ inhibition and Wnt as main control factors.

Finally, we explore spatial models to describe bone remodeling and bone metastasis. This is motivated by biological evidence that indicates the importance of spatial distribution of bone cells and molecular agents on bone remodeling and bone metastasis evolution. We finish this Thesis with concluding remarks and proposed future research to be pursued.

Keywords: bone remodeling; bone metastasis; mathematical modeling; optimal control; therapy optimization

Nomenclature

BMU	Basic multicellular unit
OCs	Osteoclasts
OBs	Osteoblasts
CCs	Cancer cells
BM	Bone mass
DT	Denosumab therapy
RT	Radiotherapy
CT	Chemotherapy
ODE	Ordinary differential equation
PDE	Partial differential equation
BCs	Boundary conditions
ICs	Initial conditions
OCP	Optimal control problem
PMP	Pontryagin's Maximum Principle
FBSM	Forward-backward sweep method
IPOPT	Interior point optimizer

Component	*Biochemical name*	*Description*
RANK	Receptor activator of nuclear factor κB	OC receptor that triggers the activation signal of bone resorption.
RANKL	Receptor activator of nuclear factor κB ligand	OB produced cytokine that binds to RANK.
OPG	Osteoprotegerin	OB produced decoy receptor that captures RANKL, preventing RANK-RANKL binding.
TGFβ	Transforming growth factor-β	Factor with pleiotropic, cellular-context dependent effects on bone cells and with promoting effects on CCs.
PTH	Parathyroid hormone	Hormone with both anabolic (bone-forming) and catabolic (bone-degrading) effects on bone.
PTHrP	Parathyroid hormone-related peptide	CC produced peptide that enhances bone resorption during bone metastasis.
ILs	Interleukins	Type of cytokines (proteins) with multiple effects on bone cells.

Contents

List of Tables

List of Figures

Introduction

1 Motivation

In this Thesis, we present a mathematical framework to study the bone remodeling process, a continuous process of bone formation-destruction required for bone homeostasis, and bone pathologies such as osteoporosis and metastatic bone disease. Osteoporosis and osteolytic lesions from bone metastases are diseases that are characterized by fragile bones. It has been estimated that 30% of women and 20% of men worldwide suffer an osteoporosis-related fracture (Mitlak et al., 2014). For metastatic bone disease, the estimated annual incidence is nearly half a million individuals (Randall, 2016). In Figure 1, we present data taken from Lipton (2004) of worldwide cancer patients prevalence, being breast cancer and prostate cancer presenting the highest number of patients. Under each label of the aforementioned Figure, we present the probability that the considered patients developed bone metastases, and we observe that multiple myeloma, although it had the lowest prevalence, it had the highest probability of developing bone metastases.

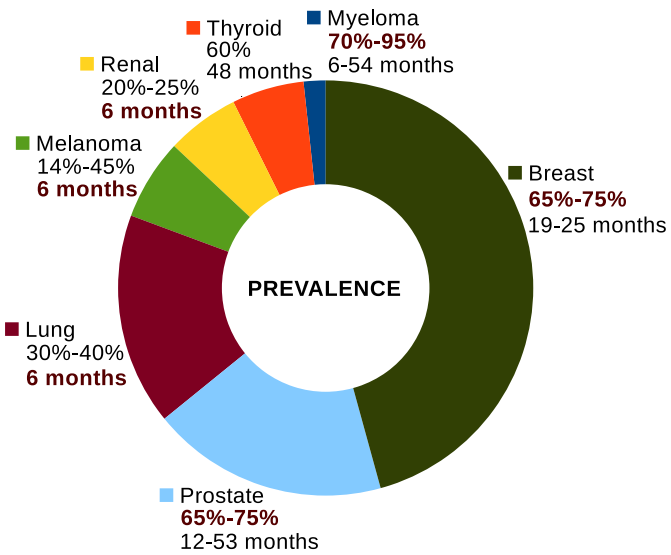

Figure 1: 5-year cancer prevalence, bone metastasis incidence and median survival (Lipton, 2004).

These and other skeletal malignancies are of great concern because of the dramatic decrease in the quality of life of the patients. However, the development of bone diseases involves a complex network of interactions among a myriad of biochemical agents and bone cells. There are multiple mechanisms that are still poorly understood. Although *in vitro* and *in vivo* experiments are crucial for bone research, it is still limited research area. Technical, economic, ethical and adequate animal models are the main factors that slow down experimental findings on bone remodeling and bone metastasis. We aim to tackle some relevant questions to better understand bone remodeling and bone metastasis vicious cycle mechanisms. Also, there is an enormous difficulty in optimizing therapies for bone diseases. In this Thesis, we also focus on applying theoretical frameworks to simulate virtual patients and find optimal therapies.

This Thesis presents a mathematical modeling approach to describe bone microenvironment dynamics with a multi-scale and multi-dimensional perspective. Concerning bone pathologies, this Thesis focus on osteoporosis and bone metastatic disease where treatments are found as solutions of optimal control problems.

2 Bone remodeling and bone metastasis

Bone is a mineralized and a dynamic tissue of the body with mechanical and metabolic functions. It provides structural support, protection to vital organs, and storage of minerals such as calcium and phosphorus. As such, maintenance of bone homeostasis is crucial. There is a myriad of molecular and cellular players involved in the adequate maintenance of bone tissue. The key cellular players are osteoclasts and osteoblasts, and the key molecular players are receptor activator of nuclear factor κB ligand (RANKL) and osteoprotegerin (OPG). Osteoclasts are bone-eater cells that are activated by RANKL. RANKL is a cytokine that has a decoy receptor called OPG, both produced by osteoblasts. Osteoblasts are bone-filler cells that have an antagonist role to osteoclasts. Altogether, these and other important molecules and cells conform a wandering team known as a basic multicellular unit (BMU).

BMUs are in charge of the bone remodeling process. First, osteoclasts from a BMU receive a trigger signal and start the resorption phase that dissolves an area of bone

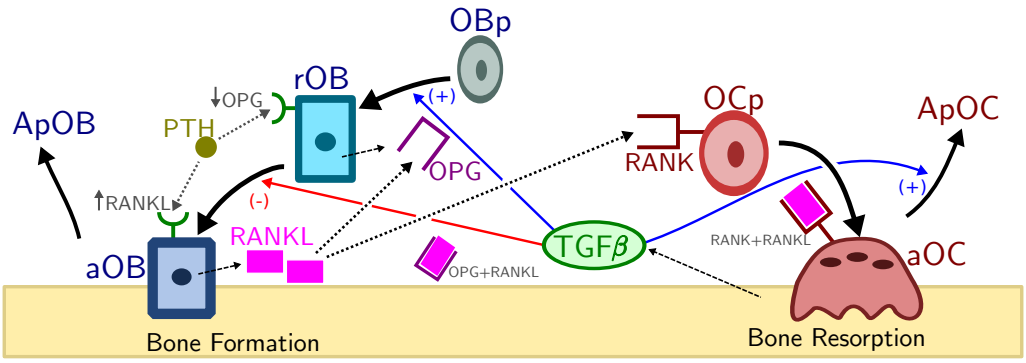

Figure 2: Schematic representation of normal bone remodeling. The different cell maturation stages are named as follows: responding osteoblasts (rOB), active osteoblasts (aOB), osteoblast apoptosis (ApOB), osteoclasts precursors (OCp), active osteoclasts (aOC) and osteoclast apoptosis (ApOC).

matrix. Then, there is a reversal (or coupling) phase thereby osteoclasts are deactivated and osteoblasts from the BMU are recruited. Finally, osteoblasts refill the previously resorbed lacunae with new bone matrix and giving an end to the remodeling process until the next triggering signal. Osteoclasts and osteoblast activities must be perfectly balanced. Bone pathologies, such as osteoporosis and bone metastasis colonization, emerge when bone remodeling gets corrupted.

Osteoporosis is a degradation of the bone. It is caused by higher levels of osteoclastic bone resorption. Several local and systemic factors are implicated as the culprits of osteoporosis. Two conventional treatments to deal with this pathology are denosumab bisphosphonates (Burkiewicz et al., 2009). Denosumab is a fully human monoclonal antibody that captures RANKL and thereby reduce osteoclast activation (Javed et al., 2018). Bisphosphonates, on the other hand, promote the apoptosis of osteoclasts (Coelho et al., 2016).

According to the classical 'Seed & Soil' hypothesis (Paget, 1889), bone metastatic cancer cells are also capable of corrupting homeostasis of bone remodeling through a vicious cycle. Cancer cells send signaling substances which distort the communication between the BMU cells. There are two broad recognized bone metastasis dynamical behaviors, see also Chappard et al. (2011); Lipton (2004); Mundy (2002):

- *Osteolytic lesion.* This disease is characterized by a significant increase of bone resorption which is likely caused by a release of activating factors of osteoclasts such as the peptide related to the parathyroid hormone (PTHrP). These factors are secreted by tumor cells in the bone environment since substances like TGF-β are released in the bone resorption process which stimulates the tumor growth. Figure 3 also shows schematically the vicious cycle of an osteolytic lesion.

- *Osteoblastic lesion.* This injury is caused by the secretion of certain substances by cancer cells that stimulate the bone formation leading to a loss of synchronization between the BMU cells. The most known factor is the protein endothelin-1 which activates the proliferation, differentiation, and activation of osteoblasts.

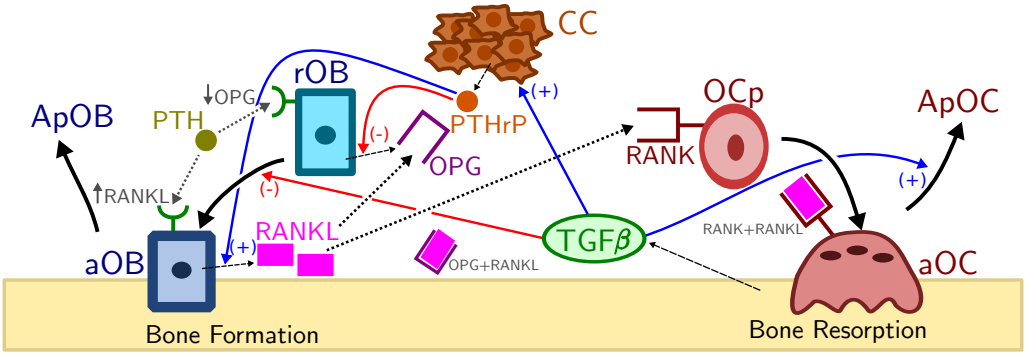

Figure 3: Schematic representation of the "vicious cycle" of bone metastasis. The different cell maturation stages are named as before with the addition of cancer cells (CC).

Both types of lesions can also appear in a patient for different periods of time which is known as the mixed metastatic lesion. All these injuries lead to weak bones and when an osteolytic lesion is present then the bone degeneration occurs at a higher rate. In all these diseases, the usual treatment is to try to recover a normal regulation of BMU. Thus, to have a better understanding of bone metastasis could allow the design of more effective treatments. In this direction with a non-invasive method using mathematical modeling, one of our goals is to identify which are the significant factors in bone metastasis.

3 Models

3.1 Bone remodeling mathematical models

Although there has been an increasing number of works in the literature that deals with bone remodeling, the number is still low compared to other biological processes. Reviews for that discuss bone remodeling models include Pivonka & Komarova (2010a); Buenzli & Pivonka (2017), while a review for cancer-induced bone disease models is found in Ryser & Komarova (2017).

In general, mathematical models for bone remodeling can be broadly classified into two groups: biochemical-detailed and biochemical-simplified. Biochemical-detailed models include both cellular and molecular players as explicit variables of the system. The majority of works from the literature follow this approach. On the other hand, biochemical-simplified models condense molecular effects as exponent parameters in a power law formulation. These models have less number of parameters and their mathematical analysis is more tractable.

3.1.1 ODE modeling

Classical bone remodeling models include Kroll (2000); Komarova et al. (2003); Lemaire et al. (2004). These works rely on the ordinary differential equations (ODE) to study bone cells and relevant molecular agents. In particular, Kroll (2000) presented an ODE model where the key elements of bone remodeling considered are PTH and IL-6. Later, Komarova et al. (2003) proposed a biochemical-simplified model that condensed paracrine and autocrine communication among bone cells through a power law approximation known as S-Systems, having only an equation for osteoclasts and another for osteoblasts. Finally, Lemaire et al. (2004) constructed a biochemical-detailed model for bone remodeling where important molecules such as RANKL, OPG, and TGFβ are considered. These works confirm the main pillars for mathematical modeling of the bone remodeling process and the exploration of *in sillico* therapeutic strategies for bone diseases such as osteoporosis.

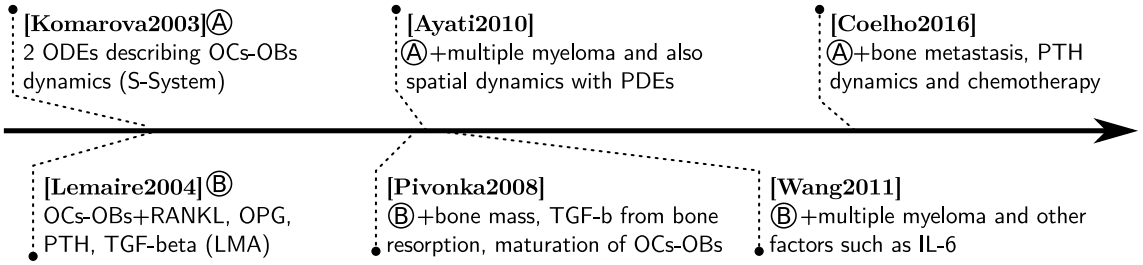

Figure 4: Relevant mathematical models based on ODEs and PDEs.

3.1.2 PDE modeling

Spatial distribution plays an important role in the dynamical evolution of biological and ecological processes. Bone processes are no exceptions. The standard mathematical framework employed to include a spatial variable is partial differential equations (PDE). In Ryser et al. (2009, 2010) a realistic, biologically relevant model with PDE is presented. This work is of great relevance since they are the precursors in spatial modeling of the bone remodeling process. Besides considering osteoclasts and osteoblasts as main model variables, RANKL and OPG are also regarded as important, explicit variables of the PDE model.

3.1.3 Other approaches

Bone tissue complexity is an obstacle to clearly understand bone remodeling and bone metastasis processes. Besides ODE and PDE modeling, in recent years research has been employing novel mathematical and computational approaches to model bone remodeling. For instance, in Garzón-Alvarado et al. (2012) a biomechanical model is proposed. This work is relevant because it is well-documented that mechanical stresses play an important role in the bone remodeling process through mechanotransduction bone cells, the osteocytes. In Jerez et al. (2018), a stochastic model is proposed. This is an important approach since noise is ubiquitous in biological processes and stochastic models are well-suited for considering noise effects on the bone remodeling process. On the other hand, the evolutionary game theory follows a Darwinian perspective in which the encounter of cells change the fitness of the corresponding populations, and in Ryser & Murgas (2017) a spatial evolutionary game for bone remodeling is proposed.

3.2 Cancer-induced bone diseases mathematical models

The main mathematical models for bone metastasis can be broadly classified into two groups: biochemical-detailed models following Lemaire et al. (2004), and biochemical-simplified models following Komarova et al. (2003).

3.2.1 Biochemical-detailed models

In Wang et al. (2011), multiple myeloma-induced bone disease is studied based on the bone remodeling model presented in Pivonka et al. (2008). In Farhat et al. (2017), the authors focus specifically to model bone metastatic prostate cancer while incorporating coupling factors such as TGFβ and Wnt.

3.2.2 Biochemical-simplified models

In Ayati et al. (2010), multiple myeloma and the BMU dynamics is studied. In Garzón-Alvarado (2012), both metastatic bone lesions are studied via a switch term included in the model. In Ryser et al. (2012), the OPG concentration is proposed as a key parameter mediating the bone metastasis. In Coelho et al. (2016), the authors include PTH concentration effects and a novel way to determine the number of active osteoclasts and osteoblasts.

3.2.3 Other approaches

In Dingli et al. (2009) and Warman et al. (2018), treatments for multiple myeloma and prostate cancer-induced bone disease are modeled as evolutionary games. In Neto et al. (2018), the authors propose to introduce fractional derivatives as to account for local diffusive characteristics.

4 Objectives

In this Thesis, we address bone metastasis dynamical interactions under the Paget's Seed & Soil paradigm. Hence, we employ mainly the ODE modeling framework and in particular the biochemical-simplified modeling approach. The objective is to gain insight into what are the key factors that contribute to the failure or success of a bone metastatic invasion.

In a successful colonization case, our aim is to discern different types of cancer cell invasion with respect to bone cell populations: osteolytic or osteoblastic lesion. To answer what are the main drivers of bone metastatic progression in the model, we perform a local stability analysis of biological meaningful equilibria, such as cancer-free and cancer-invasion steady-states. We also perform a parameter sensitivity analysis to understand qualitative dynamical behavior changes with respect to model parameters.

Another relevant question is related to oscillations in the dynamical system. This is relevant due to the fact that osteoclasts and osteoblasts couple together in a feedback fashion, which often results in oscillations. However, biological evidence is not clear about this question. Through a bifurcation analysis, we tackle this question and explore what factors may induce the origin or termination of oscillatory bifurcation points known as Hopf bifurcation.

Finally, we focus our attention on bone metastasis treatment modeling. As mentioned earlier in this Introduction, bone metastasis is considered incurable and therefore many questions arise what may be the optimal way to combine conventional or novel therapeutic approaches. Baring this in mind, we propose an optimal control approach such that the objective functional penalizes both the presence of cancer cells and the usage of treatment control functions.

5 Outline

We finish this Introduction with an outline of the Thesis. The Thesis is divided into two Parts: PRELIMINARIES and MAIN RESULTS.

PART I. PRELIMINARIES

In this Part, we present the relevant biological and mathematical background of this Thesis. In Chapter 1.1, we present the base assumptions related to the bone microenvironment that are translated into a base mathematical model used throughout this Thesis. Then, in Chapter 1.2 we show the basic elements from Optimal Control Theory that are employed to model and optimize bone disease treatments.

PART II. MAIN RESULTS

In this Part, we show the main results obtained in this Thesis. It is composed of four Chapters that we describe in what follows.

Chapter 2. Bone metastasis cellular dynamics model

Chapter 2 is based on Jerez & Camacho (2018). Here, we propose a mathematical model to describe bone metastasis dynamics. The state variables of the system are the basic multicellular unit (BMU) main cells –osteoclasts and osteoblasts– and also bone metastatic cancer cells. To construct the mathematical model, we based on the "vicious cycle" paradigm in which positive feedback between the BMU and the metastatic tumor is proposed.

Dynamics of osteoclasts and osteoblast is modeled with a power law approach where exponents simplify paracrine communication. Four significant parameters are introduced to codify the vicious cycle of bone metastasis. This model presents two biological relevant steady-states: a cancer-free equilibrium and a cancer-invasion equilibrium. We find criteria for determining local stability of the aforementioned equilibria.

The obtained theoretical results are used to explore different bone metastasis scenarios classified into two groups depending on failure or accomplishment of cancer cells to colonize the bone microenvironment. We conclude that contributions from the BMU to cancer proliferation are important in the cancer colonization of bone, having therapeutic implications and opportunities to further explore.

Chapter 3. Bone metastasis treatments as optimal control problems

Chapter 3 is based on Camacho & Jerez (2018). Here, we extend the previous model to incorporate two bone metastasis therapies: denosumab and radiotherapy. Three bone

metastatic invasions are explored: an aggressive cancer proliferation, a slow cancer proliferation, and an osteoblast-dependent cancer proliferation. We employ optimal control theory to optimize treatments that minimize the usage of therapies while minimizing the presence of cancer cells.

Denosumab is an anti-catabolic agent that aids OPG in reducing RANKL levels, thereby reducing OCs activation. Radiotherapy is a treatment that employs radiation in order to damage the DNA of fast-proliferating cells such as cancer cells. Using the bone metastasis model from the previous Chapter, we propose denosumab and radiotherapy models as optimal control problems. In order to find numerical approximations to the optimal control solutions, we employ the Maximum Principle (Pontryagin et al., 1962) and an indirect numerical method known as Forward-Backward Sweep Method (Lenhart & Workman, 2007). Optimal control solutions point out the importance of timing and dosing of the therapies depending on the metastatic scenario considered.

Chapter 4. Cellular-molecular bone microenvironment model

Chapter 4 is based on a submitted manuscript. Here, we return to the base bone remodeling model and propose the incorporation of the key coupling factors: TGFβ and Wnt. The motivation to do this is two-fold: first, these factors confirm an important communication bridge that links bone resorption with bone formation; second, treatments related to these factors are transparently modeled if they appear as explicit model variables.

In the vicious cycle paradigm of bone metastasis, TGFβ plays an important role in the positive feedback between cancer cells and osteoclasts. Thus, the previous model offers a more transparent framework than the biochemical-simplified model from Chapter 2 to better describe the vicious cycle and explore therapeutic strategies.

To explore the optimization of osteoporosis and bone metastasis treatments, we propose optimal control problems where, besides penalizing the presence of cancer cells, it penalizes different density levels of OCs and OBs. Theoretical and numerical results indicate that TGFβ has non-trivial therapeutic effects on bone diseases whereas Wnt has great potential in controlling them.

Chapter 5. Spatial bone microenvironment model

Chapter 5 is devoted to spatial modeling of bone remodeling and bone metastasis. Spatial modeling is motivated by biological evidence that points out that the spatial configuration of bone cells is important for the bone remodeling process. The spatial configuration also plays a key role in tumor progression. We incorporate a novel term that expresses an advection/convection movement, motivated by the fact the bone cells follow triggering signals that indicate the direction of the BMU throughout the remodeling process.

Next, we also incorporate cancer cells to model the spatial dynamics of bone metastasis. As a final step, we incorporate TGFβ as a key molecular player into the spatial model. Numerical simulations show qualitative differences from the ODE model, suggesting that the PDE framework may offer relevant answers related to bone diseases and the optimal therapeutic strategies to control them.

Conclusions and future work

In the last Chapter of this Thesis, we make concluding remarks of the Main Results and we point out potential lines of research to be pursued in the future.

Part I

PRELIMINARIES

Chapter 1

Preliminaries

In this Chapter, we present the biological and mathematical background required in this Thesis. First, we discuss the base biological assumptions and the base mathematical model on which the Main Results are based on, mainly Chapters 2 and 3. Then, we present a brief introduction to Optimal Control Theory that includes the main theoretical results employed in Chapters 3 and 4.

1.1 Mathematical models for bone remodeling

Bone remodeling is a multi-step process in which a team of cells, called basic multicellular unit (BMU), resorbs bone and forms new bone consecutively. The steps involved in this process are initiation, transition and termination (Matsuo & Irie, 2008). At the initiation phase, osteoclasts are recruited and activated by the BMU, and then proceed to resorb the bone. The transition phase consists of inhibition and apoptosis of osteoclasts and recruitment and activation of osteoblasts, which are responsible for new bone formation. Finally, in the termination phase osteoblasts proceed to make bone formation (deposition of osteoid) which then mineralizes, and then the BMU goes into quiescence. Some of these osteoblasts get trapped by the osteoid, which is unmineralized bone. The trapped, surviving osteoblasts differentiate into osteocytes. Osteocytes are believed to serve as a mechanostat of the bone, that is, osteocytes form a system that reacts to bone loading influences (Frost, 1987).

One of the main regulatory mechanisms of bone remodeling is the RANK/RANKL/OPG pathway. Osteoclasts express RANK which binds to the receptor activator of nuclear factor κB ligand (RANKL) cytokine produced by the osteoblastic lineage. The RANK-RANKL bindings activate osteoclasts and thereby increase bone resorption activity. Osteoblasts also produce osteoprotegerin (OPG) which is a decoy receptor for RANKL, so its expression reduces osteoclast activation by RANK-RANKL bindings. Another bone remodeling pathway of great importance is the Wnt/β-catenin signaling. Several factors may disrupt BMU intercellular communication. Cancer is one of these factors. In particular, multiple myeloma cells and bone metastasis from prostate or breast cancer have an affinity for developing a vicious cycle with the BMU. In Paget (1889) the basic 'Seed & Soil' Theory is introduced. Bone metastases do not form randomly. There is a preference for certain tissues like bone, brain, and lungs.

As mentioned in Section 3.1, there are two broad groups of mathematical models: biochemical-detailed and biochemical-simplified. In the following Sections, we first present

Diagram

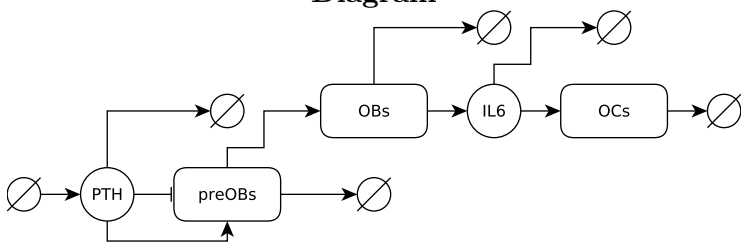

Equations

$$\frac{dY}{dt} = k_1 C_1 \frac{P}{K+P} C(t-\tau) - k_2 C_2 \left(1 - \frac{P}{K+P}\right) Y(t-2\tau) - k_Y Y$$
$$\frac{dX}{dt} = k_2 C_2 \left(1 - \frac{P}{K+P}\right) Y(t-2\tau) - k_3 X$$
$$\frac{dP}{dt} = P(t) - k_4 P$$
$$\frac{dZ}{dt} = k_5 C_3 \frac{IL6}{K_2 + IL6} - k_6 Z$$

Y: pre-osteoblasts, X: osteoblasts, Z: osteoclasts, P: PTH

Table 1.1: Kroll (2000) model.

a brief discussion on biochemical-detailed models from the literature and then we present a classic biochemical-simplified model. Next, we choose relevant biological hypotheses and proceed to codify the hypotheses into a base mathematical model used across this Thesis.

1.1.1 Biochemical-detailed model

We refer biochemical-detailed models to systems that describe explicitly the chemical reactions and the binding processes involved in bone remodeling. These are the most common type of models found in the literature. There are two main works in this line of research: Kroll (2000) and Lemaire et al. (2004). We discuss these two models in what follows.

The first of these two works is displayed in Table 1.1. In this model, the objective was to answer the paradoxical effect of parathyroid hormone (PTH) on bone mass density. The controversy arises in the sense that continuous application of PTH has catabolic effects (breakdown) on bone mass but the intermittent application has anabolic effects (construction). Thus, one of the main variables in the model is PTH. Its effects on bone cells are explicitly introduced in the model, where pre-osteoblasts, osteoblasts and osteoclasts appear also as explicit variables. One of the main features of this work is the inclusion of a time delay to the time reaction from the osteoblast lineage to PTH. This time delay is employed as a key parameter in a successive sensitivity analysis, finding possible explanations to the PTH paradox.

Later, the model presented in Table 1.2 was proposed. In this model, the explicit variables are responding osteoblasts, active osteoblasts, and active osteoclasts. Using simple biochemical mathematical modeling, non-linear functional forms are deduced in which parameters relate to molecular factors such as RANKL, OPG, and TGFβ. In this work, parameters are estimated to model different bone disease scenarios. Using a control

Diagram

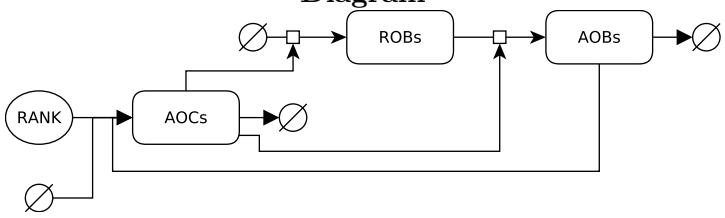

Equations

$$\frac{dB_p}{dt} = D_R \frac{C + f_0 C^s}{C + C^s} - D_B \frac{C + C^s}{C + f_0 C^s} B_p$$

$$\frac{dB}{dt} = D_B \frac{C + C^s}{C + f_0 C^s} B_p - k_B B$$

$$\frac{dC}{dt} = D_C \left(1 + \frac{I_L}{r_L}\right) \frac{k_3 K_L^P \pi_P B}{k_4 \left(1 + \frac{k_3 K}{k_4} + \frac{k_1}{k_2 k_O}\left(\frac{K_O^P}{\pi_P} B_p + I_O\right)\right)} - D_A \pi_C C$$

B_p: pre-osteoblasts, B: osteoblasts, C: osteoclasts

Table 1.2: Lemaire et al. (2004) model.

theory approach, input functions that reflect treatments such as PTH application are turned on and off at the steady-states of bone diseases to explore therapeutic options.

Both of these works propose biochemically relevant approaches to study bone remodeling. The number of parameters and the functional form of these models poses difficulties for further mathematical analysis. In this direction, biochemical-simplified models are proposed and studied.

1.1.2 Biochemical-simplified models

Another type of mathematical models are the biochemical-simplified ones. The precursor work is the one presented in Table 1.3. There are only two coupled explicit variables that describe osteoclast and osteoblast numbers. The biochemical interactions mediated by RANKL, OPG, etc., are condensed in the exponent parameters g_{ij} through a power law approximation. This approach is known as S-System modeling, which is a generalization of the law of mass actions; it was proposed in Savageau (1988).

This model has the following hypotheses:

(*H1*) There are not external influence on the osteoclast and osteoblast populations.

(*H2*) Cell apoptosis is considered to be linear.

(*H2*) Cell apoptosis is considered to be linear.

(*H3*) Biochemical interactions are approximated by an S-System, that is, a power law approximation (Savageau, 1988).

(*H4*) Concentration of molecular factors such as RANKL, OPG, etc., is assumed to depend on the number of cells.

(*H5*) The parameters g_{ij} describe the net effectiveness of biochemical interactions. When

Diagram

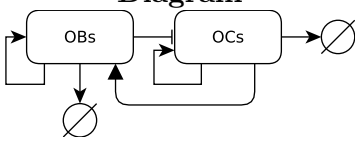

Equations

$$\frac{dx_1}{dt} = \alpha_1 x_1^{g_{11}} x_2^{g_{21}} - \beta_1 x_1$$
$$\frac{dx_2}{dt} = \alpha_2 x_1^{g_{12}} x_2^{g_{22}} - \beta_2 x_2$$

x_1: osteoclasts, x_2: osteoblasts

Table 1.3: Komarova et al. (2003) model.

$i = j$ then an autocrine interaction (same-type cells interaction) is considered, whereas $i \neq j$ refers to paracrine interactions (different-type cells interaction).

This model allows an initial mathematical analysis. The authors in Komarova et al. (2003) find the steady-state associated with the model and also present a local stability analysis. Numerical evidence of oscillations was shown but a further mathematical justification of their existence was missing. In Jerez & Chen (2015) this gap was filled. The following assumption was introduced to show mathematically the existence of periodic solutions:

(*H6*) The paracrine signaling between osteoclasts and osteoblasts regulates the growth of both populations and it is proposed as a power law function.

The *base model* to be used in this Thesis is the one from Jerez & Chen (2015) which considers the six (*H1*)–(*H6*) assumptions presented before. The equations of the simplified Komarova model are the following:

$$\begin{cases} \dfrac{dC(t)}{dt} &= C(t)(\alpha_1 B(t)^{\gamma_1} - \beta_1), \\ \dfrac{dB(t)}{dt} &= B(t)(\alpha_2 C(t)^{\gamma_2} - \beta_2), \end{cases} \tag{1.1}$$

where $C(t)$ and $B(t)$ are the number of osteoclasts and osteoblasts, respectively. The exponents γ's describe the paracrine signaling between osteoclasts and osteoblasts, and we regard $\gamma_1 < 0$ for inhibition from OBs to OCs and $\gamma_2 > 0$ for promotion from OCs to OBs. The recruitment and elimination rates of these cell populations are denoted by α's and β's, respectively. For system (2.1) in Jerez & Chen (2015), a theoretical stability analysis of its equilibria was carried out obtaining the next result:

Theorem 1.1. *System (2.1) with positive initial condition and verifying the condition*

$$\gamma_1 < 0 \quad \textit{and} \quad \gamma_2 > 0, \tag{1.2}$$

Coefficient	Value	Units
α_1	0.3	$cell^{-1}day^{-1}$
α_2	0.1	$cell^{-1}day^{-1}$
β_1	0.2	day^{-1}
β_2	0.02	day^{-1}
γ_1	-0.3	dimensionless
γ_2	0.5	dimensionless
k_1	0.07	day^{-1}
k_2	0.0022	day^{-1}

Table 1.4: BMU parameter values for a healthy person.

has a unique positive periodic solution which oscillates around the equilibrium point

$$(C^*, B^*) = \left(\left(\frac{\beta_2}{\alpha_2} \right)^{\frac{1}{\gamma_2}}, \left(\frac{\beta_1}{\alpha_1} \right)^{\frac{1}{\gamma_1}} \right). \quad \square \tag{1.3}$$

Particularly, γ_1 codifies the effects from osteoblasts to osteoclasts, such as the important RANKL-OPG pathway. As in the previous works Komarova et al. (2003); Jerez & Chen (2015), we will keep assuming a constant regulation of osteoclasts from osteoblasts by assuming $\gamma_1 < 0$. On the other hand, γ_2 is a parameter that measures the effects from osteoclasts to osteoblasts. The regulation of osteoblasts proliferation due to osteoclasts is less understood. Among the most relevant identified factors that control this communication are Ephrin2, an osteoclast transmembrane ligand that stimulates osteoblasts differentiation, Atp6v0d2, which is expressed in osteoclasts and it is believed to inhibit osteoblasts activity, and Sema4D, which also inhibits bone formation (Chen et al., 2018).

A normal bone remodeling scenario is shown in Figure 1.1. We observe the periodicity of the population of the BMU cells as Theorem 1.1 states. Notice that there is a shift between the periodic OC and OB solutions with a reciprocal behavior, that is, when osteoclasts decrease (bone resorption) then the population of osteoblasts increases (bone formation) and so on. Quantitative information about the growth and death rates for this case can be calculated from experimental data (Parfitt, 1994). In particular, we consider the parameter values β_i for $i = 1, 2$, proposed in Komarova et al. (2003). Coefficients α's and γ's are adjusted according to get a standard number of osteoblasts and osteoclasts for a healthy person. Such parameter setting is given in Table 1.4. This model and this scenario are going to serve a the base of this Thesis.

Also in Figure 1.1, we present the percentage of bone mass associated to the OC-OB system using the following bone mass equation based on the contributions of the resorption and formation processes:

$$z' = -k_1 \sqrt{\max\{C - C^*, 0\}} + k_2 \sqrt{\max\{B - B^*, 0\}}, \tag{1.4}$$

where z is total bone mass, u^* and v^* are given in (1.3) and k_1 and k_2 are the normalized activities of bone resorption and formation which are estimated to obtain the same periodicity of the osteoclast and osteoblast populations (Ayati et al., 2010; Jerez & Chen, 2015). Equation (1.4) is a modified version of the bone mass equation given in previous works (Komarova et al., 2003; Ayati et al., 2010; Jerez & Chen, 2015) in order to reduce the changes of bone mass.

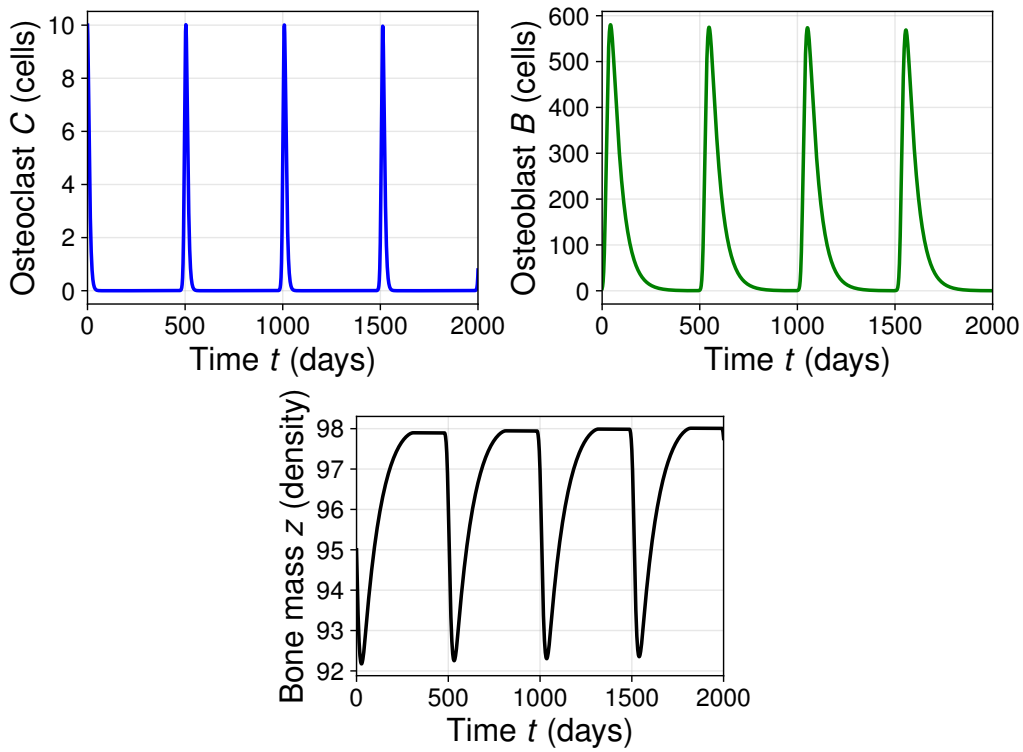

Figure 1.1: Normal behavior of OC-OB system by using (1.1) and (1.4) with initial condition $(u_0, v_0, z_0) = (10, 5, 95)$.

1.2 Introduction to Optimal Control Theory

In this Section, we present some basic elements and results from Optimal Control Theory that are used in subsequent Chapters. This Section is based on Lenhart & Workman (2007) and Berkovitz (2013).

1.2.1 General optimal control problem

Let $t \in \mathbb{R}$, $x = (x_1, \ldots, x_n) \in \mathbb{R}^n$ and $z = (z_1, \ldots z_m) \in \mathbb{R}^m$, where t is the *time variable*, x is the *state variable* and z is the *control variable*. We call *region* an open connected set. Let $\mathcal{R}$ and $\mathcal{U}$ be regions in the spaces (t, x) and z, respectively. Let $\mathcal{G} = \mathcal{R} \times \mathcal{U}$ and $f^i : G \to \mathbb{R}, \quad i = 0, 1, \ldots, n$, and let us denote $f = (f^1, \ldots, f^n)$ and $\hat{f} = (f^0, f^1, \ldots, f^n)$. Let $\mathcal{B}$ be a set of points (t_0, x_0, t_1, x_1) in $\mathbb{R}^{2n+2}$ with $t_1 > t_0$. We say that $\mathcal{B}$ is the *extremal set*. Let Ω be a function that maps $(t, x) \in \mathbb{R}$ to a subset $\Omega(t, x)$ of the region $\mathcal{U}$ in the space z. Function Ω defines the *control constraints*. Observe that if $\Omega(t, x) = \mathcal{U}$ for each (t, x) then there are no constraints because at (t, x) control z can attain any value of the domain $\mathcal{U}$.

Let us consider the following ODE:

$$\frac{dx}{dt} = f\left(t, x, u(t)\right). \tag{1.5}$$

A measurable function $u : [t_0, t_1] \to R$ is a *control* on $[t_0, t_1]$ if there exists an absolutely

continuous function $\varphi : [t_0, t_1] \to \mathbb{R}^n$ such that:

1. $(t, \varphi(t)) \in \mathcal{R}$ for each $t \in [t_0, t_1]$,
2. $\varphi'(t) = f(t, \varphi(t), u(t))$ almost everywhere on $[t_0, t_1]$.

Function φ is known as a *trajectory* associated to u. Points $(t_0, \varphi(t_0))$ and $(t_1, \varphi(t_1))$ are the *initial* and *terminal points* of the trajectory, and point $(t_0, \varphi(t_0), t_1, \varphi(t_1))$ is an *end point* of the trajectory. Control u is *admissible* if it has associated a trajectory φ such that:

1. Function $t \mapsto f^0(t, \varphi(t), u(t))$ is $L^1[t_0, t_1]$,
2. $u(t) \in \Omega(t, \varphi(t))$ almost everywhere on $[t_0, t_1]$,
3. $(t_0, \varphi(t_0), t_1, \varphi(t_1)) \in \mathcal{B}$.

If u is an admissible control and φ a trajectory associated to it then (φ, u) is known as an *admissible pair*. Let $\mathcal{A}$ be the set of every admissible pair (φ, u). Assume that $\mathcal{A}$ is not empty. Let J be the *cost functional*

$$J(\varphi, u) = g\left(t_0, \varphi(t_0), t_1, \varphi(t_1)\right) + \int_{t_0}^{t_1} f^0\left(t, \varphi(t), u(t)\right) dt, \tag{1.6}$$

where $g : \mathcal{B} \to \mathbb{R}$. Let $\mathcal{A}_1$ be a non-empty subset of $\mathcal{A}$. The *General Optimal Control Problem* can be written as follows:

GOC PROBLEM. *Find a pair* $(\varphi^*, u^*) \in \mathcal{A}_1$ *that minimizes* (1.6) *on* $\mathcal{A}_1$.

A pair (φ^*, u^*) that solves **GOC PROBLEM** is called an *optimal pair*, where φ^* is an *optimal trajectory* and u is an *optimal control*.

GOC PROBLEM is commonly known as *Bolza problem*. There are two special cases to the Bolza problem:

1. *Mayer problem.* When $f^0 \equiv 0$,
2. *Lagrange problem.* When $g \equiv 0$.

Bolza problem is equivalent to these two problems.

1.2.2 Maximum Principle

The Maximum Principle (Pontryagin et al., 1962) is one of the most important results in Optimal Control Theory. It gives a characterization of optimal controls in terms of the state variable and an additional variable called *adjoint variable*.

Let us consider again the **GOC PROBLEM** and let us assume that $g \equiv 0$ (Lagrange problem). For the Maximum Principle, we need to consider the following assumptions:

Assumption. *Region* $\mathcal{R}$ *has the form* $\mathcal{J}_0 \times \mathcal{X}_0$, *where* $\mathcal{J}_0$ *is an open interval in* $\mathbb{R}$ *and* $\mathcal{X}_0$ *is an open rectangle in* $\mathbb{R}^n$.

Assumption. *Region* $\mathcal{U}$ *is an open rectangle in* $\mathbb{R}^m$.

Assumption. *Function* $\hat{f} = (f^0, f) = (f^0, f^1, \ldots, f^n)$ *is of class* $C^1(\mathcal{X}_0)$ *for each* $(t, z) \in \mathcal{J}_0 \times \mathcal{U}$, *and is Borel-measurable on* $\mathcal{J}_0 \times \mathcal{U}$ *for each* $x \in \mathcal{X}_0$.

Assumption. *For each compact interval $\mathcal{X} \subset \mathcal{X}_0$ and for each admissible control u, there exists a function*

$$\mu = \mu(\cdot, \mathcal{X}, u)$$

defined on $\mathcal{J}_u = [t_0, t_1]$, the interval fo definition of u, such that $\mu \in L^1(\mathcal{J}_u)$ and

$$\begin{aligned} |\hat{f}\,(t, x, u(t))\,| &\leq \mu(t), \\ |\hat{f}_x\,(t, x, u(t))\,| &\leq \mu(t), \end{aligned}$$

for almost every $t \in \mathcal{J}_u$ and every $x \in \mathcal{X}$.

Assumption. *Function Ω is independent with respect to x. That is, $\Omega : t \to \Omega(t)$.*

Assumption. *Set $\mathcal{B}$ is a q-manifold of class C^1, with $0 \leq q \leq 2n+1$.*

Assumption. *Set $\mathcal{B}$ can be represented as the image of an open rectangle $\sum$ in $\mathbb{R}^q$ under*

$$\begin{aligned} t_0 &= T_0(\sigma), \quad x_0 = X_0(\sigma), \\ t_1 &= T_1(\sigma), \quad x_1 = X_1(\sigma), \end{aligned}$$

where T_i and X_i are of class $C^1(\sum)$ $(i = 0, 1)$, and the Jacobian matrix

$$(T_{0\sigma} \quad X_{0\sigma} \quad T_{1\sigma} \quad X_{1\sigma})$$

has rank q at each point of $\sum$.

Assumption. *Let H be a real function defined on $\mathbb{R} \times \mathbb{R}^n \times \mathbb{R}^m \times \mathbb{R} \times \mathbb{R}^n$ (n is related to state variable and m to control variable) as*

$$H(t, x, z, p^0, p) = p^0 f^0(t, x, z) + p \cdot f(t, x, z) = \sum_{i=0}^{n} p^i f^i(t, x, z).$$

If $\hat{p} = (p^0, p)$ we can rewrite H as

$$H(t, x, z, \hat{p}) = \hat{p} \cdot f(t, x, z).$$

Under these Assumptions, the Maximum Principle states the following:

Theorem 1.2 (Maximum Principle)**.** *Consider the Lagrange problem under the aforementioned Assumptions. Let (ϕ, u) be an optimal pair defined on $[t_0, t_1]$. Then, there exist a constant $\lambda^0 \leq 0$ and a absolutely continuous vector function $\lambda = (\lambda^1, \ldots, \lambda^n)$ defined on $[t_0, t_1]$ such that:*

1. *Vector $\hat{\lambda}(t) = (\lambda^0, \lambda(t))$ never vanishes on $[t_0, t_1]$.*

2. *For almost every $t \in [t_0, t_1]$:*

$$\begin{aligned} \phi'(t) &= H_p\left(t, \phi(t), u(t), \hat{\lambda}(t)\right), \\ \lambda'(t) &= -H_x\left(t, \phi(t), u(t), \hat{\lambda}(t)\right). \end{aligned}$$

3. For any admissible control v defined on $[t_0, t_1]$:

$$\int_{t_0}^{t_1} H(t, \phi(t), u(t)\hat{\lambda}(t))dt \geq \int_{t_0}^{t_1} H(t, \phi(t), v(t), \hat{\lambda}(t))dt. \tag{1.7}$$

4. If function $t \to \hat{f}\,(t, \phi(t), u(t))$ is continuous at $t = t_0$ and $t = t_1$, then the vector

$$(H(\pi(t_0)), -\lambda(t_0), -H(\pi(t_1)), \lambda(t_1))$$

is orthogonal to set $\mathcal{B}$ at point $(t_0, \phi(t_0), t_1, \phi(t_1))$, where

$$\pi(t_i) = (t_i, \phi(t_i), u(t_i), \hat{\lambda}(t_i)), \quad i = 0, 1.$$

Theorem 1.3. *Maximum Principle] If $\Omega(t) = \mathcal{C}$ for every t, where $\mathcal{C}$ is a fixed set, and if $\hat{f}$ is continuous on $\mathcal{R} \times \mathcal{U}$ then:*

$$H\left(t, \phi(t), u(t), \hat{\lambda}(t)\right) \geq H\left(t, \phi(t), z, \hat{\lambda}(t)\right), \tag{1.8}$$

for almost every $t \in [t_0, t_1]$ and for every $z \in \mathcal{C}$.

Observe that the Maximum Principle gives necessary but not sufficient conditions for optimal controls. For more details see Berkovitz (2013). In the next Sections, we apply the Maximum Principle to simple ODE families to illustrate its application in mathematical modeling.

1.2.3 One-dimensional problems

Let us consider the simplest Lagrange optimal control problem:

$$\begin{array}{ll} \max\limits_{u \text{ admissible}} & \displaystyle\int_{t_0}^{t_1} f\,(t, x(t), u(t))\,dt \\ \text{subject to:} & x'(t) = g\,(t, x(t), u(t))\,, \\ & x(t_0) = x_0, \\ & x(t_1) \text{ free}, \end{array}$$

Using the Maximum Principle we obtain the necessary conditions for optimal pairs (x^*, u^*):

$$\begin{array}{rrcl} \textit{(Hamiltonian)} & H(t, x, u, \lambda) & = & f(t, x, u) + \lambda \cdot g(t, x, u) \\ \textit{(Adjoint system)} & \lambda' & = & \displaystyle -\frac{\partial H}{\partial x} \quad \Rightarrow \quad \lambda' = -(f_x + \lambda g_x) \\ \textit{(Transversality condition)} & \lambda(t_1) & = & 0 \\ \textit{(Optimality condition)} & \left.\dfrac{\partial H}{\partial u}\right|_{u=u^*} & = & 0 \quad \Rightarrow \quad f_u + \lambda g_u = 0 \end{array}$$

The general approach to find optimal pairs (x^*, u^*) in simple optimal control problems is the following:

1. Conpute Hamiltonian H.

2. Obtain equations from Maximum Principle in terms of u^*, x^* y λ^*.

3. Find u^* from optimality condition in terms of x^* and λ^*.

4. Solve forward ODE with initial condition for x^* and then backward ODE with transversality condition for λ^*, substituting u^* from previous step.

5. Solve for u^*.

Henceforth, the discussion will focus on the one-dimensional problem, and then we briefly translate it to higher dimensional problems.

1.2.4 Existence of optimal pairs

There are some existence results depending on the structure of the optimal control problem. The most common ones ask for convexity and Lipschitz properties. The following is a classical existence theorem for Lagrange problems:

Theorem 1.4 (Existence, one-dimensional case)**.** *Let*

$$J(u) = \int_{t_0}^{t_1} f(t, x(t), u(t))dt$$

subject to

$$x' = g(t, x, u), \quad x(t_0) = x_0.$$

Assume that the set of admissible controls for the Lagrange problem is a set of Lebesgue integrable functions on $[t_0, t_1]$. Assume that $f(t, x, u)$ is a convex functions with respect u. Furthermore, assume that there exist constants $c_1,\ c_2,\ c_3 > 0$, c_4 y $\beta > 1$ such that:

$$\begin{aligned} g(t,x,u) &= \alpha_1(t,x) + \alpha_2(t,x)u, \\ |g(t,x,u)| &\leq c_1(1 + |x| + |u|), \\ |g(t_1,x_1,u) - g(t,x,u)| &\leq c_2|x_1 - x|(1 + |u|), \\ f(t,x,u) &\geq c_3|u|^{\beta} - c_4, \end{aligned}$$

for every $t \in [t_0, t_1]$, $x, x_1, u \in \mathbb{R}$. Then there exists an optimal control u^* that finitely maximizes $J(u)$.

1.2.5 Bounded controls

Consider the following Lagrange problem:

$$\begin{aligned} \max_{u \text{ admissible}} \quad & \int_{t_0}^{t_1} f(t, x(t), u(t))dt \\ \text{subject to:} \quad & x'(t) = g(t, x(t), u(t)) \\ & x(t_0) = x_0 \\ & a \leq u(t) \leq b. \end{aligned}$$

The Maximum Principle applied to this problem results in the same conditions as before except for the optimality condition. Now, optimal control u^* will be determined also by the sign of H_u:

$$u^*(t) = \begin{cases} a, & H_u < 0 \\ MP, & H_u = 0 \\ b, & H_u > 0 \end{cases} \tag{1.9}$$

where MP is obtained from the Maximum Principle without bounds.

1.2.6 Linear problems

Linear optimal control problems are frequently used in modeling problems. In particular for biological problems, this is because the cost functional with a linear control has a more clear interpretation than non-linear controls. The general, one-dimensional linear optimal control problem can be written as:

$$\begin{aligned} \max_{u \text{ admissible}} \quad & \int_{t_0}^{t_1} f_1(t,x) + u(t) f_2(t,x) dt \\ \text{subject to:} \quad & x'(t) = g_1(t,x) + u(t) g_2(t,x), \\ & x(t_0) = x_0, \\ & a \leq u(t) \leq b. \end{aligned}$$

The Hamiltonian is:

$$H(t,x,u,\lambda) = (f_1 \lambda g_1) + u(f_2 + \lambda g_2).$$

The optimality condition is:

$$H_u = 0 \quad \Rightarrow \quad f_2 + \lambda g_2 = 0.$$

Note that the information about u is lost in this case. The characterization of optimal control u^* is given by the sign of the *switching function* $\psi(t)$:

$$\psi(t) = H_u = f_2(t, x(t)) + \lambda(t) g_2(t, x(t)),$$

$$u^*(t) = \begin{cases} a, & \psi(t) < 0 \\ ?, & \psi(t) = 0 \\ b, & \psi(t) > 0 \end{cases}$$

If optimal control u^* satisfies $\psi = 0$ on many finite points we say that the optimal control is a *bang-bang control*. Otherwise, we say that u^* is a *singular control*. The characterization of singular controls is obtained by successively deriving H with respect to time t and u. This is known as the Legendre-Clebsh condition (Schättler & Ledzewicz, 2015) and is of the form:

$$\frac{\partial}{\partial u} \frac{d^2}{dt^2} \frac{\partial H}{\partial u} \neq 0 \quad \Rightarrow \quad u_{\text{sing}} = -\frac{\langle \lambda, [f_1, [f_1, f_2]](x) \rangle}{\langle \lambda, [f_2, [f_1, f_2]](x) \rangle}, \tag{1.10}$$

where it is assumed that the model function $f(x,u)$ can be written as $f(x,u) = f_1(x) + f_2(x)u$. The bracket notation in (1.10) refers to the Lie bracket which in this case it is

defined as:

$$[f,g](x) = f \cdot \frac{dg}{dx} - g \cdot \frac{df}{dx}. \tag{1.11}$$

1.2.7 Higher dimensional problems

Results presented previously can be extended to multi-variate optimal control problems. For instance, consider the following multi-dimensional Lagrange problem:

$$\begin{array}{ll} \max\limits_{u \text{ admissible}} & \displaystyle\int_{t_0}^{t_1} f(t, \overrightarrow{x}(t), \overrightarrow{u}(t))dt \\ \text{sujeto a} & \overrightarrow{x}'(t) = \overrightarrow{g}(t, \overrightarrow{x}, \overrightarrow{u}) \\ & \overrightarrow{x}(t_0) = \overrightarrow{x_0} \end{array}$$

with $f(\cdot) \in \mathbb{R}$, $\overrightarrow{x}(\cdot), \overrightarrow{g}(\cdot), \overrightarrow{x_0} \in \mathbb{R}^n$ y $\overrightarrow{u} \in \mathbb{R}^m$.

Hamiltonian is now expressed through the dot product:

$$H(t, \overrightarrow{x}, \overrightarrow{u}, \overrightarrow{\lambda}) = f(t, \overrightarrow{x}, \overrightarrow{u}) + \overrightarrow{\lambda}(t) \cdot \overrightarrow{g}(t, \overrightarrow{x}, \overrightarrow{u}) = f(t, \overrightarrow{x}, \overrightarrow{u}) + \sum_{i=1}^{n} \lambda_i(t) g_i(t, \overrightarrow{x}, \overrightarrow{u})$$

with $\lambda = (\lambda_1, \ldots, \lambda_n)$ y $g = (g_1, \ldots, g_n)$.

Maximum Principle in vectorial form gives the adjoint system and its corresponding transversality conditions:

$$\lambda_j'(t) = -\frac{\partial H}{\partial x_j}, \quad \lambda(t_j) = 0 \quad \forall i = 1, \ldots, n$$

Optimality conditions are:

$$\left.\frac{\partial H}{\partial u_k}\right|_{u_k = u_k^*} = 0 \quad \forall k = 1, \ldots, m$$

A simple example

Consider the Lagrange problem:

$$\begin{array}{ll} \min\limits_{u \text{ admisible}} & \displaystyle\int_0^1 x_2(t) + u(t)^2 dt \\ \text{sujeto a} & x_1'(t) = x_2 \\ & x_1(0) = 0 \\ & x_1(1) = 1 \\ & x_2'(t) = u \\ & x_2(0) = 0 \end{array}$$

It is straightforward to see that conditions from the existence theorem are satisfied. Hamiltonian is:

$$H = x_2 + u^2 + \lambda_1 x_2 + \lambda_2 u$$

Adjoint system is given by:

$$\lambda_1' = -\frac{\partial H}{\partial x_1} = 0, \quad \lambda_2' = -\frac{\partial H}{\partial x_2} = 0, \ \lambda_2(1) = 0$$

Solving for λ we obtain:

$$\lambda_1(t) = C, \quad \lambda_2(t) = -(C+1)(t-1)$$

Now, using optimality condition we obtain:

$$0 = \frac{\partial H}{\partial u} = 2u + \lambda_2 \quad \Rightarrow \quad u^* = -\frac{\lambda_2}{2} = \frac{(C+1)(t-1)}{2}$$

Then, returning to forward ODE and solving for x:

$$x_2' = u \quad \Rightarrow \quad x_2(t) = \frac{C+1}{2}\left(\frac{t^2}{2} - t\right), \ x_2(0) = 0$$

$$x_1' = x_2 \quad \Rightarrow \quad x_1(t) = \frac{C+1}{2}\left(\frac{t^3}{6} - \frac{t^2}{2}\right), \ x_1(0) = 0, \ x_1(1) = 1$$

From the algebraic equations we obtain $C = -7$. Thus, optimal pair (x^*, u^*) is given by:

$$u^*(t) = 3 - 3t, \quad x_1^*(t) = \frac{3}{2}t^2 - \frac{1}{2}t^3, \quad x_2^*(t) = 3y - \frac{3}{2}t^2 \quad \square$$

1.3 Monotone Method

In Chapter 5, we present spatial models for bone metastasis. In particular, the models presented are linear parabolic boundary-value problems. For this class of PDE problems, there exists a theory that guarantees existence and uniqueness of solutions through finding suitable upper and lower solutions. In this Section, we present the basic results of the Monotone Method based on Pao (1993).

1.3.1 Linear parabolic problem

In this Section, we present a formulation of the scalar linear parabolic equation.

Let $\Omega \subset \mathbb{R}^n$ be a bounded and open domain, and let $T \in \mathbb{R}$ be positive. Here, Ω represents the *spatial domain* while the semi-open interval $(0, T]$ represents the *time domain* with *final time* T. We define the set D_T as $D_T = (0, T] \times \Omega$. Also, we define the set S_T as $S_T = (0, T] \times \partial\Omega$. The set D_T represents the whole domain for the PDE problem, and S_T represents the boundary with respect to the space variable of D_T.

The notation $C^m(\Omega)$ for m a positive integer represents the set of all continuous functions with continuous partial derivatives of k^{th} order for $k = 1, \ldots, m$. The notation $\overline{\Omega}$ is used to denote the closure of Ω with respect to the standard topology of $\mathbb{R}^n$.

Now, let $u : D_T \to \mathbb{R}$ and let us consider the *linear parabolic problem* given by:

$$\frac{\partial u}{\partial t} - Lu + c(t, x)u = f(t, x), \quad (t, x) \in D_T, \tag{1.12}$$

with *boundary conditions* (BCs)

$$\alpha_0(t,x)\frac{\partial u}{\partial \nu} + \beta_0(t,x)u = h(t,x), \quad (t,x) \in S_T \tag{1.13}$$

where $\partial u/\partial \nu$ is the directional derivative of u in the direction of a normal vector ν pointing outward from $x \in \partial\Omega$, and *initial conditions* (ICs)

$$u(0,x) = u_0(x), \quad x \in \Omega. \tag{1.14}$$

Here, the operator L is the *advection-diffusion operator* given by

$$L = \sum_{i,j=1}^{n} a_{ij}(t,x)\frac{\partial^2}{\partial x_i \partial x_j} + \sum_{j=1}^{n} b_j(t,x)\frac{\partial}{\partial x_j}. \tag{1.15}$$

We ask the advection-diffusion operator (1.15) to be elliptic: the matrix $A = (a_{ij}(t,x))$ is positive definite in $\overline{D_T}$. We also ask the functions $c(t,x)$, $f(t,x)$, $h(t,x)$ and $u_0(x)$ in (1.12)–(1.14) to be Hölder continuous in their respective domains.

1.3.2 Monotone Method for semilinear parabolic problems

For the scalar linear parabolic problem (1.12)–(1.14), classical results of existence are available. However, in many mathematical models, the reaction functions display a nonlinear dependence on the state variables. In this Section, we focus our attention to another class of parabolic problems: the scalar semilinear parabolic problem. The objective of the *monotone method* is to use suitable functions that "bound" the semilinear parabolic problem (1.12)–(1.14) in order to guarantee existence and uniqueness of continuous solutions u. These suitable functions are the so-called upper and lower solutions of the linear parabolic problem.

Let us consider a similar problem to (1.12)–(1.14) called the *semilinear parabolic equation:*

$$u_t - Lu = f(t,x,u), \quad (t,x) \in D_T, \tag{1.16}$$

$$\alpha_0(t,x)\frac{\partial u}{\partial \nu} + \beta_0(t,x)u = h(t,x), \quad (t,x) \in S_T, \tag{1.17}$$

$$u(0,x) = u_0(x), \quad x \in \Omega. \tag{1.18}$$

We loss some linearity with respect to problem (1.12)–(1.14) in the sense that $f(t,x,u)$ may be a uniformly Hölder nonlinear functions with respect to u. Let $\tilde{u} \in C(\overline{D_T}) \cap C^{1,2}(D_T)$. We say that $\tilde{u}$ is an *upper solution* of the semilinear problem (1.16)–(1.18) if:

$$\tilde{u}_t - L\tilde{u} \geq f(t,x,\tilde{u}), \quad (t,x) \in D_T, \tag{1.19}$$

$$\alpha_0(t,x)\frac{\partial \tilde{u}}{\partial \nu} + \beta_0(t,x)\tilde{u} \geq h(t,x), \quad (t,x) \in S_T, \tag{1.20}$$

$$\tilde{u}(0,x) = u_0(x), \quad x \in \Omega. \tag{1.21}$$

On the other hand, a function $\hat{u} \in C(\overline{D_T}) \cap C^{1,2}(D_T)$ is a *lower solutions* if satisfies (1.19)–(1.21) with reversed inequalities. We also say that the pair $(\tilde{u}, \hat{u})$ is *ordered* if $\tilde{u} \geq \hat{u}$ for every $(t,x) \in \overline{D_T}$. The Monotone Method is enclosed in the following theorem (Pao, 1993,

Chapter 2, Theorem 4.1):

Theorem 1.5 (Monotone Method)**.** *Let $(\tilde{u}, \hat{u})$ be an ordered pair of upper and lower solutions of (1.16)–(1.18), respectively. Assume that f satisfies the condition*

$$-\underline{c}(u_1 - u_2) \leq f(t, x, u_1) - f(t, x, u_2) \leq \overline{c}(u_1 - u_2)$$

for some bounded functions $\underline{c}(t, x)$ and $\overline{c}(t, x)$, and for every $\hat{u} \leq u_2 \leq u_1 \leq \tilde{u}$ with $(t, x) \in D_T$. Then there exist sequences $\{\overline{u}^{(k)}\}$ and $\{\underline{u}^{(k)}\}$ that converge monotonically to a unique solution u of (1.16)–(1.18) such that

$$\hat{u} \leq \underline{u}^{(1)} \leq \underline{u}^{(2)} \leq \cdots \leq u \leq \cdots \leq \overline{u}^{(2)} \leq \overline{u}^{(1)} \leq \tilde{u}, \quad (t, x) \in \overline{D_T}.$$

The previous discussion concerns problems with only one unknown function. In many applications, we usually encounter mathematical models with a coupled relationship between unknown functions rather than decoupled systems as previously discussed. Coupled systems are the next and last object of study.

1.3.3 Coupled systems

A general representation of parabolic partial differential equation systems is given by:

$$(u_i)_t - L_i u_i = f_i(t, x, u_i, [\mathbf{u}]_{a_i}, [\mathbf{u}]_{b_i}), \quad \text{in } D_T, \tag{1.22}$$
$$B_i u_i = h_i(t, x), \quad \text{on } S_T, \tag{1.23}$$
$$u_i(0, x) = u_{i,0}(x), \quad \text{in } \Omega, \tag{1.24}$$

for $i = 1, \cdots, N$, where $\mathbf{u} = (u_i, [\mathbf{u}_{a_i}], [\mathbf{u}_{b_i}])$ such that $a_i + b_i = N - 1$, and L and B are the operators composed of

$$L_i = \alpha_i(t, x)\frac{\partial^2}{\partial x^2} + \beta_i(t, x)\frac{\partial}{\partial x}, \quad B_i = \alpha_{i,0}(x)\frac{\partial}{\partial \nu} + \beta_{i,0}(x)$$

with $\alpha_i(t, x) > 0$.

We assume that f is a *quasimonotone function*: it satisfies that $f_i(\cdot, u_i, [\mathbf{u}_{a_i}], [\mathbf{u}_{b_i}])$ is monotone nondecreasing in $[\mathbf{u}]_{a_i}$ and is monotone nonincreasing in $[\mathbf{u}]_{b_i}$.

In the context of coupled systems (1.22), we have a similar definition for upper and lower solutions. For system (1.22), functions $\tilde{\mathbf{u}}$ and $\hat{\mathbf{u}}$ in $C(\overline{D}) \cap C^{1,2}(D)$ are said to be coupled upper and lower solutions of the system if:

$$\tilde{\mathbf{u}} \geq \hat{\mathbf{u}}, \quad \text{in } \overline{D_T}, \tag{1.25}$$
$$(\tilde{u}_i)_t - L_i \tilde{u}_i \geq f_i(t, x, \tilde{u}_i, [\tilde{\mathbf{u}}]_{a_i}, [\hat{\mathbf{u}}]_{b_i}), \tag{1.26}$$
$$(\hat{u}_i)_t - L_i \hat{u}_i \leq f_i(t, x, \hat{u}_i, [\hat{\mathbf{u}}]_{a_i}, [\tilde{\mathbf{u}}]_{b_i}), \tag{1.27}$$
$$B_i \tilde{u}_i \geq h_i(t, x) \geq B_i \hat{u}_i, \tag{1.28}$$
$$\tilde{u}_i(0, x) \geq u_{i,0}(x) \geq \hat{u}_i(0, x). \tag{1.29}$$

A *sector* defined by coupled upper and lower solutions $\tilde{\mathbf{u}}$ and $\hat{\mathbf{u}}$ is given by:

$$\{\hat{\mathbf{u}}, \tilde{\mathbf{u}}\} = \{\mathbf{u} \in \mathcal{C}(\overline{D_T}) \mid \hat{\mathbf{u}} \leq \mathbf{u} \leq \tilde{\mathbf{u}}\} \tag{1.30}$$

The monotone method for coupled systems is as follows (Pao, 1993, Chapter 8, Theorem 8.1)

Theorem 1.6 (Monotone Method for Coupled Systems)**.** *Let* $\tilde{\mathbf{u}}$ *and* $\hat{\mathbf{u}}$ *be coupled upper and lower solutions of* (1.22)*, respectively. Assume that function* f *is Lipschitz and quasimonotone in* $\{\hat{\mathbf{u}}, \tilde{\mathbf{u}}\}$*. Also, assume that for each* $i = 1, \ldots, N$ *there exist functions* $\underline{c}_i \in C(\overline{D_T})$ *such that*

$$f_i(t, x, u_i, [\mathbf{u}]_{a_i}, [\mathbf{u}]_{b_i}) - f_i(t, x, v_i, [\mathbf{u}]_{a_i}, [\mathbf{u}]_{b_i}) \geq -\underline{c}_i(u_i - v_i)$$

for every $\hat{u}_i \leq v_i \leq u_i \leq \tilde{u}_i$ *with* $(t, x) \in D_T$*. Then there exist a unique solution* $\mathbf{u}^*$ *to* (1.22) *with* $\mathbf{u}^*$*.*

Part II

MAIN RESULTS

Chapter 2

Mathematical modeling for bone metastasis*

Cancer cells are characterized by uncontrolled cell growth and by their propensity to spread to other body parts from the primary site (Alberts et al., 2002; Hanahan & Weinberg, 2011), this phenomenon is known as metastasis. Bone metastasis occurs when the tumor-cell invasion reaches the skeleton. According to the American Cancer Society (2015), prostate (Keller & Brown, 2004), breast (Chen et al., 2010) and lung cancers are the most likely cancers to spread to the bone. Moreover, it is worth mentioning that in 2014 worldwide mortality by cancer was 14.6% and a 90% of these deaths were due to metastasis (Stewart & Wild, 2014).

As mentioned in the Introduction, some of the mechanisms of bone metastasis have been identified. One of the most important findings is that the osteoclast and osteoblast cells are implicated in the tumor-cell proliferation. Osteoclasts and osteoblasts are known as the basic multicellular unit (BMU) cells and they are responsible for the bone remodeling process. Bone remodeling is a complex process that consists in a particular mechanism of regulation between osteoclasts and osteoblasts via autocrine and paracrine signaling mostly controlled by the agents: RANK, RANKL, OPG and TGF-β, see Eriksen (2010); Phan et al. (2004); Raggatt & Partridge (2010). Cancer cells interfere with the osteoclast-osteoblast communication in order to obtain important growth factors which are released during bone resorption (Lipton, 2004; Mundy, 2002). This distortion in the communication between osteoclasts and osteoblasts may compromise seriously bone by excessive bone elimination of excessive bone formation.

Although the usual way to study a biological process is by experimentation, it may have certain limitations. An optional route is by mathematical modeling which is a non-invasive tool and it is usually proposed in order to get alternative information that may not be obtained experimentally.

*This Chapter is based on Jerez, S., Camacho, A. (2018). Bone metastasis modeling based on the interactions between the BMU and tumor cells. *Journal of Computational and Applied Mathematics*, 330, 866–876.

In the Introduction, we presented briefly the main mathematical models concerning bone remodeling and bone metastasis. Here, we further the discussion to make our motivation clearer. Recently, some works have been focused on modeling the role of the BMU cells in cancer-induced bone diseases, especially in the case of multiple myeloma: Ayati et al. (2010) based on a Komarova type model included a new equation for the cancer cells with a Gompertz growth function, Wang et al. (2011) extended the linear differential system proposed in Pivonka et al. (2008) by introducing a logistic equation by cancer cells, and Ji et al. (2014) modified the previous model by using Hill functions to represent the osteoclasts and osteoblasts interactions. In all these works, a numerical simulation of the behavior of the solution and a discussion of these results were carried out. Also, steady states were usually obtained but an equilibrium dynamical analysis was missed. Such analysis is particularly difficult to perform for nonlinear differential equations, although it usually provides significant information about model parameters. Therefore, this Chapter is a contribution in such direction and we are interested in modeling bone metastasis disease.

In this Chapter, we extend the nonlinear model proposed in Section 1.1.2 for the BMU process in order to describe the dynamics between the tumor, osteoclast and osteoblast cells on a site of bone remodeling. The osteoclasts and osteoblasts equations are of Komarova type. The cancer growth is defined by a logistic function and the interactions terms between the three populations are proposed according to biological information. Via a stability analysis of equilibria, we obtain knowledge about the significant factors in the success or failure of bone metastasis. Moreover, we present numerical simulations that show diverse dynamical interactions of the osteoclast-osteoblast-cancer cells. The results obtained by our model are contrasted with the known behaviors of bone mass when bone metastasis occurs. A better understanding of the interactions between the tumor and BMU cells could help to improve treatments or even to develop treatments in order to eradicate bone metastasis.

The Chapter is organized as follows: In Section 2.1, first we describe a normal cycle of the BMU cells and later we display how the cancer cells distort the osteoclasts and osteoblasts communication causing serious bone diseases. In Section 2.2, we construct a nonlinear differential system that describes the osteoclast-osteoblast-cancer interactions based on a simplified Komarova model along with a cancer logistic equation. An equilibria analysis of the two steady states –cancer-free and cancer-invasion– of the proposed system is carried out and their stability conditions are obtained in Section 2.3. In Section 2.4, numerical simulations are performed to show the different behaviors of the solution as well as to carry out a sensitivity analysis of certain significant parameters. We finish this Chapter with a summary of the results.

2.1 Bone metastasis: the role of BMU in tumor expansion

As we mentioned before, in their eagerness to proliferate cancer cells send signaling substances which distort the communication between the BMU cells. This interference in the interplay between osteoclasts and osteoblasts leads to serious bone diseases in cancer patients (Phan et al., 2004): osteoporosis, osteopetrosis, Paget's disease, osteoarthritis, periodontal disease, osteogenesis imperfecta, etc. In all these diseases, the usual treatment is to try to recover a normal regulation of BMU. For example, experimental studies show that neutralizing antibodies that act against PTHrP or using agents that specifically de-

crease expression PTHrP or treatment of OPG can prevent high bone destruction. Thus, to have a better understanding of bone metastasis could allow the design of more effective treatments. In this direction with a non-invasive method using mathematical modeling, one of our goals is to identify which are the significant factors in bone metastasis. Using the biological considerations displayed in Chapter 1.1, in the next Section we will construct a model to describe bone metastasis dynamics based on the interaction between the BMU and cancer cells.

2.2 OC-OB-CC model

We focus on the Komarova biochemical-simplified model presented in Section 1.1.2:

$$\begin{cases} C' &= C(\alpha_1 B^{\gamma_1} - \beta_1), \\ B' &= B(\alpha_2 C^{\gamma_2} - \beta_2), \end{cases} \tag{2.1}$$

where $C = C(t)$, $B = B(t)$ are the number of osteoclasts and osteoblasts, respectively, and the symbol $'$ denotes the derivative of C or B with respect to time. Recall that α and β parameters are positive, whereas $\gamma_1 < 0$ and $\gamma_2 > 0$. For discussion on the model parameters, please refer to Section 1.1.2.

In the following, we extend this model in order to include a new equation for cancer cells and incorporate new terms of the interactions between the three cell populations: osteoclasts (OCs), osteoblasts (OBs) and cancer cells (CCs). Taking into account the mechanisms of the bone metastasis dynamics exposed in the previous Section, and also the base hypotheses (*H1*)–(*H6*) from 1.1.2, we assume the following hypotheses related to cancer dynamics in constructing our model:

(*H1'*) There are not external influence on the osteoclast, osteoblast and cancer populations, that is, the OC-OB-CC system is isolated.

(*H2'*) CCs have a logistic growth which is a natural behavior when there are limited resources.

(*H3'*) CCs and OBs can have a mutualism or competitive relationship depending on the bone lesion considered.

(*H4'*) CCs and OCs have a mutualism relationship.

(*H5'*) The death of CCs is due to inherent factors in the bone microenvironment and it is assumed to be proportional to the population of cancer cells.

Based on the previous hypotheses, we propose the following OC-OB-CC model:

$$\begin{cases} C' &= \alpha_1 C B^{\gamma_1} - \beta_1 C + \sigma_1 C T, \\ B' &= \alpha_2 C^{\gamma_2} B - \beta_2 B + \sigma_2 B T, \\ T' &= \alpha_3 \left(1 - \dfrac{T}{K}\right) T + (\sigma_3 C^{\gamma_2} + \sigma_4 v^{\gamma_1}) T - \beta_3 T, \end{cases} \tag{2.2}$$

where $T = T(t)$ is the number of cancer cells; the cell production and apoptosis rates of the three cell populations are denoted by α_i and β_i for $i = 1$ (OCs), 2 (OBs), 3 (CCs); the positive coefficient K is the carrying capacity of tumor cells in the bone environment. Finally, the constants σ's represent the mutualism and competence between all cell populations.

For the mutualism case between two populations, the coefficient σ_j, for $j = 1, \ldots, 3$, is positive, otherwise a negative σ is associated to a competitive relationship. In the case $\sigma_4 > 0$ osteoblasts have a negative effect on the growth of cancer cells due to the negative exponent γ_1; the opposite effect is achieved if $\sigma_4 < 0$. Thus, taking into account hypotheses *(H3')*-*(H5')* based on experimental observations, σ_1 and σ_3 are considered positive and σ_2 and σ_4 can be positive or negative, both cases will be analyzed. The term $\sigma_3 C^{\gamma_2} + \sigma_4 v^{\gamma_1}$ that appears in the third equation of system (2.2) describes the OC-OB-contribution to the tumor growth. Notice that it is regulated by the paracrine signaling of the osteoclast and osteoblast populations which is an approximation to facilitate the posterior analysis of the system. However, a more general functional form can be considered as we will show in Section 2.4.

In order to simplify the formulation of system (2.2), we define the following dimensionless variables:

$$\bar{C} = \left(\frac{\alpha_3}{\alpha_2}\right)^{-\frac{1}{\gamma_2}} C, \quad \bar{B} = \left(\frac{\alpha_3}{\alpha_1}\right)^{-\frac{1}{\gamma_1}} B, \quad \bar{T} = \frac{T}{K}; \quad \bar{t} = \alpha_3 t.$$

Substituting them into the OC-OB-CC model we obtain the equivalent dimensionless system:

$$\begin{cases} \bar{C}' &= \bar{C}\Big(\bar{B}^{\gamma_1} + a_1\bar{T} - b_1\Big), \\ \bar{B}' &= \bar{B}\Big(\bar{C}^{\gamma_2} + a_2\bar{T} - b_2\Big), \\ \bar{T}' &= \bar{T}\Big(1 - \bar{T} + a_3\bar{C}^{\gamma_2} + a_4\bar{B}^{\gamma_1} - b_3\Big), \end{cases} \tag{2.3}$$

where

$$a_1 = \frac{K\sigma_1}{\alpha_3}, \quad a_2 = \frac{K\sigma_2}{\alpha_3}, \quad a_3 = \frac{\sigma_3}{\alpha_2}, \quad a_4 = \frac{\sigma_4}{\alpha_1}, \quad b_i = \frac{\beta_i}{\alpha_3},$$

for $i = 1, 2, 3$. Taking into account the signs of the original coefficients, we know that $a_1, a_3 > 0$, $b_i > 0$ and coefficients a_2 and a_4 can be positive or negative.

Let us define the set $\Omega^3_+ = \{(x, y, z) : x, y > 0, z \geq 0\} \subset \mathbb{R}^3_+$. Observe that the functions on the right side of system (2.3) are locally Lipschitz continuous with respect to $(\bar{C}, \bar{B}, \bar{T})$ on Ω^3_+. Thus for any initial condition $(\bar{C}_0, \bar{B}_0, \bar{T}_0) \in \Omega^3_+$ there exists a unique solution in Ω^3_+. Analogously, the previous statement is also satisfied for system (2.2).

In the next Section, we will give the stationary solutions of system (2.2). The equilibria of this system consist of two equilibrium points: one free of cancer in the bone site and the other with an invasion of cancer cells. In order to know the significant factors in the success of bone metastasis, a stability analysis of equilibria will be carried out using the dimensionless system.

2.3 Equilibria and stability analysis

System (2.3) has two steady states, so using the equivalence between the systems (2.2) and (2.3), the stationary points in the original variables are given by the following:

- *Cancer-free equilibrium.*

$$C^*_F = \left(\frac{\beta_2}{\alpha_2}\right)^{\frac{1}{\gamma_2}}, \quad B^*_F = \left(\frac{\beta_1}{\alpha_1}\right)^{\frac{1}{\gamma_1}}, \quad T^*_F = 0. \tag{2.4}$$

Notice that the T_F^* is zero since it represents the number of the cancer cells in the bone system.

- *Cancer-invasion equilibrium.*

$$\begin{cases} C_I^* &= \left(\dfrac{\alpha_1(r\beta_2+\beta_3\sigma_2-\alpha_3\sigma_2)-\sigma_4(\beta_1\sigma_2-\beta_2\sigma_1)}{d}\right)^{\frac{1}{\gamma_2}}, \\ B_I^* &= \left(\dfrac{\alpha_2(r\beta_1+\beta_3\sigma_1-\alpha_3\sigma_1)-\sigma_3(\beta_1\sigma_2-\beta_2\sigma_1)}{d}\right)^{\frac{1}{\gamma_1}}, \\ T_I^* &= \dfrac{\alpha_1\alpha_2\alpha_3-\alpha_1\alpha_2\beta_3+\alpha_1\sigma_3\beta_2+\alpha_2\sigma_4\beta_1}{d}, \end{cases} \tag{2.5}$$

where $r = \dfrac{\alpha_3}{K}$ and $d = \alpha_1\alpha_2 r + \alpha_1\sigma_2\sigma_3 + \alpha_2\sigma_1\sigma_4$. This state describes when the maximum population of cancer cells is reached due to the limit of the bone system resources.

Next, we obtain sufficient conditions for the stability of each stationary solution. To study the stability of the above states, we use the standard analysis that consists of: linearizing the OC-OB-CC system (2.3) around equilibrium solutions by calculating the Jacobian matrix of the system and to get the characteristic polynomial associated to the Jacobian matrix, $P_J(s)$ where $s := (C^*, B^*, T^*)$. As a matter of fact, the stability of the equilibrium depends on the signs of the real part of the roots of the P_J. In the case that their roots cannot be obtained explicitly a useful tool is given by the Routh-Hurwitz (R-H) criterion, see Appendix A.

2.3.1 Cancer-free equilibrium

The characteristic polynomial associated to the cancer-free equilibrium (2.4) of system (2.3) is

$$P_J(s) = \left(-b_1b_2\gamma_1\gamma_2 + s^2\right)\left(-b_1a_4 - b_2a_3 + b_3 + s - 1\right).$$

The roots of this polynomial are

$$s_1^F = +i\sqrt{-b_1b_2\gamma_1\gamma_2}, \quad s_2^F = -i\sqrt{-b_1b_2\gamma_1\gamma_2}, \quad s_3^F = 1 + b_1a_4 + b_2a_3 - b_3. \tag{2.6}$$

Since s_1^F and s_2^F do not have real part, the stability of (C_F^*, B_F^*, T_F^*) is given by the third root. For s_3^F positive, this steady state is unstable but if it is negative then a linear analysis is not conclusive. However, when the cancer-free equilibrium is attained then system (2.2) is a particular case of the OC-OB system (2.1). So, taking into account Theorem 1.1, we state the following result:

Theorem 2.1. *The OC-OB-CC system with any initial condition* $(C_0, B_0, T_0) \in \Omega_+^3$ *and verifying condition* (1.2) *has a locally stable cancer-free equilibrium solution,* $E_F := (C_F^*, B_F^*, T_F^*)$*, defined in* (2.4) *if*

$$\frac{\beta_2\sigma_3}{\alpha_2} + \frac{\beta_1\sigma_4}{\alpha_1} < \beta_3 - \alpha_3. \tag{2.7}$$

Moreover, OC-OB-CC system has a unique periodic solution which oscillates around

$$\left(\left(\frac{\beta_2}{\alpha_2}\right)^{\frac{1}{\gamma_2}}, \left(\frac{\beta_1}{\alpha_1}\right)^{\frac{1}{\gamma_1}}, 0\right).$$

If inequality (2.7) is not fulfilled then E_F is unstable.

Proof. Inequality (2.7) is obtained forcing to satisfy $s_3^F < 0$ and substituting into this inequality the original coefficients of model (2.2). The periodicity of the solution is straightforward of Theorem 1.1. □

Inequality (2.7) provides the conditions for which cancer cells can be removed from the bone system. Analyzing the biological sense of this inequality we conclude that in order to eliminate the tumor some of the following behaviors between the osteoclasts, osteoblasts and cancer cells have to be given:

- If $\sigma_4 > 0$ then a slow growth of the cancer cells along with a fast death of them ($\alpha_3 \downarrow\downarrow$ versus $\beta_3 \uparrow\uparrow$).
- If $\sigma_4 < 0$ then a fast growth of osteoblasts and a poor support of the osteoclasts to the cancer cells ($\alpha_2 \uparrow\uparrow$ versus $\sigma_3 \downarrow\downarrow$).

  Both cases will be shown in Section 2.4

2.3.2 Cancer-invasion equilibrium

In this case, it is difficult to find the roots of the characteristic polynomial associated to the Jacobian matrix on $(\bar{C}_I^*, \bar{B}_I^*, \bar{T}_I^*)$. So for simplicity we consider $\sigma_4 = 0$. Biologically, it means that the population of osteoblast cells only affects indirectly the growth of cancer cells by activating the population of osteoclast cells. Assuming that, we have:

$$\begin{aligned}
&P_J(s) = \\
&s^3 + \Big\{b_3 - b_2a_3 - 1 + \Big(a_2a_3 + 2\Big)\bar{T}_I^*\Big\}s^2 \\
&+\gamma_2\Big\{ - b_1b_2\gamma_1 + \Big(b_1a_2\gamma_1 - b_2a_1a_3 + b_2a_1\gamma_1\Big)\bar{T}_I^* + \Big(a_1a_2a_3 - a_1a_2\gamma_1\Big)(\bar{T}_I^*)^2\Big\}s \\
&+\gamma_1\gamma_2\Big\{b_1b_2(b_2a_3 - b_3 + 1) + \Big(b_1a_2(b_3 - 1) - b_1b_2(3a_2a_3 - 2) - b_2a_1(b_2a_3 - b_3 + 1)\Big)\bar{T}_I^* \\
&+\Big(2b_1a_3a_2^2 + 2b_1a_2 + a_1a_2(3b_2a_3 - b_3 + 1) + 2b_2a_1\Big)(\bar{T}_I^*)^2 - 2a_1a_2\Big(a_2a_3 + 1\Big)(\bar{T}_I^*)^3\Big\},
\end{aligned} \tag{2.8}$$

where $\bar{T}_I^* = (1 + a_3b_2 - b_3)/(1 + a_2a_3)$ is the third component of the steady state of the dimensionless system when $a_4 = 0$. Given that the coefficient a_2, from σ_2 of model (2.2), can be positive (a mutualism relationship between OBs and CCs) or negative (competitive relationship between OBs and CCs), we distinguish both cases in our analysis. The following theorem summarize the results obtained.

Theorem 2.2. *The OC-OB-CC system with any initial condition $(C_0, B_0, T_0) \in \Omega_+^3$ and verifying condition (1.2) has a locally asymptotically stable cancer-invasion equilibrium solution, $E_I := (C_I^*, B_I^*, T_I^*)$, defined in (2.5), if $\sigma_2 < 0$, $\sigma_4 = 0$ and these three inequalities*

$$(i)\ \frac{\beta_3 - \alpha_3}{\sigma_3} < \frac{\beta_2}{\alpha_2}, \qquad (ii)\ \frac{|\sigma_2|}{\alpha_2} < \frac{\alpha_3}{\sigma_3}, \qquad (iii)\ T_I^*\Big(1 - \frac{\alpha_3}{|\sigma_2|\gamma_1}\Big) < \frac{\beta_1}{\sigma_1},$$

are verified. If $\sigma_2 > 0$ then E_I is unstable.

Proof. Condition *(i)* is imposed so that the cancer-free equilibrium, E_F, is unstable and taking into account that $\sigma_4 = 0$. Now, in order to get that all the roots of the polynomial (2.8) have negative real part, we impose the Routh-Hurwitz conditions, see Appendix A. If $\sigma_2 < 0$ then $a_2 < 0$ and we get the following inequalities:

$$0 < \bar{T}_I^*; \quad \bar{T}_I^*\Big(1 + \frac{1}{a_2\gamma_1}\Big) < \frac{b_1}{a_1}; \quad -a_2 < \frac{1}{a_3}.$$

The first inequality is always satisfied and the other two give conditions *(ii)* and *(iii)* when the dimensionless coefficients are replaced by the original one. However, if $\sigma_2 > 0$ then $a_2 > 0$ and the condition (C2) in the R-H criterion is never satisfied then under these conditions the cancer-invasion equilibrium is always unstable. □

Analogously to the equilibrium E_F, we analyze the biological sense of inequalities (i)-(iii) and conclude that for a successful cancer invasion in the bone microenvironment then several of the following conditions should occur:

- Cancer cells have to have fast growth ($\alpha_3 \uparrow\uparrow$).
- Cancer should not stimulate the growth of osteoclasts too much ($\sigma_1 \downarrow\downarrow$).
- A strong competition by the resources, like TGF-β and IGF-I, between osteoblasts and the cancer cells ($\sigma_2 \uparrow\uparrow$) or more control of osteoblasts on osteoclasts ($|\gamma_1|\uparrow\uparrow$).

Next, we shall show numerical simulations of the different behaviors of the solution of the OC-OB-CC system (2.2) in order to illustrate the qualitative results proved in this Section. Unfortunately, we do not have experimental data of the populations of osteoblasts and osteoclasts in presence of cancer cells, but there is "known" information about their qualitative behavior given by the diseases associated with a bone tumor. So, we shall validate our OC-OB-CC model based on the metastatic lesions disclosed in Section 2.1.

2.4 Simulations and discussion

Here we illustrate the different behaviors of the solution of the OC-OB-CC system proposed previously in order to describe the diverse scenarios of the bone metastasis evolution. We are also interested in the changes in bone mass associated with the distinct behaviors of the three populations so the percentage of bone mass is also shown.

Numerical simulations of system (2.2) are calculated by using the values of the parameters in Table 1.4 (baseline parameters) and Table 2.1 (cancer-associated dynamics), where a carrying capacity of tumor cells of $K = 300$ is considered. We did not have access to quantitative data, from the literature or from a laboratory, to perform a parameter estimation from experiments. Thus, we estimated the values so that the number of OCs was at least 1 order of magnitude smaller than the number of OBs (Komarova et al., 2003) and such that simulations did not present blow-up of solutions. We briefly describe each scenario considered here:

- *Periodicity 1.* This is a cancer-free scenario in which the initial CC population goes extinct and where there is no contribution from OBs to CCs ($\sigma_4 = 0$).
- *Periodicity 2.* Here, we explore a hypothetical inhibited elimination of CCs due to OB factors ($\sigma_4 < 0, \gamma_1 < 0$).

Parameter *(units)*	**Cancer-Free** *Periodicity 1*	*Periodicity 2*	**Cancer-Invasion** *Mixed Lesion*	*Osteolytic Lesion*
α_3 (day^{-1})	0.045	0.055	0.055	0.055
β_3 (day^{-1})	0.05	0.05	0.05	0.05
σ_1 $(cell^{-1}day^{-1})$	0.001	0.001	0.001	0.0005
σ_2 $(cell^{-1}day^{-1})$	-0.00005	-0.00005	-0.005	-0.009
σ_3 $(cell^{-1}day^{-1})$	0.005	0.005	0.001	0.001
σ_4 $(cell^{-1}day^{-1})$	0.0	-0.015	0.0	0.0
k_1 $(cell^{-1}day^{-1})$	0.07	0.07	0.02	0.02
k_2 $(cell^{-1}day^{-1})$	0.0022	0.0022	0.003	0.003

Table 2.1: Parameter values for system (2.2) and bone mass equation (1.4). Additionally, $K = 300$ is considered for the four cases.

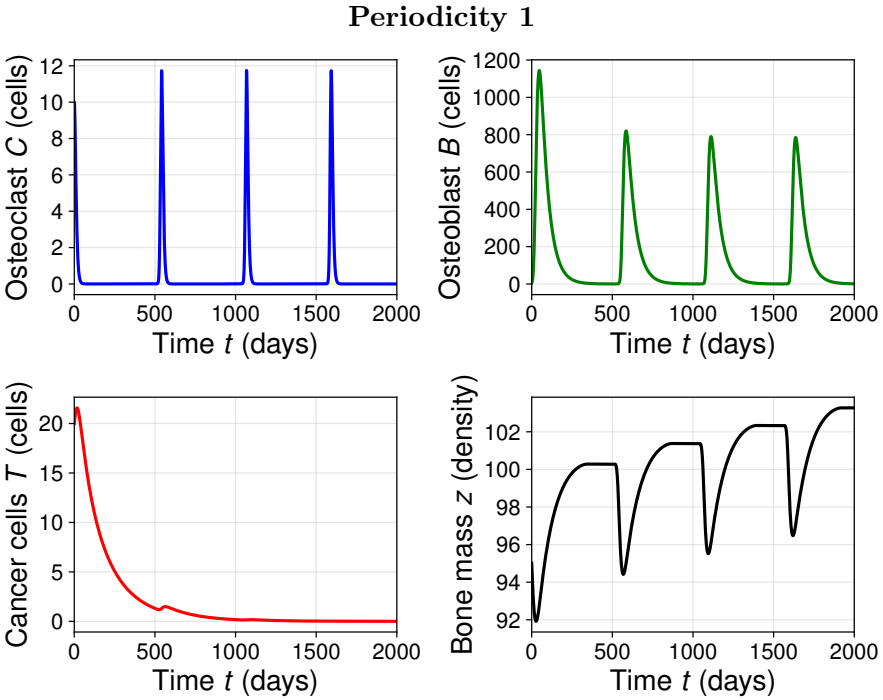

Figure 2.1: Cancer-free behavior of OC-OB-CC system (2.2) and bone mass (1.4) for a patient with bone metastasis with initial condition $(C_0, B_0, T_0, z_0) = (10, 5, 20, 95)$ using parameters of the *Periodicity 1* column.

- *Mixed Lesion.* In this scenario, tumor invades bone such that OCs and OBs increase considerably. Bone mass increases abnormally and then decreases due to inhibition of OBs.

- *Osteolytic Lesion.* Here, a persistent number of OCs and CCs co-exist at considerable levels while the number of OBs decreases. Bone mass is reduced rapidly.

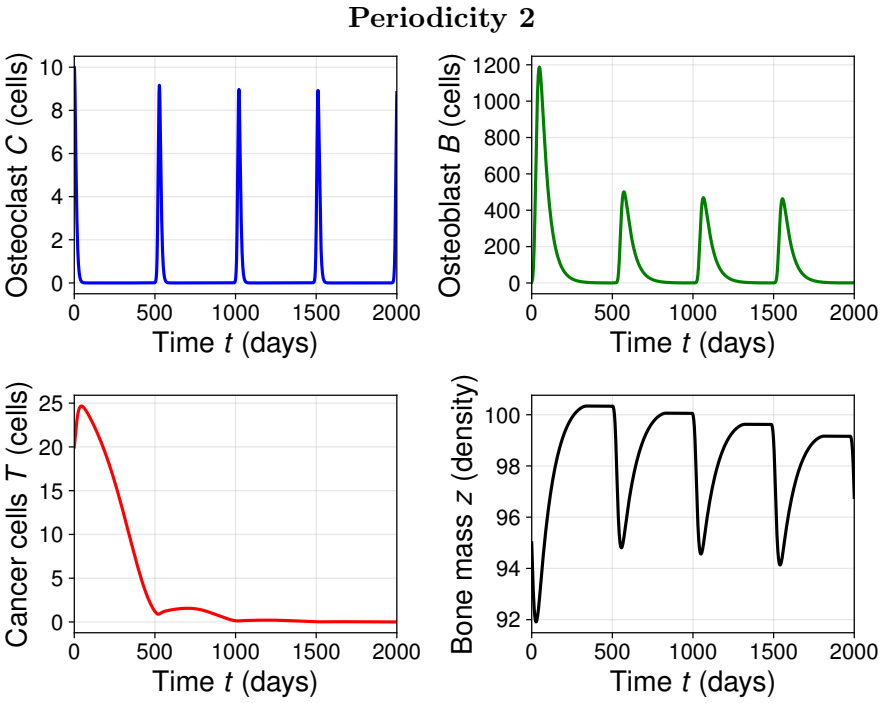

Figure 2.2: Cancer-free behavior of OC-OB-CC system (2.2) and bone mass (1.4) for a patient with bone metastasis with initial condition $(C_0, B_0, T_0, z_0) = (10, 5, 20, 95)$ using parameters of the *Periodicity 2* column.

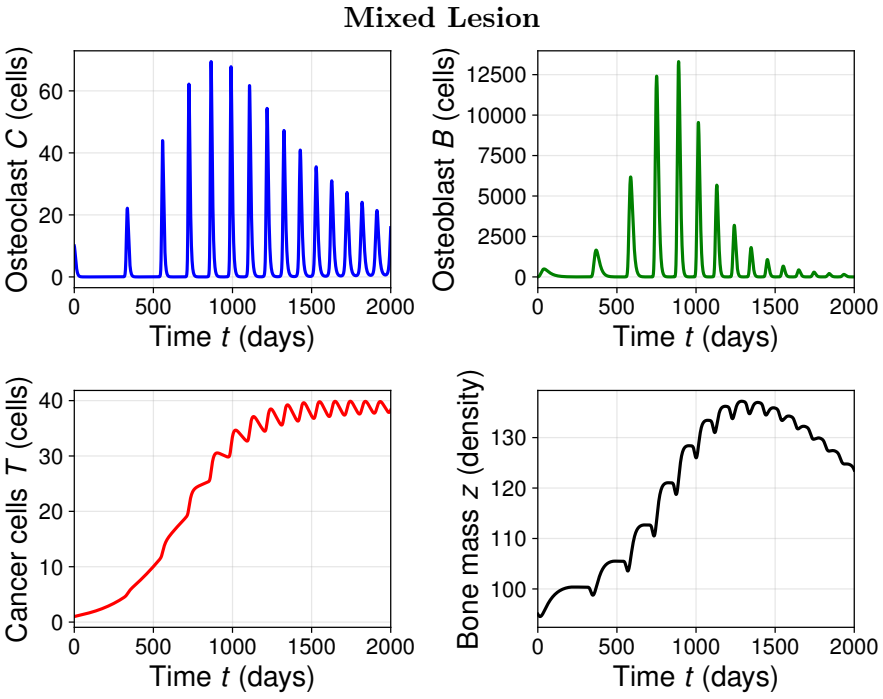

Figure 2.3: Cancer-invasion behavior of OC-OB-CC system (2.2) and bone mass (1.4) for a patient with bone metastasis with initial condition $(C_0, B_0, T_0, z_0) = (10, 5, 1, 95)$ using parameters of the *Mixed Lesion* column.

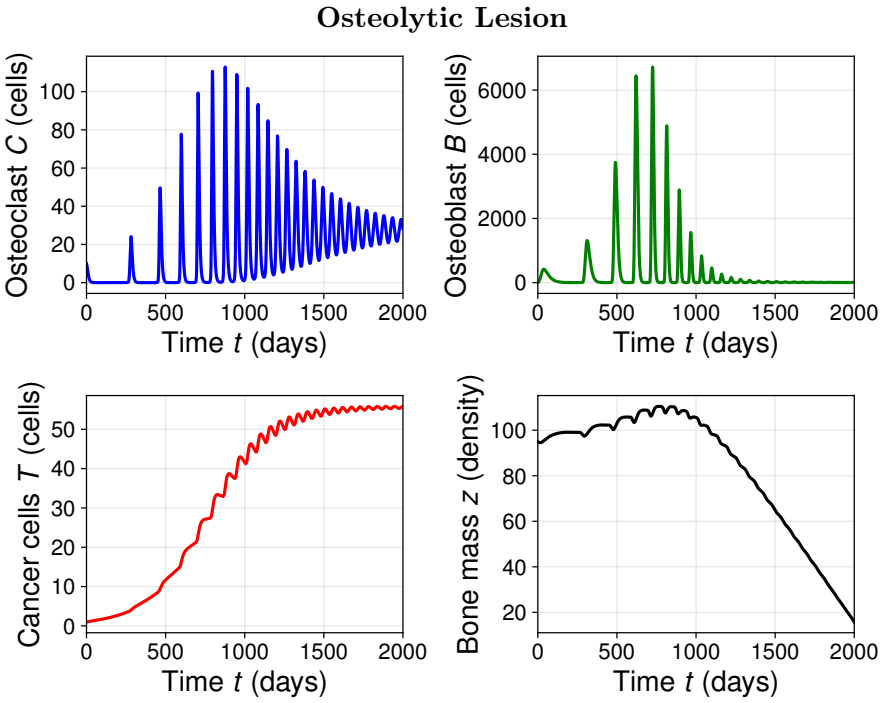

Figure 2.4: Cancer-invasion behavior of OC-OB-CC system (2.2) and bone mass (1.4) for a patient with bone metastasis with initial condition $(C_0, B_0, T_0, z_0) = (10, 5, 1, 95)$ using parameters of the *Osteolytic Lesion* column.

For the cancer-free equilibrium, if the death rate of cancer cells is greater than its growth rate then, there is a fast decline of the tumor and a normal periodicity of osteoclasts and osteoblasts is recovered, see Figure 2.1. However, when $\alpha_3 > \beta_3$ it is necessary that $\sigma_4 < 0$ in order to get a stable cancer-free stationary state. An example of the behavior of the solution for this case is also shown in Figure 2.2. Notice that the periodicity of the OC, OB and bone mass solutions is recovered as time increases. In both periodicity cases, the parameter setting from Table 2.1 satisfies the stability conditions from Theorem 2.1. In Figures 2.3 and 2.4, we show the behaviors of the solution curves for system (2.2) and bone mass equation (1.4) when cancer does not disappear but reaches its maximum population limit. For such cancer-invasion case, the ravages of cancer on the bone matrix structure are reflected in the percentage of bone mass. In Figure 2.3, a mixed metastatic lesion is shown; initially, a high bone formation is presented followed by strong bone resorption. On the other hand, in Figure 2.4, we also show a lesion of the osteolytic type on the right graphs. In both cases, notice that there is an abnormal increase in the values of osteoclasts and osteoblasts which triggers a malfunction of the BMU cells. Observe that the type of lesions is directly linked to the values of the coefficients σ_1 and σ_2, which give information about how cancer affects the osteoclast and osteoblast populations.

A bifurcation analysis provides interesting results since changes of the sign of the coefficient σ_4 leads to different stationary states of the solution. We chose to explore this parameter because the role of osteoblasts on the growth of the tumor is still under research. Thus, we consider σ_4 as a bifurcation parameter. Varying it, we obtain the diagram given in Figure 2.5 where we show the stability and instability of the two equilibrium solutions

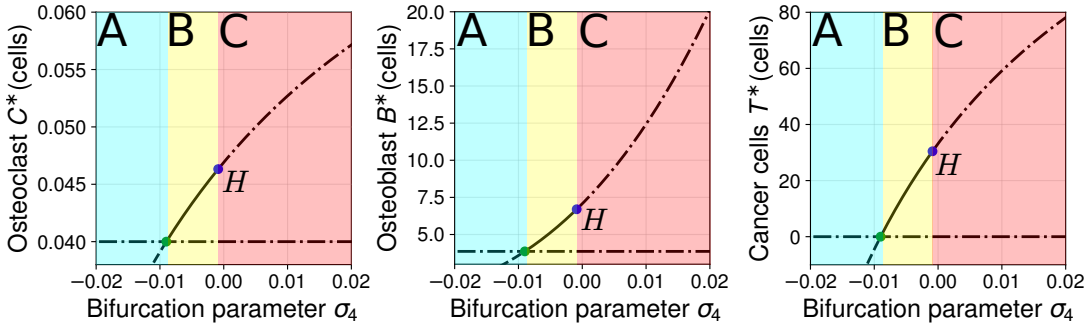

Figure 2.5: Bifurcation diagrams with respect to σ_4 using *Periodicity 2* column in Table 2.1. **Solid lines:** Stable. **Dashed lines:** Unstable. **Dashed-dot lines:** Oscillations.

for the population of cancer cells. Notice the small parameter regime where the cancer cells can not survive. Also, along the branch of cancer-invasion, periodic solutions can be found. Therefore, showing a potential coexistence between all type of cells. In summary, there are three regions where different behavior is found:

- *Region* **A**: In this region, CCs go extinct and the BMU returns to a periodic, cancer-free oscillatory behavior.
- *Region* **B**: In this region, the cancer-invasion steady-state appears as a stable equilibrium, showing a transient co-existence of OCs, OBs and CCs.
- *Region* **C**: In this region, a Hopf bifurcation H appears, and the dynamical system oscillates unstably around the cancer-invasion steady-state.

2.4.1 A generalized term

As we mentioned previously, here we propose a more general functional form for the term that describes the contribution of osteoclasts and osteoblasts to the tumor growth. So, we replace the third equation of the OC-OB-CC model (2.2) for the following generalized cancer equation:

$$T' = \alpha_3 \left(1 - \frac{T}{K}\right) T + (\sigma_3 C^{\gamma_3} + \sigma_4 v^{\gamma_4}) T - \beta_3 T, \tag{2.9}$$

and we refer to the new system as the generalized OC-OB-CC model.

In the following, we analyze numerically the generalized system varying the value of the exponents γ_3 and γ_4. According to the relationships between the three populations, we assume that $\gamma_3 > 0$, however, it is not clear how is the OB-CC paracrine-signaling which is represented by γ_4. Thus, we first consider $\sigma_4 = 0$ and vary γ_3 between 0 and 1 and then we study the more general case fixing γ_3 and varying the values of σ_4 and γ_4. As expected, the changes in the value of γ_3 affect the magnitude of the populations and the time period of the BMU cycles but the profile of the OC-OB-CC equilibrium solution is conserved, see Figure 2.6. Now we consider the parameters values proposed in the Periodicity 2 column of Table 2.1, fix $\gamma_3 = 0.5$ and give three different values of the exponent γ_4 (positive and negative). We obtain three different solutions which are shown in Figure 2.7 on the left graphs. Analogously, considering $\sigma_4 = 0.001$ and the parameter

setting given in mixed lesion column in Table 2.1 we present in the same figure on the right graphs the profile of the solutions associated to the same three values of γ_4. We can observe that the equilibrium solution does not change although γ_4 is modified. Thus, we can conclude that the inclusion of the equation (2.9) in the OC-OB-CC model does not change the qualitative behavior of the OC-OB-CC solution.

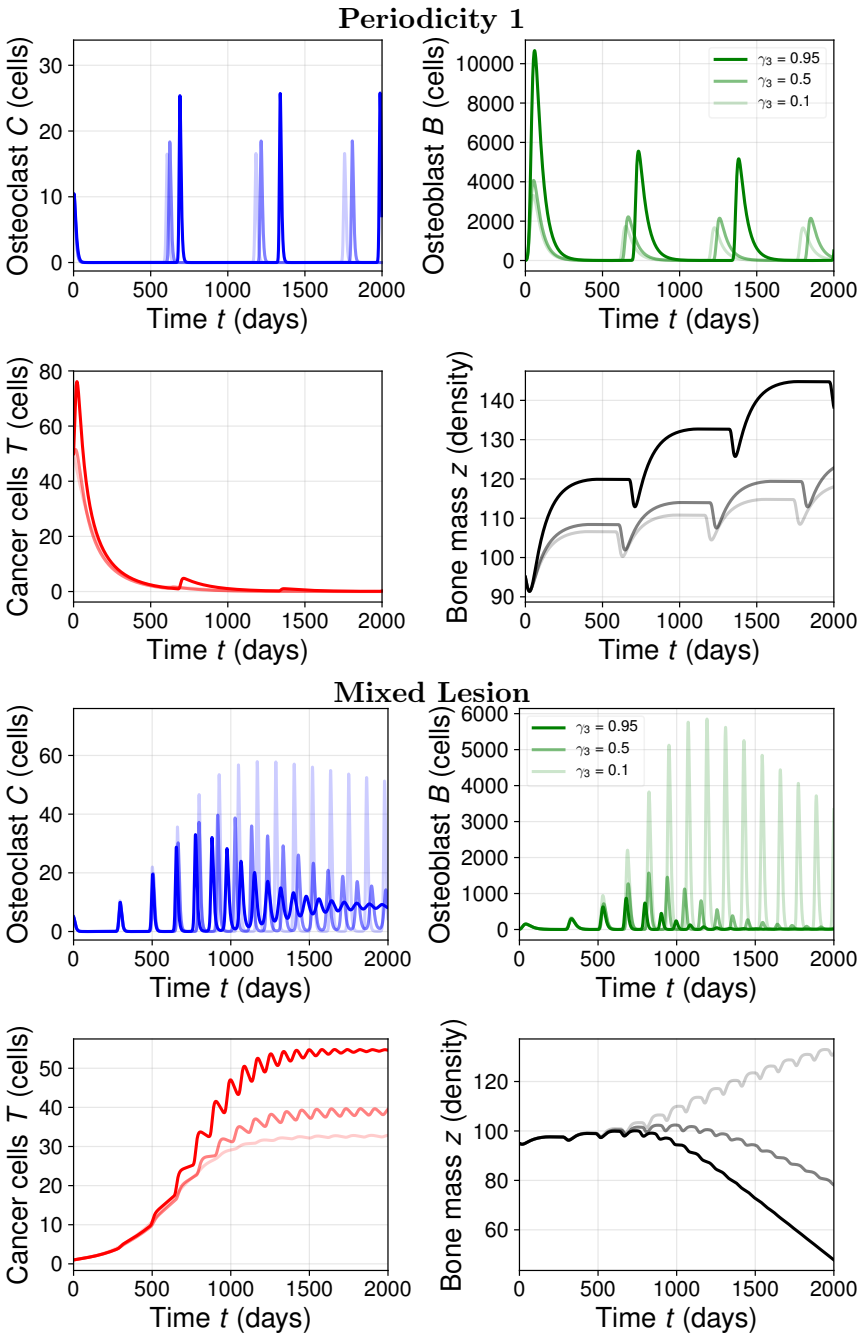

Figure 2.6: Sensitivity analysis for (2.9) with respect to γ_3 considering parameters of *Periodicity 1* column with initial condition $(C_0, B_0, T_0, z_0) = (10, 5, 50, 95)$ (**left**) and *Mixed Lesion* column with $(C_0, B_0, T_0) = (5, 5, 1)$ (**right**).

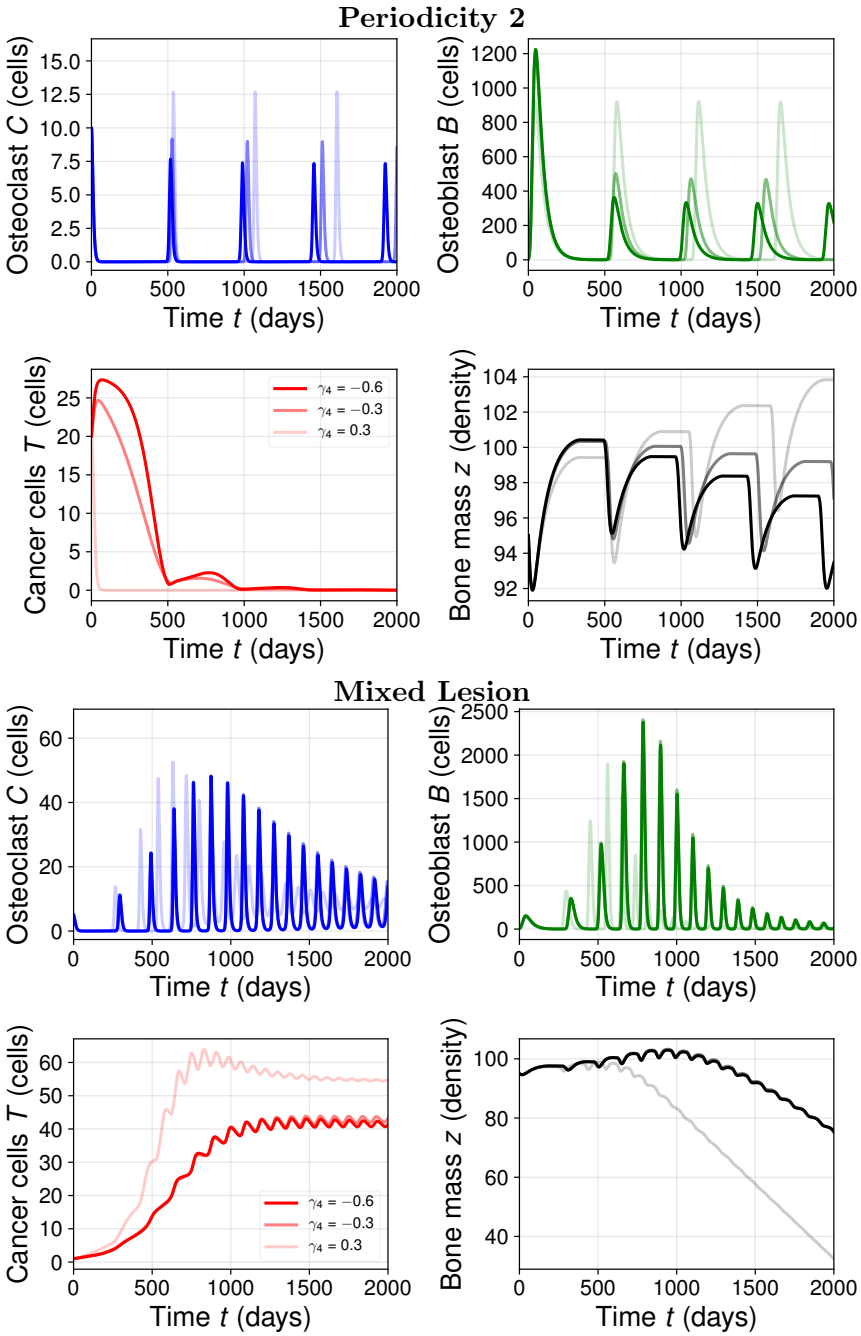

Figure 2.7: Sensitivity analysis for (2.9) with respect to γ_4 considering parameters of *Periodicity 2* column with initial condition $(C_0, B_0, T_0) = (10, 5, 20)$ (**left**) and *Mixed Lesion* column with $(C_0, B_0, T_0) = (5, 5, 1)$ (**right**).

Discussions

In this Chapter, we constructed a model that describes the evolution of bone metastasis disease based on the interactions between the osteoclast, osteoblast and cancer cells. Such a model was derived according to the experimental knowledge of the osteoclast-osteoblast relationship and the 'vicious cycle' hypothesis for bone metastasis. The model fills a gap in the literature since we couple cancer dynamics with the BMU dynamics, a feature not considered in Ayati et al. (2010).

In our model, there are two equilibrium solutions: one cancer-free and another cancer-invasion. What are the key elements that could dictate that cancer cells sometimes colonize bone and sometimes they do not? A stability analysis could answer partially this questions. Stability conditions for model parameters were obtained for both steady states, which were useful to deduce the most significant coefficients in the success or failure of bone metastasis. We found that the colonization of cancer cells depends on convoluted relationships between BMU parameters (that is, OCs-OBs system without cancer) and cancer dynamics. Here, mathematical and biological knowledge must face each other. The stability conditions may pose experimental settings to corroborate or refute the mathematical conditions for failure or success of a bone metastatic invasion. This is an essential feedback loop in Applied Mathematics, and we hope to find interested colleagues in performing experiments that may be suggested by our mathematical model.

In order to give support to the analytical results, we also performed numerical simulations. We found different behaviors of the solution of the OC-OB-CC model. Parameter setting for simulations was given according to qualitative experimental data. As mentioned earlier, further quantitative experiments may serve to perform a more accurate parameter fitting. A novel bone mass equation was proposed, based on the comparison of the number of osteoclasts and osteoblasts with an OC-OB reference value for a healthy person. Via simulations, we realized that our model is able to describe the different three types of bone diseases caused by bone metastasis: osteolytic lesion, osteoblastic lesion, and mixed lesion. Numerical results validated and illustrated the cancer-free and cancer-invasion equilibrium solutions. We discovered, with a numerical bifurcation analysis, that there is a key coefficient for the change of stability of the equilibria and also for the existence of bifurcation points. In particular, we recovered an oscillatory regime for cancer-invasion dynamics that resembles the one of the OCs-OBs system from Komarova et al. (2003).

In the next Chapter, we focus on using optimal control tools in order to describe the effects of different treatments for bone metastasis disease.

Chapter 3

Conventional bone metastasis treatments as optimal control problems*

As mentioned in the previous Chapter, several factors may disrupt the cross-talk between osteoclasts and osteoblasts, thereby causing bone diseases such as osteoporosis or osteopetrosis. In particular, the presence of metastatic cancer cells at the bone microenvironment is one of these factors (Florencio-Silva et al., 2015). Metastasis occurs when cancer cells spread from an initial body part, -like breast or prostate cancer-, to distant tissues, -like brain, lungs or bone-. The 'Seed & Soil' theory (Paget, 1889) explains that cancer cells (*the seeds*) have preference to certain microenvironments (*the soil*) to metastasize. Breast and prostate cancers are the most common cancers that have high potential to form bone metastases; the former is known to cause osteolytic lesions, while the latter usually exhibits osteoblastic lesions. There is multiple evidence that supports the idea that there are many complex biochemical interactions between metastatic cells and the bone microenvironment, bringing up the hypothesis of the development of a *vicious cycle* that the BMU cells support cancer cells proliferation (Mundy, 2002; Theriault & Theriault, 2012).

Considering that one of the main causes of death in cancer patients is metastases formation (Massagué & Obenauf, 2016), this disease has received much attention in the last years so to understand its mechanisms. It is known the difficulty and limitations of *in vivo* and *in vitro* bone metastasis experiments (Kwakwa et al., 2017), thus mathematical modeling may be another approach to obtain insights about the disease and try to validate some posed biological hypotheses. The number of this kind of works is considerably reduced. Lemaire extensions that model these phenomena include: Wang et al. (2011) in which multiple myeloma-induced bone disease is studied based on the bone remodeling model presented in Pivonka et al. (2008), and Farhat et al. (2017) which focuses specifically to model bone metastatic prostate cancer. Biochemical-simplified models that consider BMU-disregulation due to cancer are: Ayati et al. (2010) which focus on multiple myeloma and the BMU dynamics; Garzón-Alvarado (2012) where both metastatic bone lesions are studied via a switch term included in the model; in Ryser et al. (2012) the OPG concentration is proposed as a key parameter mediating the bone metastasis; Coelho et al.

*This Chapter is based on Camacho, A., Jerez, S. (2019). Bone metastasis treatment modeling via optimal control. *Journal of Mathematical Biology*, 78(1–2), 497–526.

(2016) include parathyroid hormone concentration effects and a novel way to determine the number of active osteoclasts and osteoblasts; and Chapter 2 where a logistic cancer equation is coupled to a Komarova bone remodeling model for describing the bone metastasis vicious cycle. From a new approach, in Dingli et al. (2009) and Warman et al. (2018) treatments for multiple myeloma and prostate cancer-induced bone disease are modeled as evolutionary games.

Despite important advances in understanding bone metastasis mechanisms, this disease is still considered incurable (Juárez et al., 2017). Palliative treatments for bone metastases are used to reduce pain and to prevent adverse consequences such as bone fractures and spinal cord compression. In this Chapter, we focus on two bone metastasis palliative treatments: denosumab and radiotherapy. Denosumab is a fully human monoclonal antibody to RANKL that acts similarly as OPG and its effectiveness in delaying the appearance of skeletal-related events has been proved (Theriault & Theriault, 2012). Some of the side-effects of denosumab are urinary tract infection, upper respiratory infection, hypocalcemia, and osteonecrosis of the jaw (Lipton et al., 2016). On the other hand, radiotherapy is a treatment that consists of using radiation beams in localized areas of the body to kill cancer cells by damaging their DNA (Lutz et al., 2017). It is estimated that around 50% of cancer patients receive this treatment (Barker et al., 2015). Bone loss is one of the side-effects related to radiotherapy (Zhang et al., 2018). The search for optimal schedules and doses for these bone metastasis treatments continues (Chow et al., 2014; Lipton et al., 2016; Ganesh et al., 2017).

As we mentioned before, it is difficult to make *in vivo* or *in vitro* experiments to study the precise effects of bone metastasis treatments, so mathematical modeling can be an alternative approach. A way to model treatments for some disease is via an optimal control problem associated with the differential model that describes the disease. This framework is based on the idea of minimizing an expression that involves the cost of using a treatment while reducing the hazardous effects by the presence of the disease over time (Lenhart & Workman, 2007). This mathematical tool was used by Lemos et al. (2016) to model treatments for multiple myeloma but has also been employed to study treatments in other biomedical models (Swan, 1990; Fister et al., 1998; Pillis & Radunskaya, 2003). Here, we are interested to find optimal treatments for the denosumab and radiation therapies since significant information about effects on BMU and collateral damage is known for both treatments. The latter is essential for the mathematical modeling process and model validation. It is important to remark that there are other novel treatments with intrinsic relevance; unfortunately, we do not have enough information about them. It is our hope that this Chapter can be used to motivate the generalization of our results for different therapies.

In the present Chapter, we propose two optimal control models: one for denosumab treatment, and another for radiotherapy. Both of them are based on the bone metastasis biochemical-simplified model proposed in Chapter 2, that describes the dynamics between cancer cells and the main BMU cells. We consider this model as a starting point since it is possible to obtain explicitly the steady-states associated with the cancer-free and cancer-invasion scenarios. Furthermore, we have conditions for the local stability of these equilibria. We also prove the existence and uniqueness of solutions for both optimal control models mentioned previously. Such mathematical achievement is of paramount importance for the numerical analysis of the models. The simulations that we obtain agree qualitatively with clinical observations about the evolution of metastatic tumors on

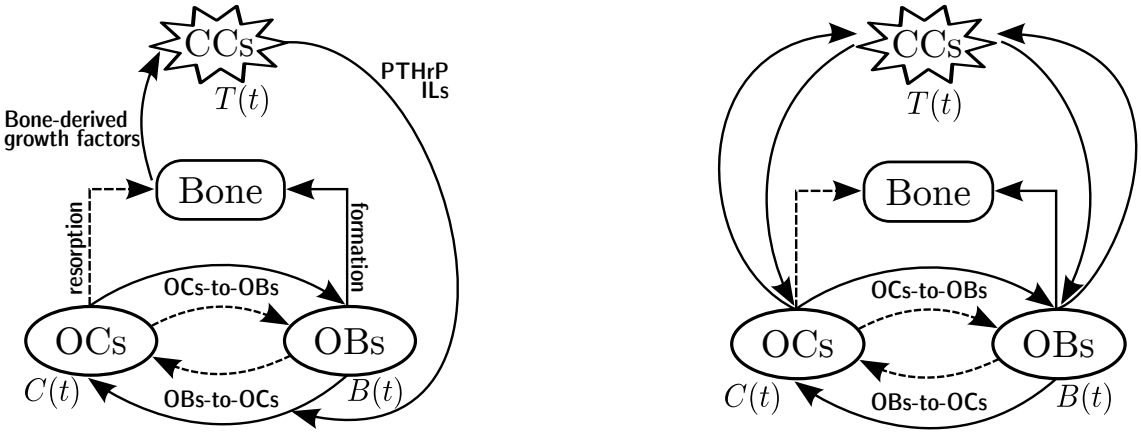

Figure 3.1: Diagrams representing simplified interaction networks in an osteolytic lesion (*left*) and in an osteoblastic or mixed lesion (*right*). Dashed lines represent inhibition/degradation (negative) effects, and solid lines represent promotion/formation (positive) effects.

in silico experiments and on animal models. Moreover, we explore cancer-BMU dynamics for each treatment under different cancer-invasion scenarios.

The Chapter is organized as follows. In Section 3.1, the bone metastasis base model is presented and discussed. Next, in Section 3.2 we propose mathematical models for two bone metastasis treatments (denosumab and radiotherapy) as optimal control problems. In Sections 3.3 and 3.4, an optimal control framework is utilized to show existence and uniqueness of solutions, and also to pose the corresponding optimality systems. Finally, in Section 3.5 qualitative effects of treatment regimes are obtained computationally. Numerical simulations and discussions are presented.

3.1 Bone metastasis base model

The base model can be found in Section 1.1.2 and in the previous Chapter. Here, we recall the main biological assumptions:

- There are autocrine and paracrine communications between osteoclasts (hereafter OCs) and osteoblasts (hereafter OBs) which modifies the recruitment and inhibition rates of the cells (Florencio-Silva et al., 2015). This cross-talk is approximated as a power-law (Komarova et al., 2003). See also Chapter 1.1.

- Bone metastatic cells (hereafter CCs) express a number of biochemical factors that modify bone homeostasis, such as parathyroid hormone-related peptide (PTHrP) and interleukins (ILs) (Mundy, 2002; Ottewell, 2016). For instance, PTHrP enhances OBs expression of RANKL, thereby increasing the number of active OCs; also, OCs resorb bone which causes the release of growth factors such as TGF-β than increase the production of PTHrP (Mundy, 2002). Thus, we assume that the communication between OCs and CCs have positive effects on both populations (mutualism).

- The OBs–CCs communication loop is not completely known (Ottewell, 2016). In the case of an osteolytic lesion, the presence of OBs may not directly impact the prolifer-

ation of CCs and vice versa. On the other hand, for an osteoblastic lesion, the OBs population may increase due to osteoblast-promoting factors produced by CCs such as IL-6. Therefore, we assume that the communication between OBs, and CCs may have positive, negative or null effects on these populations.

- Finally, we also assume that CCs population satisfies a logistic equation which is penalized by a linear elimination rate that reflects the adaptability of CCs to the bone microenvironment (Farhat et al., 2017).

For a schematic representation of the assumptions see Fig. 3.1.

Let us denote by $C(t)$, $B(t)$ and $T(t)$ the population of OCs, OBs and CCs at a certain time t, respectively. Thus, the base model is as follows:

$$\frac{dC(t)}{dt} = \underbrace{\alpha_1 C(t)B(t)^{g_1}}_{\text{OCs inhibition by OBs}} - \beta_1 C(t) + \underbrace{\sigma_1 C(t)T(t),}_{\text{OCs promotion by CCs}} \tag{3.1a}$$

$$\frac{dB(t)}{dt} = \underbrace{\alpha_2 C(t)^{g_2} B(t)}_{\text{OBs promotion by OCs}} - \beta_2 B(t) + \underbrace{\sigma_2 B(t)T(t),}_{\text{CCs net effect on OBs}} \tag{3.1b}$$

$$\frac{dT(t)}{dt} = \alpha_3 T(t)\left(1 - \frac{T(t)}{m}\right) - \beta_3 T(t) + \underbrace{\sigma_3 C(t)^{g_2} T(t)}_{\text{CCs promotion by OCs}} + \underbrace{\sigma_4 B(t)^{g_1} T(t)}_{\text{OBs net effect on CCs}}. \tag{3.1c}$$

For a discussion of the model parameters, we refer the reader to Section 1.1.2.

3.1.1 Cancer-free and cancer-invasion equilibria

In Chapter 2, the existence of cancer-free and cancer-invasion steady-states of the model (3.1) is assured and explicit expressions for them are found. Here, we recall those results. The cancer-free equilibrium is given by:

$$\left(\left(\frac{\beta_2}{\alpha_2}\right)^{\frac{1}{g_2}}, \left(\frac{\beta_1}{\alpha_1}\right)^{\frac{1}{g_1}}, 0\right),$$

which is locally stable if $g_1 g_2 < 0$ and $\frac{\beta_2\sigma_3}{\alpha_2} + \frac{\beta_1\sigma_4}{\alpha_1} < \beta_3 - \alpha_3$. On the other hand, the cancer-invasion equilibrium, denoted by $E_I = (C_I, B_I, T_I)$, can be expressed as:

$$\begin{aligned} C_I &= \left(\frac{\alpha_1(r\beta_2 + \beta_3\sigma_2 - \alpha_3\sigma_2) - \sigma_4(\beta_1\sigma_2 - \beta_2\sigma_1)}{\alpha_1\alpha_2 r + \alpha_1\sigma_2\sigma_3 + \alpha_2\sigma_1\sigma_4}\right)^{\frac{1}{g_2}}, \\ B_I &= \left(\frac{\alpha_2(r\beta_1 + \beta_3\sigma_1 - \alpha_3\sigma_1) - \sigma_3(\beta_1\sigma_2 - \beta_2\sigma_1)}{\alpha_1\alpha_2 r + \alpha_1\sigma_2\sigma_3 + \alpha_2\sigma_1\sigma_4}\right)^{\frac{1}{g_1}}, \\ T_I &= \frac{\alpha_1\alpha_2\alpha_3 - \alpha_1\alpha_2\beta_3 + \alpha_1\sigma_3\beta_2 + \alpha_2\sigma_4\beta_1}{\alpha_1\alpha_2 r + \alpha_1\sigma_2\sigma_3 + \alpha_2\sigma_1\sigma_4}, \end{aligned} \tag{3.2}$$

where $r = \alpha_3/m$. If $\sigma_2 < 0$ and $\sigma_4 = 0$, then the cancer-invasion steady-state E_I is locally stable if these three inequalities hold:

$$\frac{\beta_3 - \alpha_3}{\sigma_3} < \frac{\beta_2}{\alpha_2}, \quad \frac{|\sigma_2|}{\alpha_2} < \frac{\alpha_3}{\sigma_3}, \quad \text{and} \quad C_I\left(1 - \frac{\alpha_3}{|\sigma_2| g_1}\right) < \frac{\beta_1}{\sigma_1}. \tag{3.3}$$

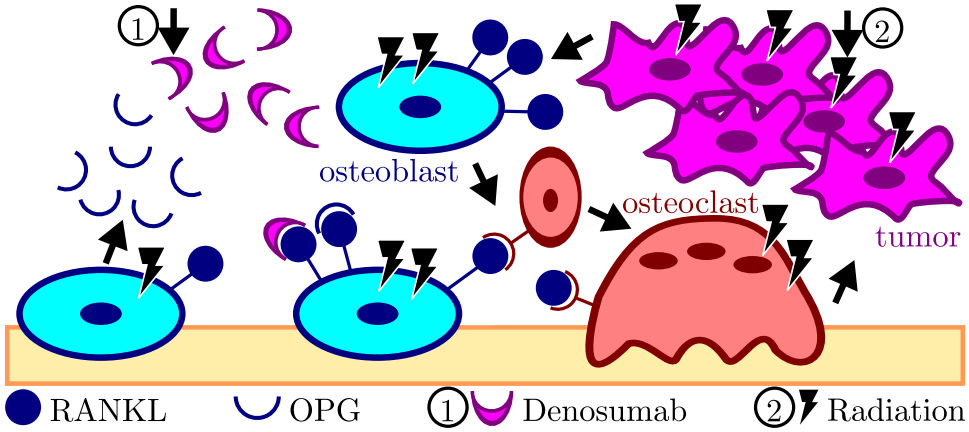

Figure 3.2: Diagrams representing simplified interaction networks in an osteolytic lesion (*left*) and in an osteoblastic or mixed lesion (*right*). Dashed lines represent inhibition/degradation (negative) effects, and solid lines represent promotion/formation (positive) effects.

Note that if we let $\sigma_2 > 0$ and $\sigma_4 = 0$ then E_I is unstable. Also, note that these are sufficient conditions for E_I to be locally stable but not necessary conditions.

Up until now, we have not presented new results. The objective of this Chapter is to explore control strategies for bone metastasis. As such, we predict the local behavior of the solutions around the corresponding steady-states, being the cancer-invasion equilibrium of great importance. If the cancer-invasion equilibrium is locally stable, then CCs may colonize the bone tissue if there are enough of these cells; if this equilibrium is unstable, then an erratic invasion (increasing oscillations) or an elimination of CCs may occur. This information is be used on Section 3.5 for the numerical simulations results.

3.2 Bone metastasis treatment models

In this Section, we present two mathematical models for bone metastasis treatments: denosumab and radiotherapy treatments. These two treatments modify the cellular behavior of OCs, OBs and CCs. Since these three cellular populations are intertwined in an intricate communication network mediated mainly by biochemical factors, it is difficult to predict the overall dynamics of the BMU under treatments. Our goal is to understand the CCs-BMU dynamics and to address the question about the best way to dose those two treatments. For that matter, we use the optimal control framework where a cost function that includes an input (the treatment) and also undesirable variables (bone metastases) is minimized (Lenhart & Workman, 2007). Such optimal control cost includes abstractly an economic cost and the side-effects of the treatment.

3.2.1 Denosumab treatment model

Denosumab affects the main bone remodeling signaling pathway RANK/RANKL/OPG (Florencio-Silva et al., 2015). The main biological mechanisms that we consider and their corresponding mathematical assumptions are:

- When OBs produce RANKL and this molecule binds to RANK then OCs are activated.

Denosumab neutralizes RANKL and it is used to treat bone metastasis to slow down excessive bone resorption caused by the vicious cycle CCs → OBs → OCs (Mundy, 2002; Lipton et al., 2016). For the model, we propose that denosumab alters the cell activity of OCs in a proportional way.

- Denosumab has various side-effects on the patient, such as osteonecrosis of the jaw (Theriault & Theriault, 2012). We propose to combine these side-effects and the economical cost of this treatment in a function that measures both components.

Let us denote by $u_D(t)$ the effect of denosumab on the activity of OCs. Considering the previous assumptions, we propose the following denosumab model:

$$\min_{u_D} J(u_D(t)) \quad \text{where} \quad J(u_D(t)) = \int_0^{t_f} \underbrace{w_D u_D(t)^2}_{\text{DT cost and side-effects}} + T(t)^2 dt \tag{3.4a}$$

subject to:

$$\frac{dC(t)}{dt} = \alpha_1 \underbrace{(1-u_D(t))}_{\text{DT effects on OCs}} C(t)B(t)^{g_1} - \beta_1 C(t) + \sigma_1 C(t)T(t), \tag{3.4b}$$

$$\frac{dB(t)}{dt} = \alpha_2 C(t)^{g_2} B(t) - \beta_2 B(t) + \sigma_2 B(t)T(t), \tag{3.4c}$$

$$\frac{dT(t)}{dt} = \alpha_3 T(t)\left(1 - \frac{T(t)}{m}\right) - \beta_3 T(t) + \sigma_3 C(t)^{g_2} T(t) + \sigma_4 B(t)^{g_1} T(t), \tag{3.4d}$$

$$C(0),\ B(0),\ T(0) > 0 \quad \text{given}, \tag{3.4e}$$

$$0 \le u_D(t) \le u_D^{\max} < 1 \quad \text{for all} \quad 0 \le t \le t_f, \tag{3.4f}$$

where DT stands for denosumab therapy, $u_D \equiv 0$ means that no denosumab is applied and $u_D \equiv u_D^{\max}$ reflects the maximum effectivity of denosumab in nullifying the activity of OCs. The cost functional $J(u_D(t))$ measures the economical cost and side-effects of using denosumab and stores the net side-effects due to the presence of CCs. To construct the cost functional, we follow the standard notion of non-linear cost functionals (Lenhart & Workman, 2007). In particular, the cost per unit of time of the presence of CCs is measured by $T(t)^2$, while the use of denosumab produces a cost per unit of time in term of its effectivity $u_D(t)^2$. Note that $u_D(t)$ and $T(t)$ have significant differences in their orders of magnitude. Thus, in the cost functional (3.4a), the parameter w_D is a weight control parameter that represents the normalized cost of using denosumab. The normalization is done with respect to the order of magnitude of $T(t)^2$. We assume a fixed time window from a starting day 0 to a final day denoted by t_f.

3.2.2 Radiotherapy treatment model

Another treatment option for patients with bone metastasis is radiotherapy. In Zhang et al. (2018) the authors offer a landscape of what is known about the effects of radiation on the bone cells, particularly on OCs and OBs. We now mention the key biological aspects of radiotherapy and the associated mathematical assumptions:

- The main action of radiotherapy is to disrupt CCs proliferation by damaging their DNA; however, it also affects non-cancerous cells of the body like OCs and OBs (Vakaet

& Boterberg, 2004; Brenner, 2008; Zhang et al., 2018). Therefore, we propose that radiation increases the elimination rates of OCs, OBs, and CCs.

- Radiation may cause hematological toxicity, nausea and vomiting (Chow et al., 2014). Taking into account this fact, we include the use of radiation with a function that measures these effects along with the economic cost of the treatment.

- It has been observed that irradiation may impair bone remodeling in the long run (Oest et al., 2015; Zhang et al., 2018). We propose that the effects of a radiation dose decay exponentially rather than instantly on the BMU.

Let us denote by $u_R(t)$ the cell-killing rate due to radiation on the BMU. Considering the mentioned assumptions, we propose the following radiotherapy model:

$$\min_{u_R} J(u_R(t)) \quad \text{where} \quad J(u_R(t)) = \int_0^{t_f} \underbrace{w_R u_R(t)^2}_{\text{RT cost and side-effects}} + T(t)^2 dt, \tag{3.5a}$$

subject to:

$$\frac{dC(t)}{dt} = \alpha_1 C(t) B(t)^{g_1} - \underbrace{(\beta_1 + \psi_1 u_R(t))}_{\text{RT effects on OCs}} C(t) + \sigma_1 C(t) T(t), \tag{3.5b}$$

$$\frac{dB(t)}{dt} = \alpha_2 C(t)^{g_2} B(t) - \underbrace{(\beta_2 + \psi_2 u_R(t))}_{\text{RT effects on OBs}} B(t) + \sigma_2 B(t) T(t), \tag{3.5c}$$

$$\frac{dT(t)}{dt} = \alpha_3 T(t)\left(1 - \frac{T(t)}{m}\right) - \underbrace{(\beta_3 + u_R(t))}_{\text{RT effects on CCs}} T(t) + \sigma_3 C(t)^{g_2} T(t) + \sigma_4 B(t)^{g_1} T(t), \tag{3.5d}$$

$$C(0),\ B(0),\ T(0) > 0 \quad \text{given}, \tag{3.5e}$$

$$0 \le u_R(t) \le u_R^{\max} \quad \text{for all} \quad 0 \le t \le t_f. \tag{3.5f}$$

where RT stands for radiotherapy, the parameters $u_R^{\max}$ and w_R are the analogues of $u_D^{\max}$ and w_D as in the denosumab case. Here, we propose to increase linearly the CCs elimination rate β_3 by $u_R(t)$. To account for adverse effects on the proliferation of OCs and OBs, we assume that their respective elimination rates are also affected by radiation as well. For that reason, we introduce the coefficients ψ_1 and ψ_2 that act as rescaling parameters of the radiation effect $u_R(t)$ on OCs and OBs, respectively.

3.3 Optimal solution for the denosumab model

In order to explore these bone metastasis treatment models, it is important to guarantee the existence of optimal solutions, $u_D(t)$ and $u_R(t)$, that satisfy the corresponding problems (3.4) and (3.5). In this Section, we prove the existence and also the uniqueness of an optimal control solution to the denosumab treatment model (3.4), and we discuss how the radiotherapy model (3.5) has analogous results.

3.3.1 Existence of optimal solutions

We are interested in studying the effects of bone metastasis treatments on the BMU when the tumor has the potential to establish or has already established a successful invasion. To accomplish this, we assume two possible scenarios related to the boundness and positivity of the solutions for the non-treatment model (3.1):

Assumption A *The cancer-invasion equilibrium is locally stable and the initial conditions are located nearby.*

Assumption B *The cancer-invasion equilibrium is locally unstable, then we assume a priori that the state variables remain inside a compact subset.*

Assumption A is valid if the steady-state (3.2) satisfies conditions (3.3). Assumption B is a reasonable assumption that has been proposed in other optimal control problems, see for instance (Bara et al., 2017). In either case, these assumptions lead us to consider a compact subset near the cancer-invasion equilibrium from which the solutions stay in that subset for every positive time $t > 0$.

Now, let us denote the state variables as $x(t) = (C(t), B(t), T(t))$. Also, let Ω be a compact subset of the natural domain of model (3.1) defined by $\Omega^+ = \{(C(t), B(t), T(t)) \mid x_i > 0,\ i = 1, 2, 3\}$. In this subset, the state variables $(C(t), B(t), T(t))$ are uniformly bounded because Ω is a compact subset of Ω^+. This means that, for all $t \in [0, t_f]$, we have

$$C(t) \leq C^{\max} \quad \text{and} \quad B(t) \geq B^{\min}.$$

To prove the existence of an optimal control we employ Theorem 4.1 from Fleming & Rishel (1975). Such result states that the the following conditions are sufficient to guarantee the existence of an optimal control solution for (3.4):

$(H1'')$ The right-hand side of the model (3.4b)–(3.4d) is composed of continuous functions, and for each one of these functions f_i there exist positive constants C_1, C_2 such that $|f_i(t, x, u_D)| \leq C_1(1 + |x| + |u_D|)$ and $|f_i(t, \bar{x}, u_D) - f_i(t, x, u_D)| \leq C_2|\bar{x} - x|(1 + |u_D|)$ for all $0 \leq t \leq T$ and $i = 1, 2, 3$.

$(H2'')$ There exists at least one pair $(x(t), u_D(t))$ satisfying both (3.4b)–(3.4d) and (3.4f).

$(H3'')$ The set of admissible controls is closed and convex.

$(H4'')$ The right-hand side of the model is bounded above by a sum of the states and the control, and it can be written as a linear function with respect the control.

$(H5'')$ The integrand of cost functional is convex with respect the control and it is bounded above by $C_3|u_D|^n - C_4$ for some fixed $C_3 > 0$, $C_4 \in \mathbb{R}$ and $n > 1$.

We proceed to show such conditions.

Lemma 1. *The model (3.4) satisfies $(H1'')$.*

Proof It is straightforward since the model functions are of class C^2 in Ω. □

Lemma 2. *There exists at least one pair $(x(t), u_D(t))$ with $u_D \in \mathcal{U}$ such that equation (3.4b)-(3.4d) is satisfied.*

Proof The condition $(H2'')$ is satisfied by the Carathéodory's existence theorem (see Theorem 9.2.1 from (Lukes, 1982)), which guarantees the existence of solutions for Cauchy problems. □

Lemma 3. *The set of admissible controls is closed and convex.*

Proof Since $0 \leq u_D(t) \leq u_D^{\max}$ then the lemma requirements are satisfied. □

Lemma 4. *The right-hand side of (3.4b)-(3.4d) is continuous, also it is bounded from above by a sum of the states and the control, and it can be written as a linear function of the control.*

Proof Let $f(t, x, u_D)$ be the vector function defined by the right-hand side of (3.4b)-(3.4d). As mentioned above, f is continuous on Ω. Now we have to find suitable bounds for the states. Since $0 < C(t) \leq C^{\max}$, $B^{\min} \leq B(t)$ and $0 < T(t) \leq C^{\max}$, where the constants $C^{\max}$, $B^{\min}$ and $C^{\max}$ come from the definition of the domain Ω, then:

$$\begin{aligned}
\frac{dC(t)}{dt} &= \alpha_1 C(t) B(t)^{g_1}(1-u_D) - \beta_1 C(t) + \sigma_1 C(t) T(t) \\
&\leq \alpha_1 C(t) B(t)^{g_1} - \beta_1 C(t) + \sigma_1 C(t) T(t) \\
&\leq \alpha_1 C(t) m_1 - \beta_1 C(t) + \sigma_1 C(t) T(t) \quad (g_1 < 0 \text{ and } m_1 := (B^{\min})^{g_1}) \\
&\leq \alpha_1 C(t) m_1 + \sigma_1 C(t) T(t) \\
&= C(t)(\alpha_1 m_1 + \sigma_1 C^{\max}),
\end{aligned} \tag{3.6}$$

so $dC(t)/dt$ is bounded from above by the linear equation (3.6). Similarly,

$$\frac{dB(t)}{dt} \leq B(t)(\alpha_2 m_2 + \sigma_2 C^{\max}),$$

where $m_2 := (C^{\max})^{g_2}$. Taking into account that: $\sigma_2 \geq 0$ or $\sigma_2 < 0$, then

$$\frac{dB(t)}{dt} \leq \begin{cases} B(t)(\alpha_2 m_2 + \sigma_2 C^{\max}) & \text{if } \sigma_2 \geq 0 \\ B(t)\alpha_2 m_2 & \text{if } \sigma_2 < 0. \end{cases} \tag{3.7}$$

Hence, $B(t)$ is also bounded from above by a linear equation. Analogous to $C(t)$ and $B(t)$ and considering that $\sigma_4 \leq 0$, we have

$$\frac{dT(t)}{dt} \leq T(t)\left(\alpha_3 - \beta_3 + \sigma_3 m_2\right). \tag{3.8}$$

From inequalities (3.6)-(3.8), we know that the model is bounded from above by a linear system. Thus, the solutions are bounded for a finite final time. Observe that there are two cases given by the sign of σ_2. These inequalities, together with the triangle inequality, also give:

$$\begin{aligned}
&|f(t, x, u_D)| \\
&= \left| \left(\frac{dC}{dt}, \frac{dB}{dt}, \frac{dT}{dt} \right)^{\intercal} \right| \\
&= \left| \begin{pmatrix} \alpha_1 m_1 + \sigma_1 C^{\max} & 0 & 0 \\ 0 & \alpha_2 m_2 + \sigma_2 C^{\max} & 0 \\ 0 & 0 & \alpha_3 - \beta_3 + \sigma_3 m_2 \end{pmatrix} \begin{pmatrix} C \\ B \\ T \end{pmatrix} \right| + \left| \begin{pmatrix} \alpha_1 C^{\max} m_2 \\ 0 \\ 0 \end{pmatrix} u_D \right|
\end{aligned}$$

$$\leq C_1(|x|+|u_D|), \tag{3.9}$$

where C_1 depends on the model parameters and the bounds of its solutions. The case for $\sigma_2 < 0$ is analogous. □

Lemma 5. *The integrand from (3.4a) is convex in the control, and it is bounded from above by $C_3|u_D|^n - C_4$ with $C_3 > 0$ and $n > 1$.*

Proof The integrand $L(t, x, u_D) = T(t)^2 + w_D u_D^2$ is convex respect u_D, and also

$$L(t, x, u_D) = T(t)^2 + w_D u_D^2 \geq w_D u_D^2 = C_3|u_D|^n, \tag{3.10}$$

with $C_3 = w_D > 0$ and $n = 2 > 1$. □

The above discussion allows us to state the following result:

Theorem 3.1. *The denosumab treatment model (3.4), considering the domain Ω, has an optimal control u_D^*.* □

3.3.2 Optimality system

Under Assumption A or Assumption B, we have proved the existence of at least one optimal control. Here, we use Pontryagin's Maximum Principle (Pontryagin et al., 1962; Lenhart & Workman, 2007) to derive necessary conditions that every optimal control satisfies. Let H be the Hamiltonian defined by

$$\begin{aligned} H = &\left(\alpha_1 C(t) B(t)^{g_1} \left(1 - u_D(t)\right) - \beta_1 C(t) + \sigma_1 C(t) T(t)\right) \lambda_1(t) \\ &+ \left(\alpha_2 C(t)^{g_2} B(t) - \beta_2 B(t) + \sigma_2 B(t) T(t)\right) \lambda_2(t) \\ &+ \left(\alpha_3 T(t) \left(1 - \frac{T(t)}{m}\right) - \beta_3 T(t) + \sigma_3 C(t)^{g_2} T(t)\right) \lambda_3(t) \\ &+ T(t)^2 + w_D u_D(t)^2. \end{aligned} \tag{3.11}$$

From (3.11) we get the following adjoint system for denosumab model (3.4):

$$\frac{d\lambda_1}{dt} = -\lambda_1 \left(\alpha_1 B^{g_1} \left(1 - u_D\right) - \beta_1 + \sigma_1 T\right) - \lambda_2 \left(\alpha_2 g_2 C^{g_2 - 1} B\right) - \lambda_3 \left(\sigma_3 g_2 C^{g_2 - 1} T\right), \tag{3.12a}$$

$$\frac{d\lambda_2}{dt} = -\lambda_1 \left(\alpha_1 g_1 C B^{g_1 - 1} \left(1 - u_D\right)\right) - \lambda_2 \left(\alpha_2 C^{g_2} - \beta_2 + \sigma_2 T\right), \tag{3.12b}$$

$$\frac{d\lambda_3}{dt} = -\lambda_1 \sigma_1 C - \lambda_2 \sigma_2 B - \lambda_3 \left(\alpha_3 \left(1 - \frac{2T}{m}\right) - \beta_3 + \sigma_3 C^{g_2}\right) - 2T, \tag{3.12c}$$

$$\lambda_1(t_f) = \lambda_2(t_f) = \lambda_3(t_f) = 0. \tag{3.12d}$$

The optimality condition for (3.4), obtained also by means of the Pontryagin's Maximum Principle, is the following:

$$u_D^*(t) = \max\left\{0, \min\left\{1, \frac{\alpha_1 C(t) B(t)^{g_1} \lambda_1(t)}{2 w_D}\right\}\right\}, \tag{3.13}$$

which is the characterization of every optimal solution u_D^* for (3.4) in terms of the state variables, the adjoint variables and the parameters of the model. A direct use of the Maximum Principle gives us:

Theorem 3.2. *Let u_D^* be an optimal control for the denosumab model (3.4) and $x = (C, B, T)$ its associated state-variable. Then there exist functions $\lambda_1(t)$, $\lambda_2(t)$ and $\lambda_3(t)$ that satisfy the adjoint system (3.12). Also, the optimal control u_D^* satisfies the optimality condition (3.13).* □

3.3.3 Uniqueness of optimal solutions

In order to prove the uniqueness of an optimal control problem, we follow the steps proposed in Fister et al. (1998) and state the next theorem:

Theorem 3.3. *There exists a final time t_f such that the model (3.4) has a unique optimal control solution.*

Proof See Appendix B. □

3.4 Optimal solution for the radiotherapy model

Besides the denosumab treatment, we also explore the radiotherapy effects on the dynamics of the bone metastasis model. In this Section, we give the optimality system and discuss the existence and uniqueness of the optimal control for the radiotherapy model (3.5).

3.4.1 Existence of optimal solutions

The five lemmas for the existence of solutions of the denosumab model are proved in the same way for the radiotherapy treatment model since they have a similar structure: an *a priori* bounded domain, a bounded control u_R, and the model is linear respect to u_R. Thus, similar algebraic manipulations give the existence of solutions for the radiotherapy model.

3.4.2 Optimality system

Analogously as in the denosumab model, using the Maximum Principle we obtain the following optimality system for the radiotherapy model (3.5):

$$\frac{dC}{dt} = \alpha_1 C B^{g_1} - (\beta_1 + \psi_1 u_R^*)C + \sigma_1 CT, \tag{3.14a}$$

$$\frac{dB}{dt} = \alpha_2 C^{g_2} B - (\beta_2 + \psi_2 u_R^*)B + \sigma_2 BT, \tag{3.14b}$$

$$\frac{dT}{dt} = \alpha_3 T\left(1 - \frac{T}{m}\right) - (\beta_3 + u_R^*)T + \sigma_3 C^{g_2} T + \sigma_4 B^{g_1} T, \tag{3.14c}$$

$$\frac{d\lambda_1}{dt} = -\alpha_2 g_2 \lambda_2 C^{g_2-1} B - \sigma_3 g_2 \lambda_3 C^{g_2-1} T - (\alpha_1 B^{g_1} + \sigma_1 T - \beta_1 - \psi_1 u_R^*)\,\lambda_1, \tag{3.14d}$$

$$\frac{d\lambda_2}{dt} = -\alpha_1 g_1 \lambda_1 C B^{g_1-1} - \sigma_4 g_1 \lambda_3 B^{g_1-1} T - (\alpha_2 C^{g_2} + \sigma_2 T - \beta_2 - \psi_2 u_R^*)\lambda_2, \tag{3.14e}$$

$$\begin{aligned}\frac{d\lambda_3}{dt} = &-\sigma_1 \lambda_1 C - \sigma_2 \lambda_2 B - \left(\sigma_3 C(t)^{g_2} + \sigma_4 B^{g_1} - \alpha_3\left(\frac{T}{m} - 1\right)\right.\\ &\left. -\beta_3 - u_R^* - \frac{\alpha_3 T}{m}\right)\lambda_3 - 2T,\end{aligned}$$

$$C(0), B(0), T(0) \quad \text{given}, \tag{3.14f}$$

$$\lambda_1(t_f) = \lambda_2(t_f) = \lambda_3(t_f) = 0, \tag{3.14g}$$

$$u_R^*(t) = \max\left\{0, \min\left\{1, \frac{\psi_1 C(t)\lambda_1(t) + \psi_2 B(t)\lambda_2(t) + T(t)\lambda_3(t)}{2w_R}\right\}\right\}. \tag{3.14h}$$

3.4.3 Uniqueness of optimal solutions

The uniqueness of optimal solutions for the radiotherapy model is analogous to the denosumab case since changes in the model (ODEs, cost functional or control restrictions) produce a similar effect in the optimality system (adjoint system and optimality condition).

3.5 Numerical results and discussion

The existence and uniqueness of solutions guarantee that a convergent numerical method will get the approximation to the unique optimal solution. Taking advantage of that, here we use the forward-backward sweep method (FBSM) (Lenhart & Workman, 2007). This numerical scheme is based upon the iterative use of the Maximum Principle. Considering the optimal control problem for the denosumab model (3.4) together with its adjoint system (3.12) and the optimality condition (3.13), the steps involved in the FBSM are the following:

Forward-Backward Sweep Method

1. Propose an initial control $u_D^0(t)$.
2. Solve forward in time the state variable system (3.4).
3. Solve backward in time the adjoint system (3.12).
4. Use the Maximum Principle to get a new control update u_D^k for step k. Here, we consider (Lenhart & Workman, 2007):

$$u_D^k(t) \hookleftarrow \mu u_D^k(t) + (1-\mu)u_D^{k-1}(t).$$

   If a convergence criteria is met, e.g., the control update is close to previous control, then STOP; else, return to STEP 2.

For solving the forward and backward ODEs, we used a fourth order Runge-Kutta scheme with a variable time step. Let us point out that the problem about the convergence of the FBSM is discussed in (McAsey et al., 2012). In that work, the authors prove results about the convergence of the FBSM, and the main hypotheses required to guarantee such convergence are Lipschitz conditions, an appropriate length for the integration interval and boundedness of the adjoint system. Some of these conditions, in particular the last one, are difficult to satisfy *a priori* because of the non-linearities of the treatment models.

To achieve convergence, here we set the maximum value of the control u_D to $u_D^{\max} = 0.6$ instead of using $u_D^{\max} = 1$. From a modeling perspective, this means that we assume that the treatment does not have a complete effectiveness. An example of this approach, used in a different problem, can be found in (Stephenson et al., 2017). Also, we initialized the

control u^0 for the FBSM as $u^0 \equiv u_D^{\max}$. We have convergence of the simulations when μ takes values within the interval $0.15 \leq \mu \leq 0.6$.

3.5.1 Parameters for numerical simulations

After exploring numerous combinations for the parameter values, and in an effort to agree with experimental data (Komarova et al., 2003; Farhat et al., 2017; Araujo et al., 2014), we considered a fixed set of values for certain parameters depicted in Table 3.1 for models (3.4) and (3.5). Next, we discuss their selection:

- Initial condition $(C(0), B(0), T(0))$: We chose the initial conditions $C(0) = 4 \times 10^{-6}$, $B(0) = 4$ and $T(0) = 1000$ according with Section 1.1.2. In particular, these initial conditions allow the system to begin close to the periodic solution.

- The net effectiveness parameters g_1 and g_2: We preserved OBs-induced inhibition on OCs by taking $g_1 = -0.3$ as in Section 1.1.2. However, in this Chapter we increased g_2 from 0.5 (Chapter 2) to 0.7 in order to have a more active remodeling process, that is, larger amplitudes and shorter periods for the OCs and OBs solutions without cancer.

- The cell activity parameters α_1 and α_2: By fixing values of g_1 and g_2 we estimated through trial and error these parameters to obtain standard numbers of OCs and OBs with and without cancer.

- The elimination rates β_1 and β_2: They are proposed as in Komarova et al. (2003).

- Coefficients for CCs: The elimination rate β_3 is considered zero since we include its effect in α_3, having a net production rate for CCs. For the production rate of CCs, α_3, we take a realistic interval based on Ayati et al. (2010); Farhat et al. (2017). We estimated a normal carrying capacity for the CCs, m, using Farhat et al. (2017) .

- Rates of the OCs–CCs and OBs–CCs interactions σ_i $(i = 1, ..., 4)$: They are difficult to estimate *a priori* since we do not have experimental data. So, a trial and error parameter space exploration was made. Election criteria for their values took into consideration the cancer-invasion equilibrium value (3.2) together with its stability conditions (3.3),

Parameter	Value	Description	Reference
g_1 $(dimensionless)$	-0.3	net paracrine effectiveness on OCs	Chapter 2
g_2 $(dimensionless)$	0.7	net paracrine effectiveness on OBs	Assumed
α_1 $(cell^{-1}day^{-1})$	0.5	activity on OCs production	Assumed
α_2 $(cell^{-1}day^{-1})$	0.05	activity on OBs production	Assumed
β_1 (day^{-1})	0.2	OCs removal rate	Komarova et al. (2003)
β_2 (day^{-1})	0.02	OBs removal rate	Komarova et al. (2003)
β_3 (day^{-1})	0	elimination rate of CCs	Assumed
σ_2 $(cell^{-1}day^{-1})$	0	rate of OBs production by cancer	Assumed
m $(cell)$	10^4	CCs carrying capacity	Farhat et al. (2017)
ψ_1, ψ_2 $(dimensionless)$	1	effect of radiation on OCs and OBs	Assumed
$u_D^{\max}$ $(dimensionless)$	0.6	Denosumab max. effectivity	Assumed
$u_R^{\max}$ (day^{-1})	0.05	Radiotherapy max. elimination rate	Assumed

Table 3.1: Fixed global parameter values, see Subsection 3.5.1 for discussion.

Parameter	*Scenario 1*	*Scenario 2*	*Scenario 3*
α_3 (day^{-1})	1.5×10^{-2}	1×10^{-4}	1×10^{-4}
σ_1 $(cell^{-1}day^{-1})$	1×10^{-6}	1×10^{-6}	0.0
σ_3 $(cell^{-1}day^{-1})$	1×10^{-3}	1×10^{-3}	1×10^{-8}
σ_4 $(cell^{-1}day^{-1})$	0.0	0.0	-1×10^{-4}

Table 3.2: Parameters for three different scenarios of the metastatic invasion.

see Fig. 3.4. Values for these parameters were discarded when erratic numbers of OCs or OBs were presented.

- The radiotherapy control parameters ψ_j $(j = 1, 2)$: They are equal to 1 as a first approach. This selection arises from the observation that other values do not change the qualitative behavior of the optimal solutions in our parameter space exploration.

To complement these fixed parameters, we varied the values for α_3, σ_1, σ_3 and σ_4 and obtained three metastatic invasion scenarios; their values are condensed in Table 3.2. These three scenarios are of biological relevance because they are associated with different dynamics of invasion which may be presented in different physiological settings (Mundy, 2002; Ottewell, 2016).

3.5.2 Denosumab treatment

As mentioned before, the function of denosumab is to inhibit osteoclasts activation through RANK-RANKL bindings. Since it is only a palliative treatment, it is expected that only osteoclasts-dependent bone metastatic invasions are heavily affected by means of denosumab administration. This is a palliative treatment because it is intended to slow down bone metastatic progression by reducing RANKL-induced fueling on the vicious cycle.

Scenario 1: Aggressive metastasis

In this case, the proliferation of CCs is rapid and so this scenario represents an aggressive type of bone metastasis tumor. It may be noted that we are considering in this case that OBs do not affect directly the CCs dynamics ($\sigma_4 = 0$). Recall that u_D affects parameter α_1, which is the activity on OCs production rate, or the recruitment/differentiation rate. In Fig. 3.4, we show that the cancer-invasion steady-state is unstable for all relevant values of constant treatment effectivity u_D. Also, it can be noted that the cancer-coordinate does not change its value in this range. That means that the steady-state is not changed in this coordinate albeit a treatment is applied. Because of the oscillations, it is not straightforward to predict the evolution of the cellular dynamics under treatment.

In Fig. 3.5, it can be noted that the optimal treatment obtained is an aggressive one: the maximum amount of effectivity ($u_{\max}$) is maintained during almost all the time range, and then is suspended abruptly. Also, we observe that OCs waves appear at the same time but they present lower amplitudes when the effectivity increases. Due to the cross-regulation between bone cell populations, this will also cause the same effect on the OBs wave. However, CCs are indifferent to the decrease of OCs and OBs. We assume

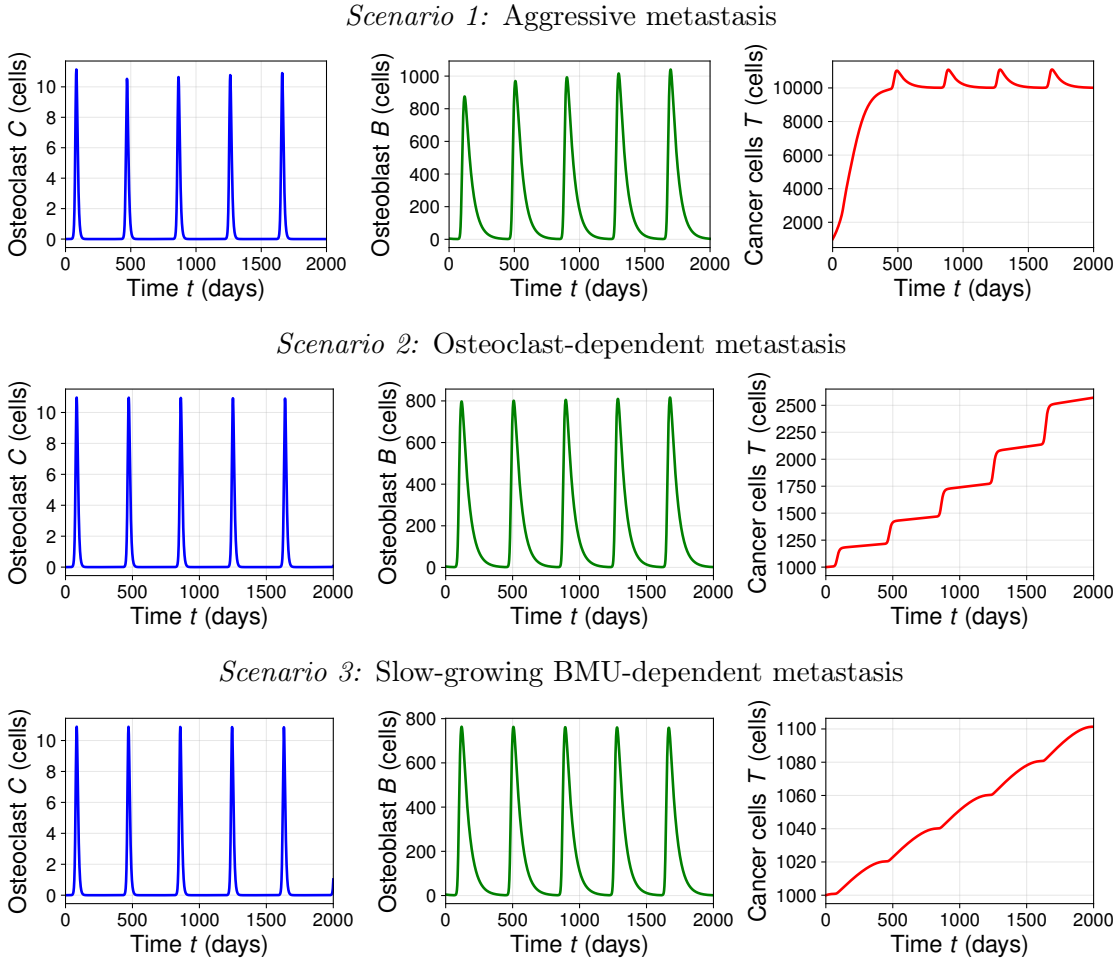

Figure 3.3: Baseline uncontrolled scenarios considered in this Chapter.

that the proliferation α_3 is high enough to pull the dynamics of CCs away from the bone resorption contribution σ_1. Thus, this scenario presents a metastatic tumor that does not rely completely on the BMU dynamics. As such, the treatment shows to be ineffective, which is clinically observed on advanced aggressive bone metastatic patients (Coelho et al., 2016).

Scenario 2: Osteoclasts-dependent metastasis

In this case, the metastatic tumor has a noticeable change when the OCs waves are reduced. In Fig. 3.4 there is a similar bifurcation diagram as in scenario 1: stability and value of the cancer coordinate do not change with variations of u_D as a constant parameter.

It can be noted in Fig. 3.6, that the optimal solution obtained has a maximum amplitude (having a value around 0.6) almost the half of the value of $u_{\max}$; also, its shape is similar to the one of the OCs wave. The treatment applied causes the OCs wave to diminish in amplitude but preserves its appearance in time. The effect of this is also a smaller amplitude on the OBs wave. By contrast from the first case, the CCs population has a visible effect (reduction of 5% compared with the non-treatment case). This is a metastatic invasion that depends more on the BMU dynamics than the previous scenario.

The parameters election for this scenario suggests that the tumor depends on the OCs dynamics rather than on the OBs evolution ($\sigma_3 > 0$ and $\sigma_4 = 0$). In this case, treatment regimes show to be more effective than the previous scenario; this is due to the OCs-activity dependence of the CCs proliferation.

Scenario 3: Slow, BMU-dependent metastasis

In Fig. 3.4 a different bifurcation diagram is present for scenario 3. The steady-state branch now goes to zero when the parameter u_D increases. This suggests that a strong inhibition over the OCs activation would lead the CCs population to be eradicated.

In Fig. 3.7, however, the optimal solution obtained is to apply the treatment almost to the lowest levels. The amplitudes of the OCs and OBs waves decrease by a small amount and the CCs burden maintains nearly to the same quantity. This simulation suggests that, in this scenario, the optimal strategy is to not apply treatment for the weight parameters chosen. In other words, in terms of the cost functional J, the number of CCs prevented by

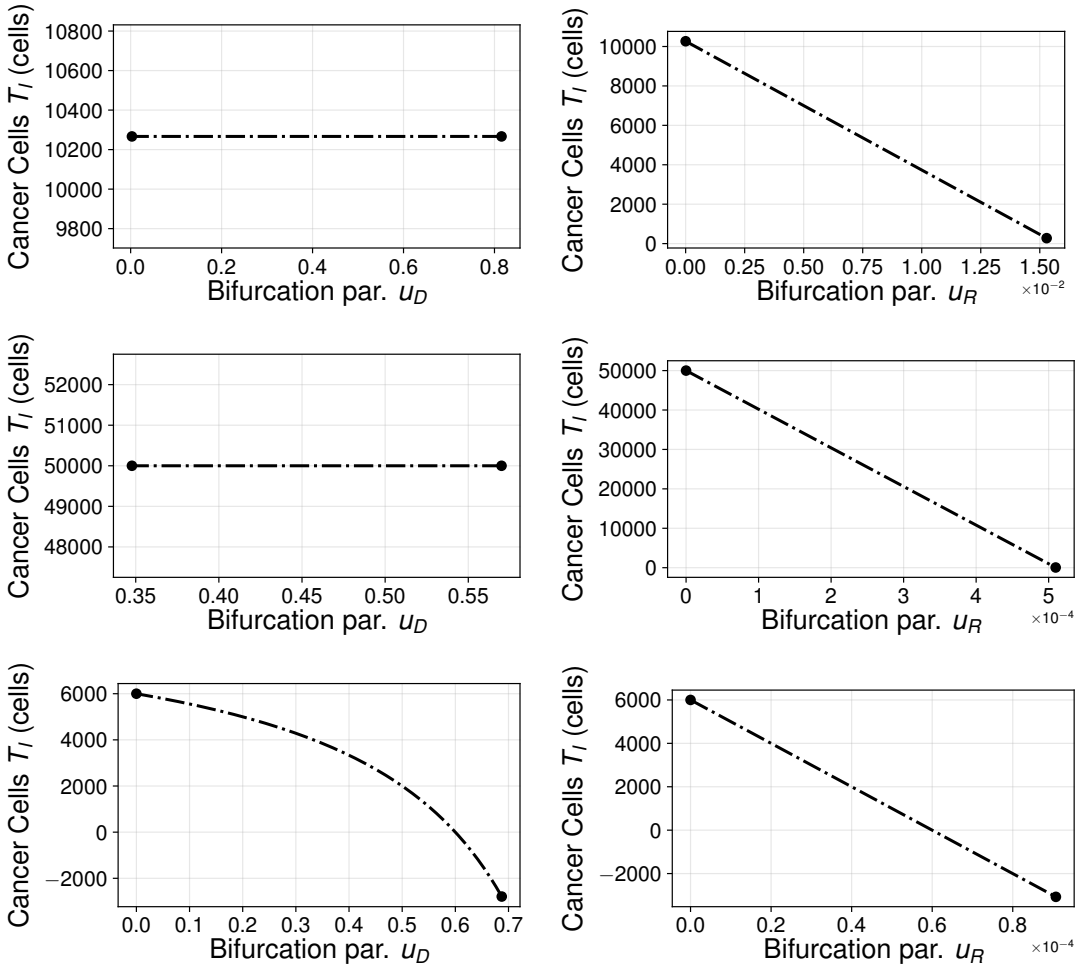

Figure 3.4: Bifurcation diagrams corresponding to Scenarios 1–3. Dash-dot linestyle represents oscillations. **Left.** Denosumab treatment model with bifurcation parameter u_D. **Right.** Radiotherapy model with bifurcation parameter u_R.

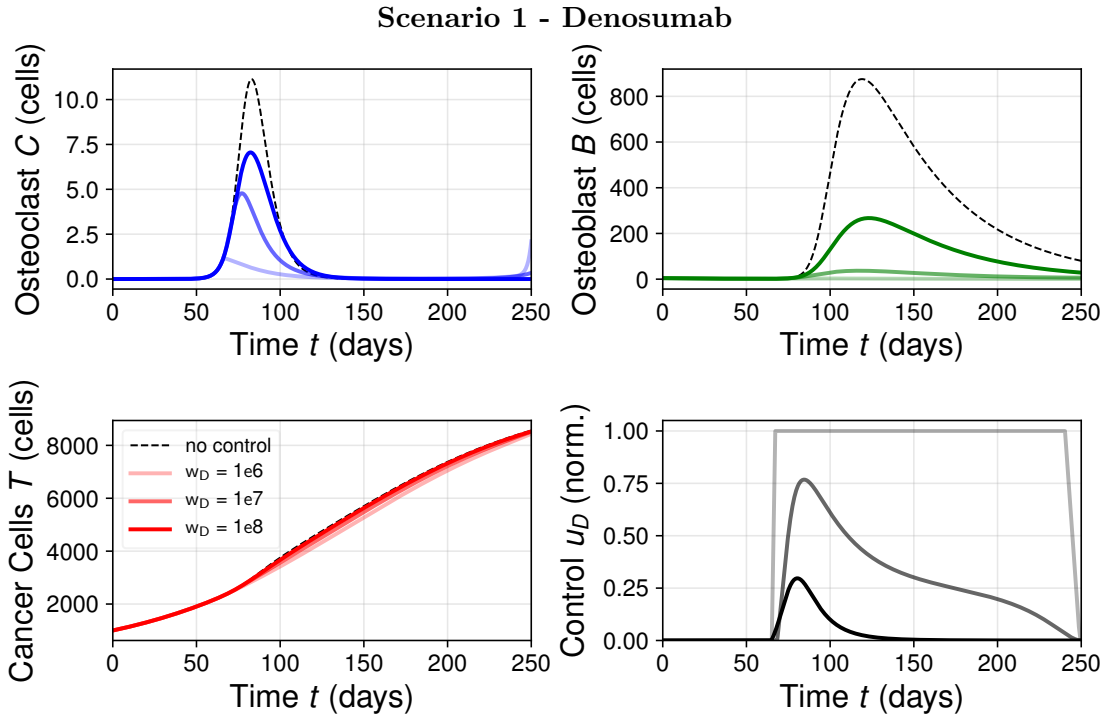

Figure 3.5: Scenario 1 for denosumab treatment model for three different cost weight values. Note that the control is normalized with respect to its possible maximum value $u_D^{\max} = 0.6$.

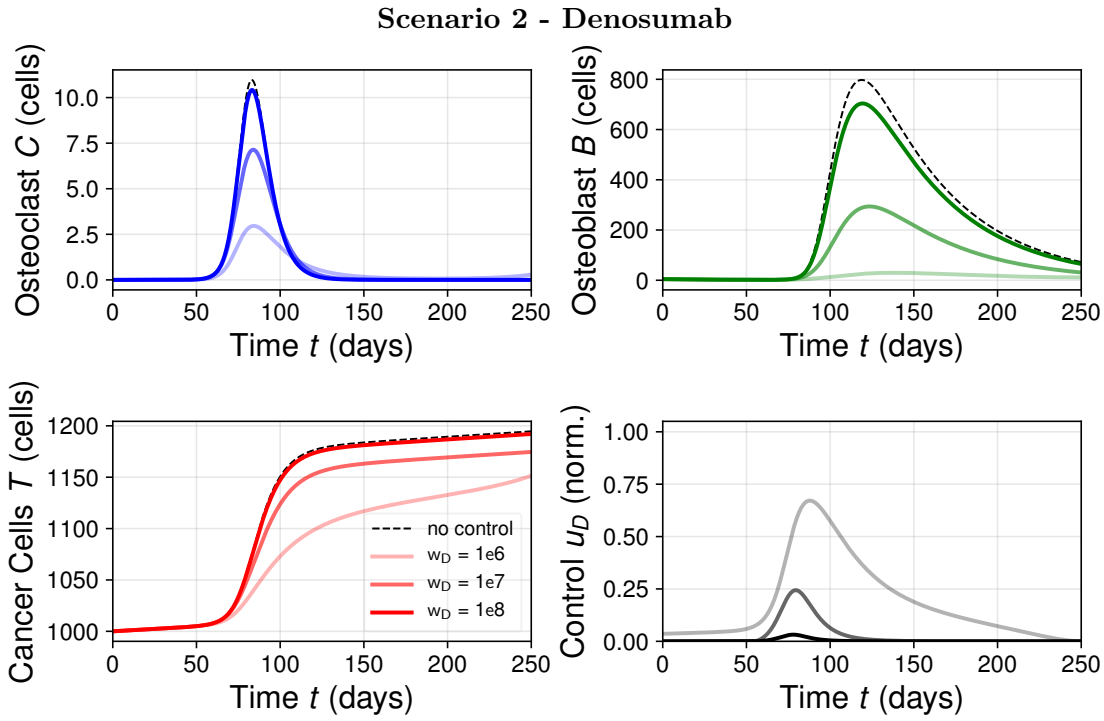

Figure 3.6: Scenario 2 for denosumab treatment model. Note that the control is normalized with respect to its possible maximum value $u_D^{\max} = 0.6$.

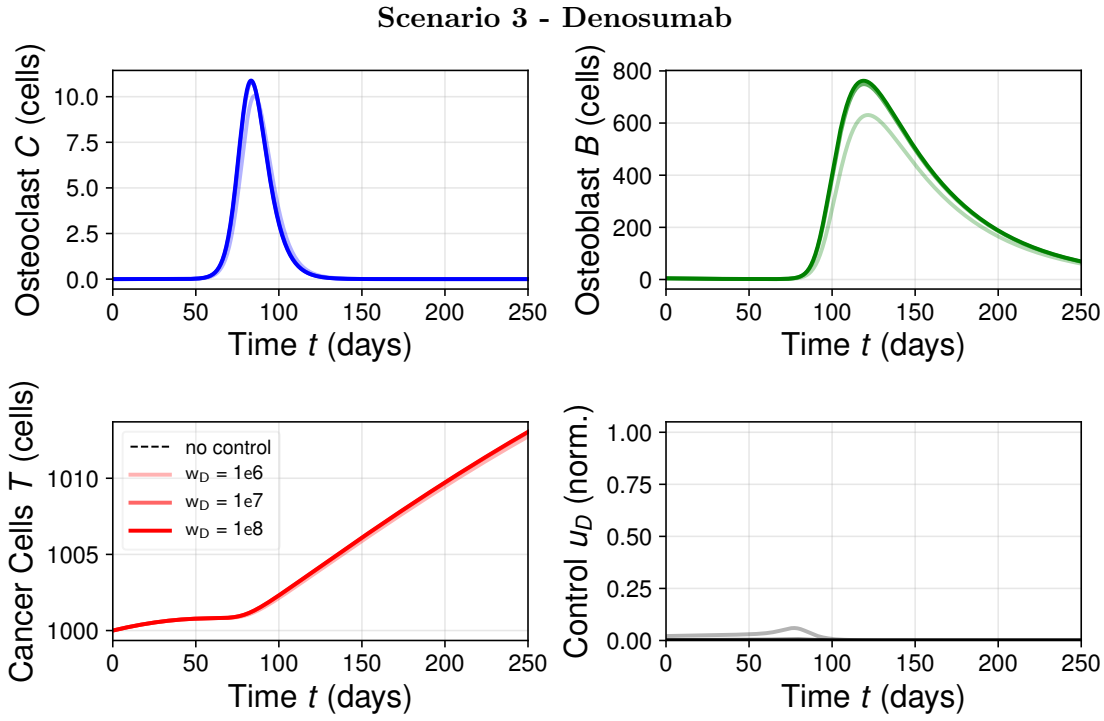

Figure 3.7: Scenario 3 for denosumab treatment model. Note that the control is normalized with respect to its possible maximum value $u_D^{\max} = 0.6$.

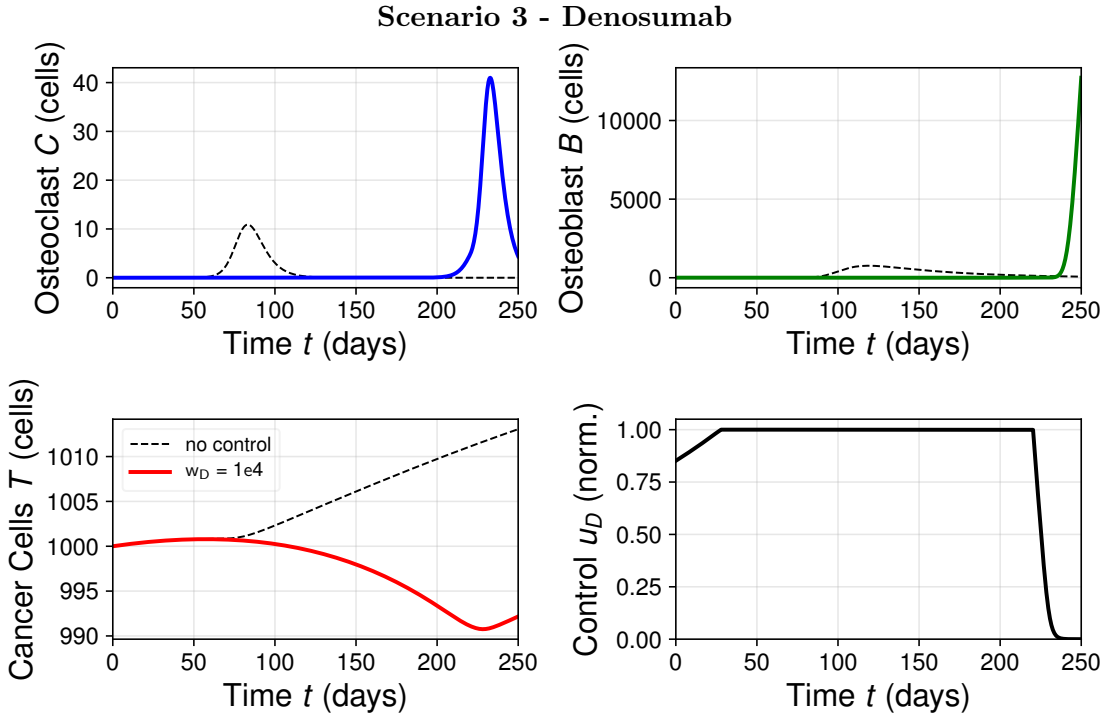

Figure 3.8: Scenario 3 for denosumab treatment. The cost parameter is changed to $w_D = 1 \times 10^4$. Note that the control is normalized with respect to its possible maximum value $u_D^{\max} = 0.6$.

the treatment does not compensate with the cost of the treatment: it is more expensive the treatment than the desired result. Note that, however, it is predicted from the optimality system that if the value of w_D is lowered then the optimal solution would take into account a stronger inhibition on OCs.

We tested such hypothesis by changing the value of w_D to 1×10^4. The results of the simulation are shown in Fig. 3.8. The inhibition of OCs activation lasts longer and the metastatic burden decreases more than with the previous values of w_D. Yet, the OCs wave appearance delays considerably due to the inhibition applied by the treatment and so the amplitude of the OCs wave increases considerably (3-fold the usual). Thus, the OBs wave also increases to drastic levels compared to the untreated case. Both abnormal waves have a positive effect on the metastatic tumor at the end of the treatment. Here, we note that it may be interesting to study how the secondary effects of a treatment may impact the appearance and the amplitude of the OCs and OBs waves.

3.5.3 Radiotherapy treatment

We adapted the FBSM to find approximations of optimal solutions also for the radiotherapy model (3.14a). For this model convergence of the method was less sensitive than the denosumab treatment model. In Figs. 3.9-3.11 are shown the same three scenarios given by Tables 3.1 and 3.2 but using the radiotherapy treatment model (3.14a).

Scenario 1: Aggressive metastasis

In the first scenario, in Fig. 3.9), there are two optimal solutions that are aggressive (maximum radiation effectivity present). The effects on the OCs and OBs populations are similar under the three treatment regimes. The CCs population decreases its proliferation rate considerably but maintains a prevalent level. It can be noticed that during the OCs wave activation there is a slight increase in the CCs population.

Scenario 2: Osteoclasts-dependent metastasis

In the second scenario, Fig. 3.10, only one treatment regimen reaches the maximum value $u_R^{\max} = 0.05$. The difference in the effects of applying the treatment is more noticeable than in the first scenario. But, as in the previous one, OCs and OBs populations do not change much. It is interesting to observe that under the first two treatments (with $w_R = 1 \times 10^9$ and $w_R = 1 \times 10^{10}$) the CCs population shows a slight increase during the remodeling wave activation; in these two regimes the CCs population drops down to lower levels.

Scenario 3: Slow, BMU-dependent metastasis

The third scenario, Fig. 3.11, is rather similar to the second one. The main difference is that, in this case, the CCs population does not show a significant increase during activation of OCs and OBs waves.

3.5.4 Summary of numerical simulations

In this Section, we explored three scenarios corresponding to different responses of the bone metastatic tumor to the microenvironment: an aggressive tumor, a tumor that relies

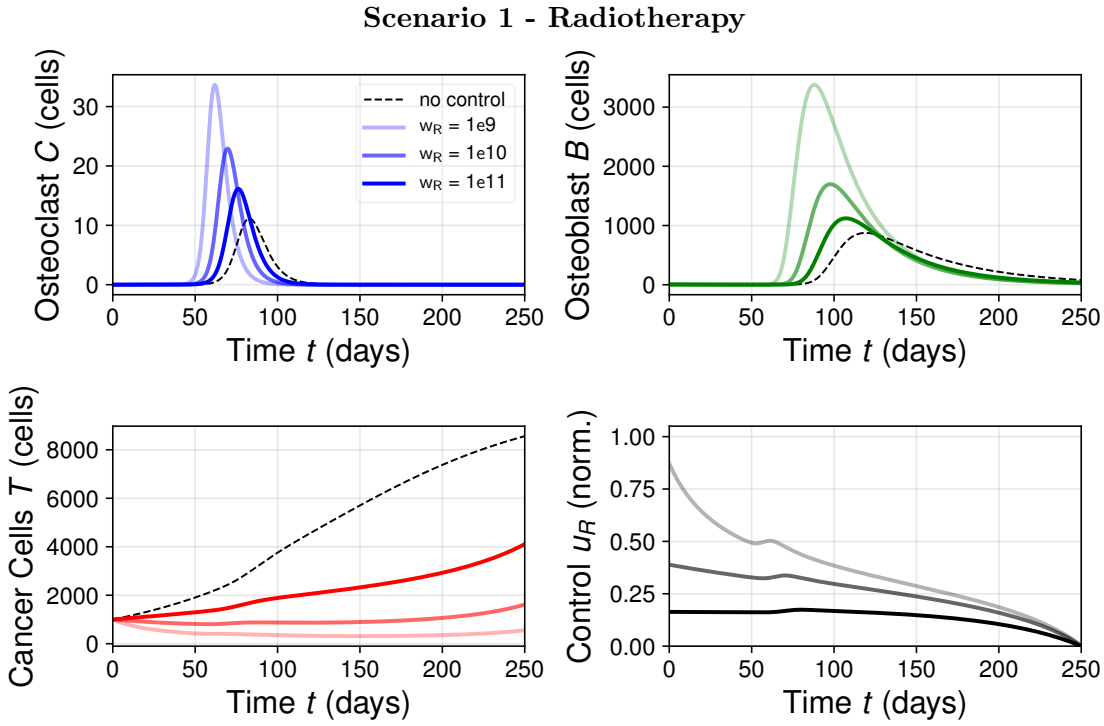

Figure 3.9: Scenario 1 for radiotherapy treatment model for three different cost weight values. Note that control is normalized with respect to its possible maximum value $u_R^{\max} = 0.05$.

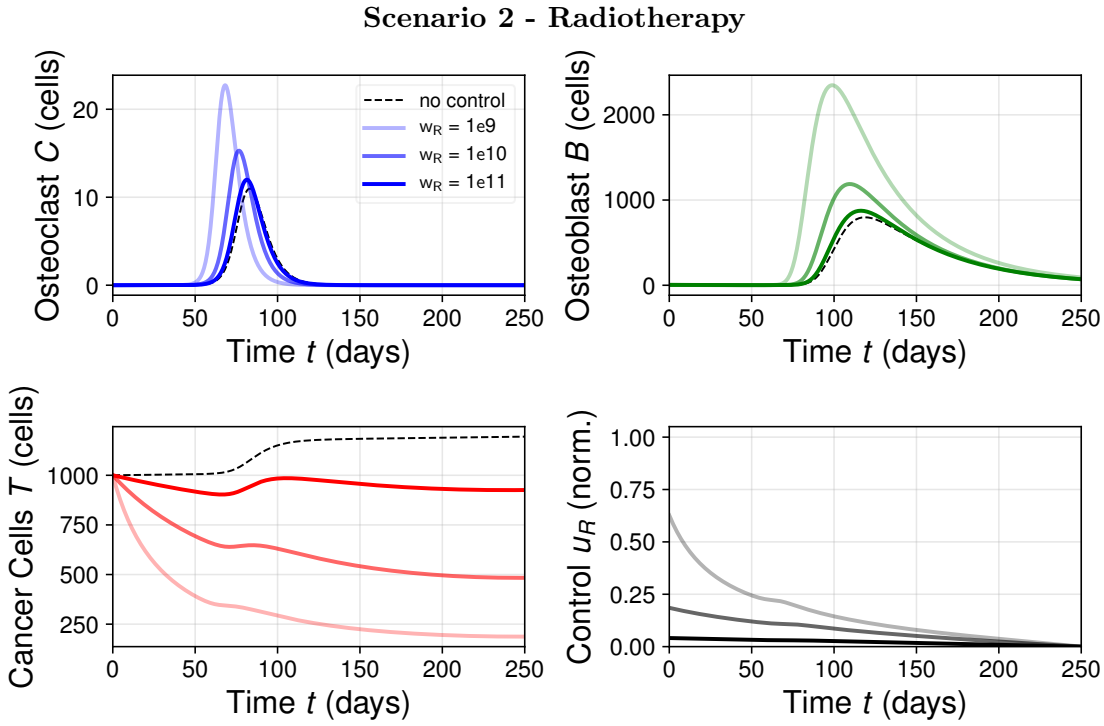

Figure 3.10: Scenario 2 for radiotherapy treatment model. Note that control is normalized with respect to its possible maximum value $u_R^{\max} = 0.05$.

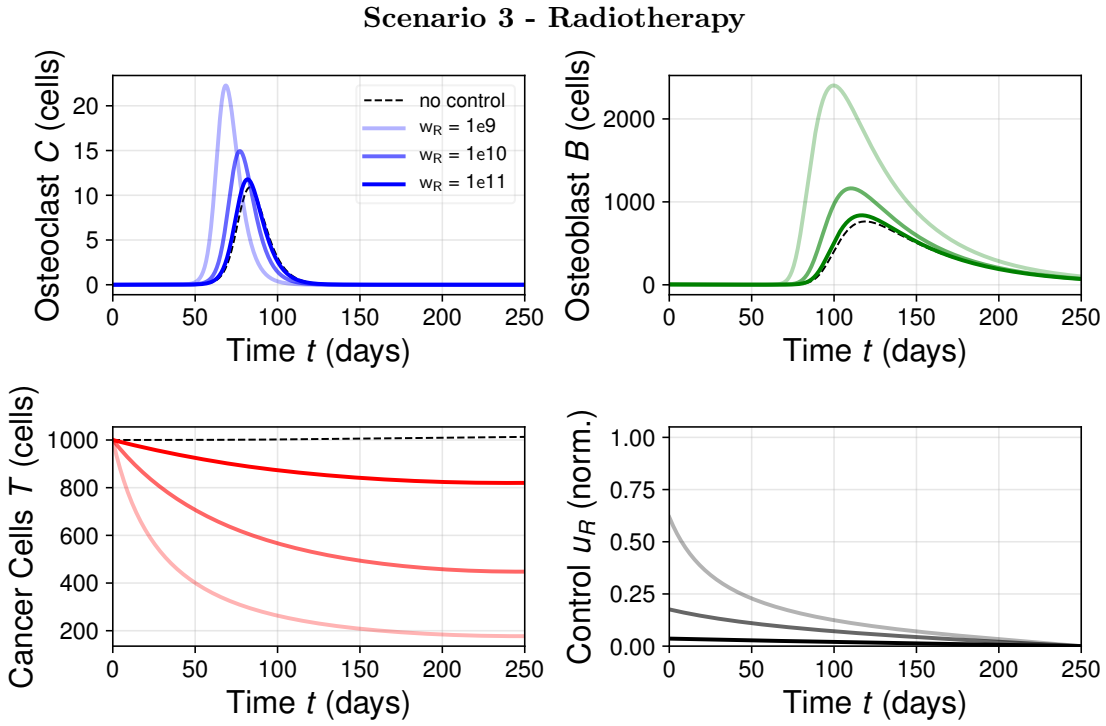

Figure 3.11: Scenario 3 for radiotherapy treatment model. Note that control is normalized with respect to its possible maximum value $u_R^{\max} = 0.05$.

on bone resorption, and a tumor that depends on both bone cell populations.

By bifurcation diagram from Fig. 3.4, we could predict that, for the particular values of the model parameters, the denosumab treatment is only effective in the third scenario, which is the BMU dependent tumor. And even so, when the weight parameter w_D is large enough then a stronger denosumab treatment is more expensive even if it has the ability to reduce the tumor size. The simulations from Figs. 3.5–3.8 reflect some possible outputs for the cellular dynamics changes under a denosumab treatment that seeks to minimize economic cost and side-effects.

Similarly, the radiotherapy model was numerically explored in Figs. 3.9–3.11. In contrast to the denosumab treatment model, the bifurcation diagram reveals that radiation has a high potential to bring down the tumor at equilibrium. Another difference in comparison to the denosumab treatment model is that for the radiotherapy model we assumed that radiation also alters the elimination rates of the bone cells. The numerical simulations show interesting cellular dynamics.

Even though that in appearance the radiotherapy shows a better performance in reducing the bone metastasis tumor that the denosumab treatment, it is important to point out that in the numerical simulations radiation has weight parameters that surpass by at least three orders of magnitude the ones assigned for the denosumab treatment. This implies that radiation was assigned a higher cost in terms of economical cost and also from the point of view of the side-effects. Increasing the weight parameters for radiation would translate in affecting less the growth of the tumor.

3.6 Mixed therapies

From the previous Sections, we can see that denosumab timing is really important and that despite reducing osteoclast activation for certain time the next remodeling wave may be higher than normal. On the other hand, radiotherapy treatments reduce significantly tumor burden but bone cells may also present an undesirable increase on the bone cell populations. In this Thesis, we further explore the question about how the mixed therapy of denosumab and radiotherapy perform together. The corresponding mixed therapy model and its associated optimality system are readily obtained by incorporating the corresponding individual terms from denosumab and radiotherapy models presented before.

For the mixed therapy model, we also explored the same three metastatic Scenarios. We gathered our results in Figures 3.12, 3.13, 3.14 and 3.15. In Figures 3.12 (Scenario 1) and 3.13 (Scenario 2) we observe a synergistic effect between denosumab and radiotherapy: tumor burden is significantly reduced while maintaining bone cell populations under control. We also observe this in Figure 3.14 (Scenario 3), but as with the denosumab model we note that denosumab is barely activated. Similar as we did with the denosumab model, we decreased the weight parameter associated with the usage of denosumab, obtaining Figure 3.15. Usage of denosumab causes increased activation of osteoclasts and osteoblasts, but it is still a more controlled increase in comparison to the denosumab model.

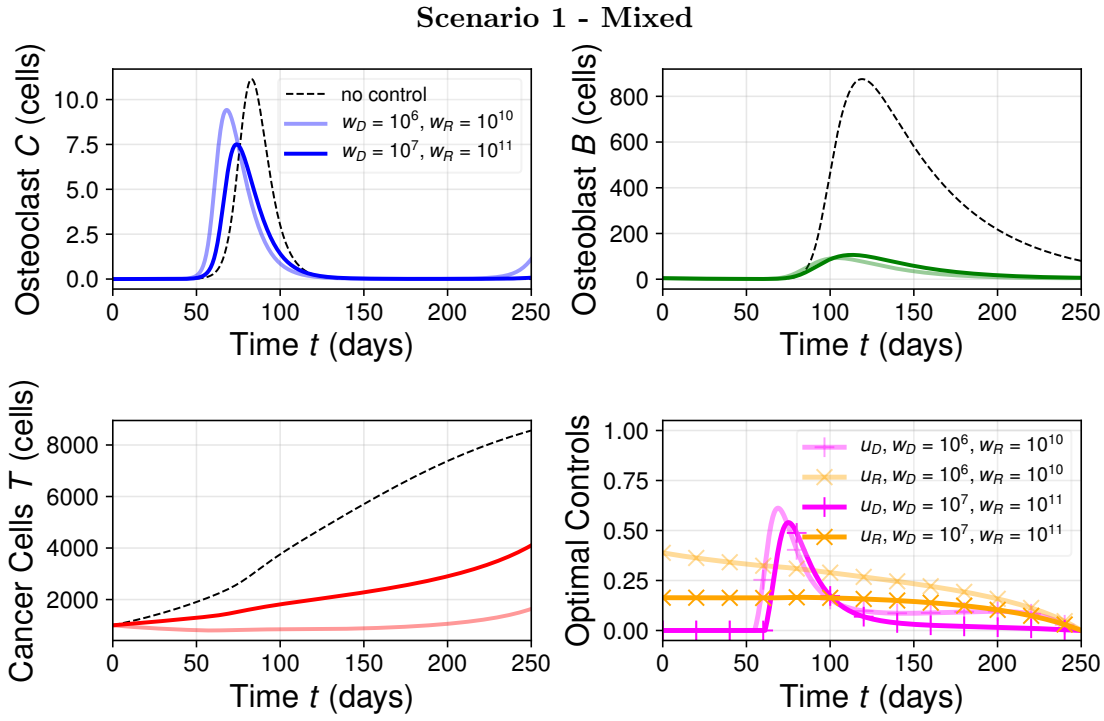

Figure 3.12: Scenario 1 for mixed treatment model.

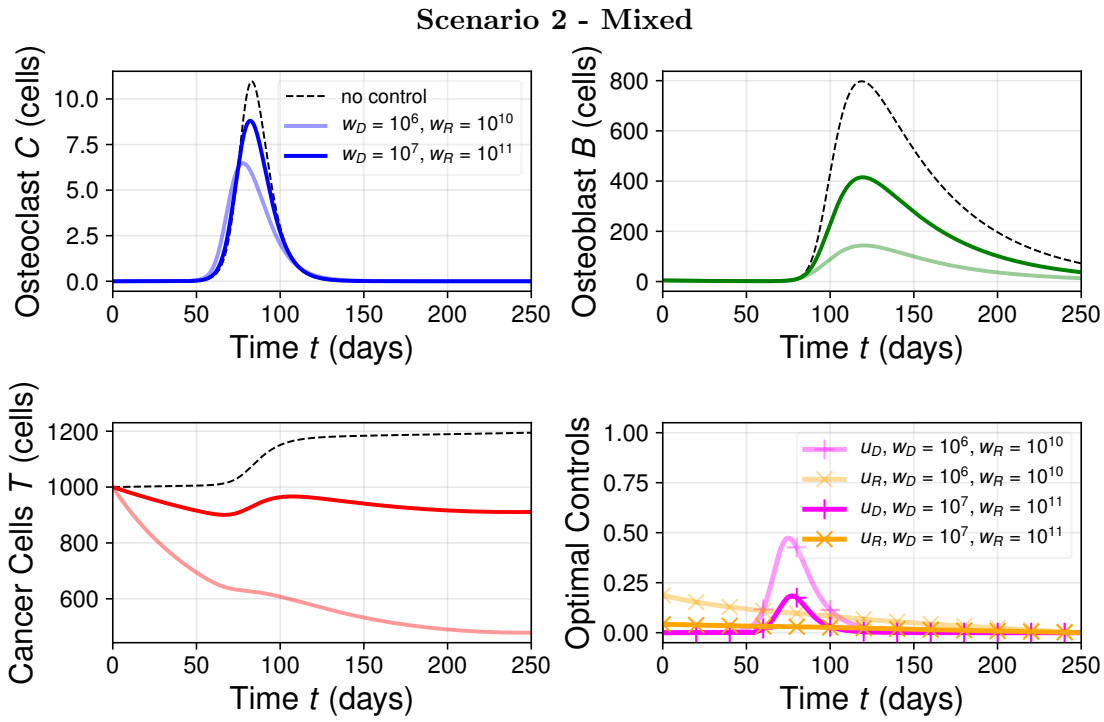

Figure 3.13: Scenario 2 for mixed treatment model.

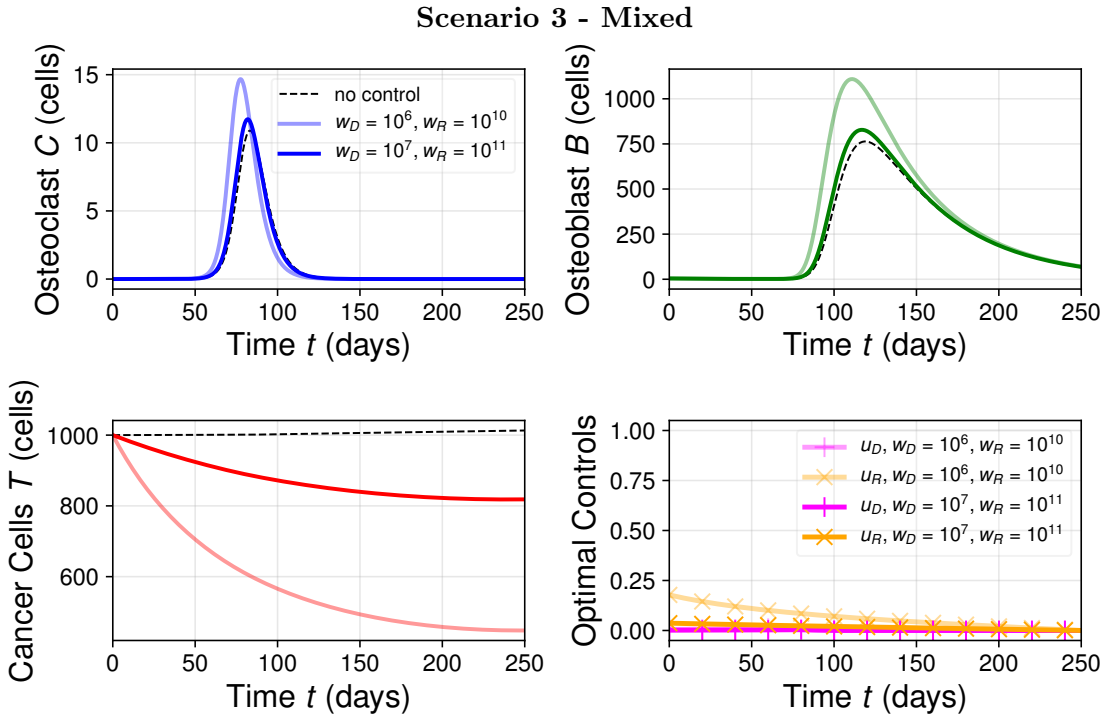

Figure 3.14: Scenario 3 for mixed treatment model.

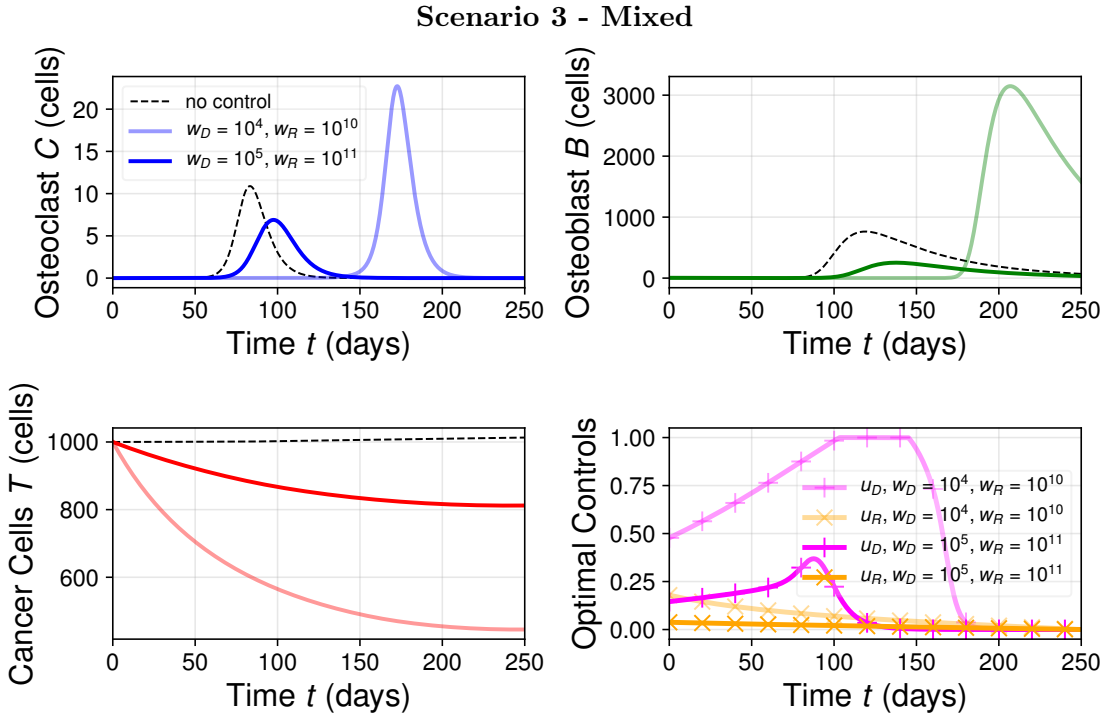

Figure 3.15: Scenario 3 for mixed treatment model.

Discussions

In this Chapter, two bone metastasis treatment models are presented, extending a previous model that studies the dynamics of the BMU cells (osteoclasts and osteoblasts) and bone metastatic cancer cells with the addition of two control functions. Having explicit expressions for the steady-states and conditions for their local stability, an exploration of parameters was made in order to find a multitude of dynamics that have already been seen qualitatively in experiments. Our objective was to find and analyze treatment regimes for two kinds of treatments –denosumab and radiotherapy–, and also to study their effects on cellular dynamics. An optimal control approach incorporates a cost function of the treatment use reflecting the economic cost and also side-effects.

We presented simulations that allowed us to verify if denosumab and radiation treatments are effective to reduce cancer cell levels. We considered a number of possible relevant scenarios of bone metastatic evolution under treatment, and we found interesting results that were not straightforward to predict. In all the scenarios, the optimal treatment regime obtained depends on the manipulation of the remodeling wave (amplitude or time of appearance). In some cases, the cancer cell populations are already aggressive enough to be influenced by the inhibition of osteoclasts. In other cases, their dependence is rather low and so the metastatic burden is not decreased enough, or it may be decreased at cost of disrupting the osteoclasts-osteoblasts cross-talk in a negative way. Thus, the inhibition of osteoclasts is not always the optimal strategy, and it depends on the type of metastatic cancer residing in the bone microenvironment. As predicted, denosumab treatment poses a weak choice in terms of controlling the growth of the tumor in general. Radiation treatment has a higher potential than the previous one, but the effects on the bone cells still need to be analyzed. Also, radiation has long-run side-effects and important economical cost that limit its applicability. A treatment that respects the natural microenvironment while attacking cancer cells would be more effective and desirable. Despite these interesting numerical results, it is important to point out that it is a difficult task to translate them into practical tools. There are two main reasons for this. First, we are considering a sole BMU being attacked by a sole metastatic tumor, but in reality there are multiple of these units acting at different places of bone and time. Thus, the next step could be to scale up the model and find optimal control solutions at a tissue level. Second, the optimal control solutions depend on predicting the appearance or the start of the bone remodeling cycle, but experimental work is still tackling this important question.

In the next Chapter, we now incorporate two key molecular factors that couples bone resorption with bone formation, and also use the optimal control framework to explore different therapeutic strategies.

Chapter 4

Modeling TGFβ and Wnt in bone diseases*

In the previous Chapters, we have studied a rather general, biochemical-simplified model for bone metastasis. Here, our objective is to decouple two important biochemical agents that have been under-studied in mathematical models.

Recall that there are three main steps in bone remodeling: bone resorption due to osteoclasts, a reversal phase and bone formation due to osteoblasts (Florencio-Silva et al., 2015). As mentioned in the previous Chapters, during the bone resorption phase osteoclast activity is regulated by osteoblasts through RANKL, a promoter of osteoclast activation, and by its decoy receptor OPG. Next, the reversal phase is thought to be the coupling phase whereby osteoclast activity is inhibited and osteoblast activity is promoted (Matsuo & Irie, 2008). The coupling phase is governed by numerous pathways, being the transforming growth factor (TGFβ) and the Wnt pathways two key coupling regulators (Weivoda et al., 2016). In particular, TGFβ promotes active osteoclast apoptosis while Wnt promotes osteoblast precursors differentiation. In this Chapter, we focus our attention to incorporate these two factors in a mathematical model for a better understanding of the coupling phase and how this coupling is affected under pathological conditions such as osteoporosis and bone metastasis.

Also, recall that, among the mathematical models, there are two broad research lines that are characterized by the biological scales incorporated: biochemical-detailed models and biochemical-simplified models. Some important biochemical-detailed models are Peterson & Riggs (2010) in which calcium homeostasis dynamics is incorporated, and Pivonka & Komarova (2010b) that explores theoretically specific bone remodeling molecular disruptions. Of importance, TGFβ and Wnt are incorporated in these biochemical-detailed models, but the dimensionality of the systems make a mathematical analysis intricate. Here we propose a model that combines the mathematical tractability of biochemical-simplified models to describe cellular dynamics and the biological relevance of biochemical-detailed models to incorporate TGFβ and Wnt molecular dynamics.

Among the questions regarding the bone remodeling process is the possibility of an oscillatory behavior between osteoclast and osteoblast activities and their corresponding molecular factors. It has been estimated that the mean time between successive remodeling events at the same location is 2 years (Manolagas, 2000). In Komarova et al. (2003) an

*This Chapter has been submitted to *Journal of Theoretical Biology*.

oscillatory bone remodeling behavior is associated with random bone remodeling. However, in another recent biochemical-simplified model proposed in Coelho et al. (2016) it is pointed out that there is still no biological evidence that such behavior occurs in a biological setting. In this Chapter we try, through our proposed mathematical model, to find possible mechanisms related to TGFβ and Wnt that may trigger the appearance of oscillatory behavior in the bone remodeling process.

After studying homeostasis in the bone remodeling process, we turn our attention to bone diseases. Bone diseases pose challenging questions regarding the best therapeutic strategies to fight against them (Marie, 2015). These pathologies are characterized by unbalanced bone mass production due to corrupted communication between osteoclasts and osteoblasts. Current osteoporosis treatments focus mainly on blocking the catabolic effect from osteoclasts. In particular, bisphosphonates are employed to increase the active osteoclast apoptosis rate, whereas denosumab is a RANKL antibody that prevents osteoclast activation (Burkiewicz et al., 2009). Some of the previously mentioned models study osteoporosis as a case study, and they mainly focus on anti-catabolic treatment. In Javed et al. (2019) a biochemical-simplified model is specifically used to predict dynamical properties of bone cells in an osteoporotic scenario. Recent research indicates that Wnt proteins may be a potential anabolic therapeutic option for osteoporosis (Weivoda et al., 2016). Here, we use osteoporosis disease as a case study to explore through the proposed mathematical model the effects of anabolic control strategies.

Another bone disease of great importance is the metastasis-associated bone disease. Two of the main culprits associated with the success of the bone metastasis vicious cycle are TGFβ and Wnt signaling pathways (Mundy, 2002; Baron & Gori, 2018). As such, therapies involving TGFβ inhibition have been proposed as potential control strategies for bone metastasis (Juárez & Guise, 2011; Cook et al., 2016), as well as inhibition of cancer-induced Wnt antagonists (Sousa & Clézardin, 2018).

Finding appropriate bone-associated diseases models is still an active and important research field, and these include *in vitro*, *in vivo* and also *in silico* models (Madrasi et al., 2018; Kähkönen et al., 2019). Mathematical and computational models for cancer-associated bone disease have also been extensively developed in the literature. Recent computational models for prostate cancer bone disease have been proposed in the work of Araujo et al. (2014); Cook et al. (2016); Araujo et al. (2018) where a hybrid computational automaton method was employed. This computational framework serves as an *in silico* laboratory to test a number of biological settings across the tissue, cellular and molecular scales. For the mathematical models, for instance, multiple myeloma bone disease has been studied from a biochemical-simplified philosophy (Ayati et al., 2010) as well from a biochemical-detailed perspective (Wang et al., 2011). Recently, cancer bone disease has been explored in a biochemical-simplified models (Coelho et al., 2016; Camacho & Jerez, 2018) and in a biochemical-detailed model (Farhat et al., 2017). Of great interest to us is this latter model proposed in Farhat et al. (2017) since the authors incorporate both TGFβ and Wnt as state variables, but a mathematical analysis discussion is limited. In this Chapter, we aim to fill a gap between the bone dynamics biology and the proposed mathematical model with a preliminary theoretical based on mathematical tools such as steady-state and bifurcation analyses.

Finally, after having gained insight into the bone remodeling and bone metastasis processes, we incorporate control functions as a way to model treatment strategies. Particularly, we are interested in disease control strategies that are connected to the TGFβ

and Wnt signaling pathways. For the case of bone remodeling, an osteoporosis treatment model is proposed, whereas for the bone metastasis dynamics we aim to model the therapeutic control of an osteolytic lesion. Additionally, we address the question about how chemotherapy-free multi-agent therapies could perform to reduce bone metastasis proliferation compared to chemotherapy-included therapies.

The optimal control framework has been employed in different biological contexts (Lenhart & Workman, 2007), like in hepatitis virus (Shah et al., 2019), cancer dynamics (Carrère, 2017) and acute myeloid leukemia (Sharp et al., 2019). However, this approach has been used scarcely in the literature for bone remodeling and bone metastasis. In Moroz (2012) an optimal control problem is posed as to describe mechanical stress effects and regulation on the BMU dynamics. In Lemos et al. (2016) the optimal control approach is employed to describe chemotherapy effects on the multiple myeloma bone invasion dynamics.

In summary, this Chapter is organized as follows: In Section 4.1 we propose a mathematical model for bone remodeling which is based on biological assumptions with emphasis on the roles of TGFβ and Wnt. The proposal combines both the mathematical tractability from biochemical-simplified models to describe cellular dynamics and the biological relevance from biochemical-detailed models to describe molecular dynamics. Then, we extend the proposed bone remodeling model to study bone metastasis dynamics in Section 4.2. In both Sections, we derive well-posedness, local stability and oscillatory properties of the systems and connect them with their biological contexts. Based on the theoretical results obtained earlier, in Section 4.3 we propose optimal control problems to model osteoporosis and cancer-induced disease treatments. In particular, through the optimal control approach, we try to identify the theoretical optimal performance of combination treatments that include both conventional and novel control strategies like bisphosphonates and TGFβ inhibition. Finally, we present some concluding remarks.

4.1 Bone remodeling

Intense research has been done in understanding the coupling between osteoclast-derived bone resorption and osteoblast-derived bone formation. Besides the amply studied RANKL and OPG signaling osteoblast-mediated regulation pathways to osteoclasts. The other main coupling factors are believed to be the TGFβ and Wnt signaling pathways (Weivoda et al., 2016). TGFβ is a cytokine that belongs to a superfamily of ligands. This cytokine is known for its multiple effects on numerous cellular processes. For instance, TGFβ plays an important role in bone homeostasis by regulating the main RANKL/OPG pathway. Recently, it has been pointed as the principal factor responsible for the transition (or reversal) phase in bone remodeling in which osteoclast-driven bone resorption is stopped while osteoblast-driven bone formation starts (Matsuo & Irie, 2008). The bone resorption-bone formation coupling is regulated in part via TGFβ by inducing the osteoclast expression of Wnt and thereby recruiting osteoblasts (Ota et al., 2013; Weivoda et al., 2016). Also, it has been found experimentally that TGFβ induces downstream signaling in osteoclasts that make them express Wnt1, and that this cytokine promoted osteoblasts migration and proliferation (Weivoda et al., 2016).

TGFβ is abundant in the bone matrix. This cytokine is released in latent form and then activated by osteoclast activity (Weivoda et al., 2016). At early stages of osteoblast differentiation, TGFβ increases osteoblast precursor migration and proliferation; at later phases, TGFβ inhibits osteoblast differentiation and bone mineralization. Moreover, TGFβ blocks

the apoptosis (programmed cell death) of osteoblasts during their conversion into osteocytes. Activation of TGFβ by osteoclasts inhibits further osteoclastogenesis. Depending on the context, TGFβ can inhibit or promote osteoclast differentiation (Weivoda et al., 2016; Juárez & Guise, 2011).

For the development of our model we assume the following hypotheses:

(H1"') Osteoblasts (**precursors** and **active**) have a regulatory effect on osteoclasts via the RANK/RANKL/OPG pathway (Florencio-Silva et al., 2015). See also Chapter 1.1.

(H2"') TGFβ is released from bone matrix and it is activated by **active** osteoclast bone resorption (Janssens et al., 2005).

(H3"') TGFβ promotes osteoblast **precursors** proliferation (Janssens et al., 2005; Juárez & Guise, 2011).

(H4"') TGFβ activation reduce osteoclastogenesis (maturation of **osteoclast precursors**) in the presence of osteoblast **lineage** by up-regulating OPG and down-regulating RANKL (Janssens et al., 2005; Takai et al., 1998).

(H5"') **Mature** osteoblast apoptosis is blocked by TGFβ (Janssens et al., 2005).

(H6"') Wnt has a positive density-dependent effect on osteoblast **precursors** (Weivoda et al., 2016).

(H7"') Wnt is expressed by osteoclasts via TGFβ (Weivoda et al., 2016).

(H8"') We assume that cells and molecules have first-order elimination (Komarova et al., 2003; Farhat et al., 2017).

These are the main assumptions for developing our mathematical model for bone remodeling. In Figure 4.1 a schematic representation of these interactions is presented.

4.1.1 Mathematical model

As mentioned in the introduction, we are interested in introducing TGFβ and Wnt as state variables. We do so by incorporating them in a modified version of the base model presented in Section 1.1.2:

$$\begin{cases} \dfrac{dx_C}{dt} = \alpha_C x_C x_B^{g_1} - \beta_C x_C, & (4.1) \\ \dfrac{dx_B}{dt} = \alpha_{BW} x_B x_C^{g_2} - \beta_B x_B, & (4.2) \end{cases}$$

where x_C and x_B are the osteoclast and osteoblast densities, respectively. For further discussion about the model and its parameters, the reader is referred to Section 1.1.2. As in Section 1.1.2, we will keep assuming a constant regulation of osteoclasts from osteoblasts by assuming $g_1 < 0$. For simplicity, we assume that $g_1 = -1$ as an inversely linear regulation.

TGFβ is regarded as indirect paracrine signaling from osteoclasts to osteoblasts and also as an osteoclast autocrine signaling. Thus, in order to modify the base model, we drop out some of the exponents related to these signalings and incorporate the TGFβ

Figure 4.1: Left: Bone remodeling coupling interactions. **Right:** Bone metastasis vicious cycle. The presence of cancer cells interfere with the bone cell communications. C: active osteoclasts, B: osteoblast lineage, T: active TGFβ, W: Wnt protein, M: bone metastasis cancer cells.

density as an explicit variable. The corresponding exponent in the reduced model (4.1)–(4.2) is g_2 which will therefore be assumed $g_2 = 0$. In their place, the meaning of the parameter g_2 will be encoded in explicit molecular agents that resembles this paracrine communication between osteoblasts and osteoclasts. A similar approach of decoupling the power-law approximation was used in Ryser et al. (2010) where RANKL and OPG were modeled explicitly.

Taking all together the previous discussion and the hypotheses *(H1)–(H8)*, we propose the following model:

$$\begin{cases} \dfrac{dx_C}{dt} = \underbrace{\alpha_C x_B^{-1}}_{RANKL/OPG} - \underbrace{\beta_C x_C}_{OC\ apopt.} - \underbrace{\beta_{CT} x_C x_T}_{TGF\beta\ induced\ apop.}, & (4.3) \\ \dfrac{dx_B}{dt} = \underbrace{\alpha_{BW} x_B x_W}_{Wnt\text{-}induced\ prolif.} - \underbrace{\beta_B x_B}_{OB\ apop.}, & (4.4) \\ \dfrac{dx_T}{dt} = \underbrace{\alpha_T x_C}_{Resorp.} - \underbrace{\beta_T x_T}_{Degra.}, & (4.5) \\ \dfrac{dx_W}{dt} = \underbrace{\alpha_W x_T x_C}_{OC\text{-}induced\ prod.} - \underbrace{\beta_W x_W}_{Degra.}, & (4.6) \end{cases}$$

where $x_C(t)$, $x_B(t)$, $x_T(t)$ and $x_W(t)$ denote the densities of **active** osteoclasts, osteoblast **lineage** cells, **active** TGFβ, and Wnt at time t, respectively; α_i are recruitment (x_C and x_B), release (x_T) or expression (x_W) rates, and β_i are elimination rates; β_{CT} represents osteoclastic apoptosis due to TGFβ.

One of the first tasks arising while constructing a mathematical model is to check the feasibility of such a model. In a biological context, it is important to check if the model is well-posed in terms of non-negativity. The following result is related to this property:

Theorem 4.1. *The set $\mathbb{R}^4_+$ is a positive-invariant set of the system (4.3)–(4.6).*

Proof. The boundary of $\mathbb{R}^4_+$ is the union of four sets: $\Omega_C = \{0\} \times \mathbb{R}^4_+ \times \mathbb{R}^4_+ \times \mathbb{R}^4_+$, $\Omega_B = \mathbb{R}^4_+ \times \{0\} \times \mathbb{R}^4_+ \times \mathbb{R}^4_+$, $\Omega_T = \mathbb{R}^4_+ \times \mathbb{R}^4_+ \times \{0\} \times \mathbb{R}^4_+$, and $\Omega_W = \mathbb{R}^4_+ \times \mathbb{R}^4_+ \times \mathbb{R}^4_+ \times \{0\}$.

In order to prove that $\mathbb{R}^4$ is positively invariant, we may prove that the vector field X' defined by the ODE system points inwards from the boundary or it is tangent to it.

For Ω_C, note that $x_C = 0$ and thus, from (4.3)–(4.6), we get:

$$\frac{dx_C}{dt} = \alpha_C x_B^{-1} > 0, \tag{4.7}$$

and thus the vector field X' points inwards to $\mathbb{R}^4$ from Ω_C.

For Ω_T, note that $x_T = 0$ and thus, from (4.3)–(4.6), we get:

$$\frac{dx_T}{dt} = \alpha_T x_C \geq 0, \tag{4.8}$$

and thus the vector field X' points inwards to $\mathbb{R}^4$ from Ω_T.

For Ω_W, note that $x_W = 0$ and thus, from (4.3)–(4.6), we get:

$$\frac{dx_W}{dt} = \alpha_W x_T x_C \geq 0, \tag{4.9}$$

and thus the vector field X' points inwards to $\mathbb{R}^4$ from Ω_W.

Finally, for Ω_B, we take $x_B \to 0^+$. Then, from (4.3)–(4.6) and for fixed x_W, we get:

$$\frac{dx_B}{dt} = x_B(\alpha_{BW} x_W - \beta_B) \to 0 \tag{4.10}$$

as $x_B \to 0^+$. Thus the vector field X' becomes tangent to $\mathbb{R}^4$ from as we approach to Ω_B. Therefore, $\mathbb{R}^4$ is positively invariant. □

The previous result guarantees that given positive initial conditions the solutions are going to be positive for any time. Now we focus our attention on the equilibrium points of the model to study long-term behavior of the system.

Theorem 4.2. *The system (4.3)–(4.6) has a unique steady-state given by:*

$$\widehat{x}_W = \frac{\beta_B}{\alpha_{BW}}, \tag{4.11}$$

$$\widehat{x}_T = \sqrt{\frac{\beta_W}{\alpha_W}\frac{\alpha_T}{\beta_T}\widehat{x}_W} = \sqrt{\frac{\beta_W}{\alpha_W}\frac{\alpha_T}{\beta_T}\frac{\beta_B}{\alpha_{BW}}}, \tag{4.12}$$

$$\widehat{x}_C = \frac{\beta_T}{\alpha_T}\widehat{x}_T = \sqrt{\frac{\beta_W}{\alpha_W}\frac{\beta_T}{\alpha_T}\frac{\beta_B}{\alpha_{BW}}}, \tag{4.13}$$

$$\widehat{x}_B = \frac{\alpha_C}{\widehat{x}_C(\beta_C + \beta_{CT}\widehat{x}_T)}. \tag{4.14}$$

Straightforward from setting the left-hand side of (4.3)–(4.6) equal to zero and solving the system. □

After finding the steady-states of the system another question of relevance is related to the local stability of these equilibrium points. Recall that if a steady-state is locally stable then the system converges to this point if initial conditions are sufficiently near to the steady-state. From Theorem 4.2, assuming local stability of the steady-state, we can

Symbol	Description	Value	Source
$x_C(0)$	Initial active osteoclast density	5.0	Assumed
$x_B(0)$	Initial osteoblast density	1.0	Assumed
$x_T(0)$	Initial active TGFβ density	0.0	Assumed
$x_W(0)$	Initial Wnt density	0.0	Assumed
α_C	Active osteoclast production	3.0	Komarova et al. (2003)
β_C	Active osteoclasts apoptosis	0.3	Farhat et al. (2017)
β_{CT}	Active osteoclasts inhibition (TGFβ)	0.13	Ross et al. (2017)
α_{BW}	Osteoblasts production (Wnt)	0.26	Farhat et al. (2017)
β_B	Osteoblasts apoptosis	1.0	Assumed
α_T	TGFβ activation	100.0	Assumed
β_T	TGFβ degradation	499.1	Farhat et al. (2017)
α_W	Wnt production	1.0	Assumed
β_W	Wnt degradation	1.0	Assumed

Table 4.1: Parameter description and assumed values for model (4.3)–(4.6).

obtain the following observations:

1. The Wnt steady-state level $\widehat{x}_W$ affects directly the equilibrium values of bone cells and TGFβ. This suggests that Wnt is a potent coupling mechanism at par of TGFβ.

2. Osteoclast equilibrium level $\widehat{x}_C$ controls inversely proportional the equilibrium level of osteoblast population. This is a direct effect of the RANKL/OPG regulatory mechanism from osteoblast to osteoclast.

The next natural question is about the behavior near the equilibrium point of the system. In other words, we would like to determine its local stability. In C.1 we gathered the associated characteristic polynomial and the corresponding conditions to guarantee local stability of the obtained steady-state. Due to the non-linearities of the model, it is difficult to extract a simplified, transparent list of biological conditions that guarantee local stability. However, this result may be used as a guide to explore the parameter space to identify different solution profiles of the model. In the following Section, we employ these preliminary theoretical results to perform a numerical analysis of the model.

4.1.2 Numerical results

Even though we are considering a multi-scale problem (cells and molecules), for the numerical simulations we consider normalized densities. Thus, the unitary value will be regarded as a standard reference value for all the variables. This is motivated by works such as Pivonka & Komarova (2010b) where a quantity of interest is the osteoclast to osteoblast population as a way to visualize bone turnover.

Baseline parameters

For the case of bone remodeling, we gathered some parameter values from the literature in Table 4.1. The resulting numerical simulation can be found in Figure 4.2 where it can be observed that the first wave of osteoclast originates the appearance of a marked osteoblast wave. This is due to the coupling between osteoclasts and osteoblasts. Over

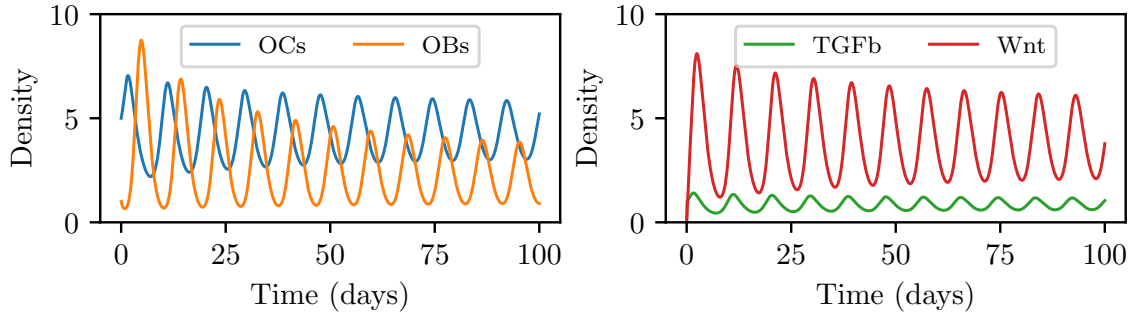

Figure 4.2: Bone remodeling oscillatory coupling. **Left:** Cell population densities. **Right:** Molecule densities.

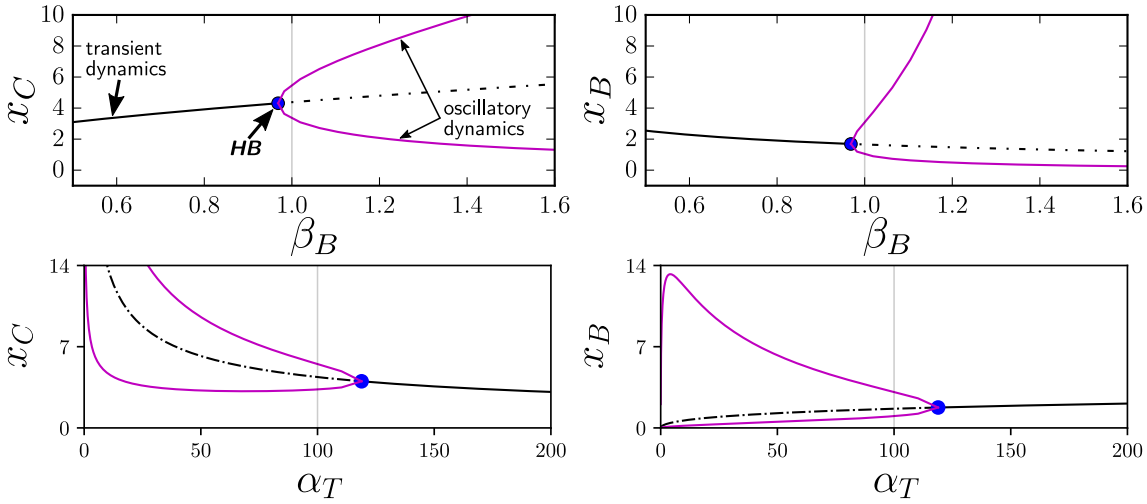

Figure 4.3: Bifurcation diagrams for osteoclast (x_C) and osteoblast (x_B) equilibrium densities with respect to osteoblast elimination rate β_B (**up**) and TGFβ release α_T (**down**). As β_B increases, a Hopf bifurcation point **HB** emerges and gives rise to oscillations; the opposite happens with α_T. The lines marked with "oscillatory dynamics" represent the maximum and minimum values of the periodic solutions. The **gray lines** correspond to baseline parameter values. Solid lines represent stable equilibrium whereas dashed lines represent unstable equilibrium.

time the coupling favors the osteoclast population and thus we associate this behavior to an osteoporotic profile. We will bring back this discussion in Section 4.3.1.

Oscillations

Due to its nonlinear nature, model (4.3)–(4.6) poses a challenge in regards to the analytical study of the stability of the steady-state (4.11)–(4.14). We can see in Figure 4.2 that using the baseline parameters we obtain an oscillatory bone remodeling process. We wondered if there may be some parameters involved in switching from an oscillatory to transient behavior. To test this hypothesis, we employed a computational tool called `PyDSTool` which is a Python module to obtain numerical approximations to bifurcation diagrams (Clewley et al., 2007).

Because of its role in the feedback loop of the bone remodeling process, we tested

Parameter ↗	Range	OCs?	OBs?	Period?
α_C	$(1.0, 3.0)$	↘	↗	—
β_C	$(0.3, 1.0)$	—	—	↘
β_{CT}	$(0.07, 0.14)$	↘	↘	↘
α_{BW}	$(0.1, 0.5)$	↘	↗	↗
β_B	$(0.1, 1.0)$	↗	↘	↘
α_T	$(10.0, 100.0)$	↘	↘	↘
α_W	$(0.1, 2.0)$	↘	↗	↗
β_W	$(1.0, 5.0)$	↗	↘	↘

Table 4.2: Qualitative parameter sensitivity analysis. The first column depicts the parameter that was increased. The second to fourth columns show how osteoclast density, osteoblast density and the period of oscillations were modified with respect to the parameter.

the hypothesis that the parameters β_B (osteoblast elimination rate) and α_T (release and activation rate of TGFβ) may be able to create or destroy an oscillatory behavior. In particular, Hopf bifurcations dictate the transition from a latent state to an oscillatory one. These points may arise when certain model parameters are varied in an interval of interest where the imaginary parts of the roots of the characteristic polynomial have a change of sign (Kuznetsov, 2013).

Exploring the parameter space, using steady-state values from Theorem 4.2 to maintain normalized values, we obtained Figure 4.3 where the appearance of Hopf bifurcations is shown. From this figure we can obtain the following observations:

1. Osteoblast elimination rate β_B is involved in the emergence of oscillatory behavior, whereas α_T favors the emergence of transient behavior.

2. When oscillations emerge, control of the bone remodeling process becomes more difficult due to non-linear periodic behavior.

3. Decreasing the release/activation of TGFβ produces the following scenario: After the emergence of the Hopf bifurcation, there is a regime in which osteoblasts oscillate with increasing amplitude, perhaps to compensate the osteoclastic increase of activity. However, due to lack of TGFβ mediated activation, osteoblastic activity ceases.

These observations lead to the hypothesis that for a bone remodeling process scenario that favors osteoclast activity (e.g. osteoporosis) the inhibition of osteoblast apoptosis or the increase of TGFβ levels may be appropriate control measures. Also, these numerical results shed some light in regards to our question of the creation or elimination of an oscillatory bone remodeling process.

Parameter sensitivity

For the bone remodeling system, we performed a sensitivity analysis for the model parameters. We regarded parameters from Table 4.1 as baseline parameters. We plotted in Figure 4.4 the most representative changes in the behavior of the solutions with respect to some parameters. In Table 4.2 we gathered the qualitative changes observed for all the

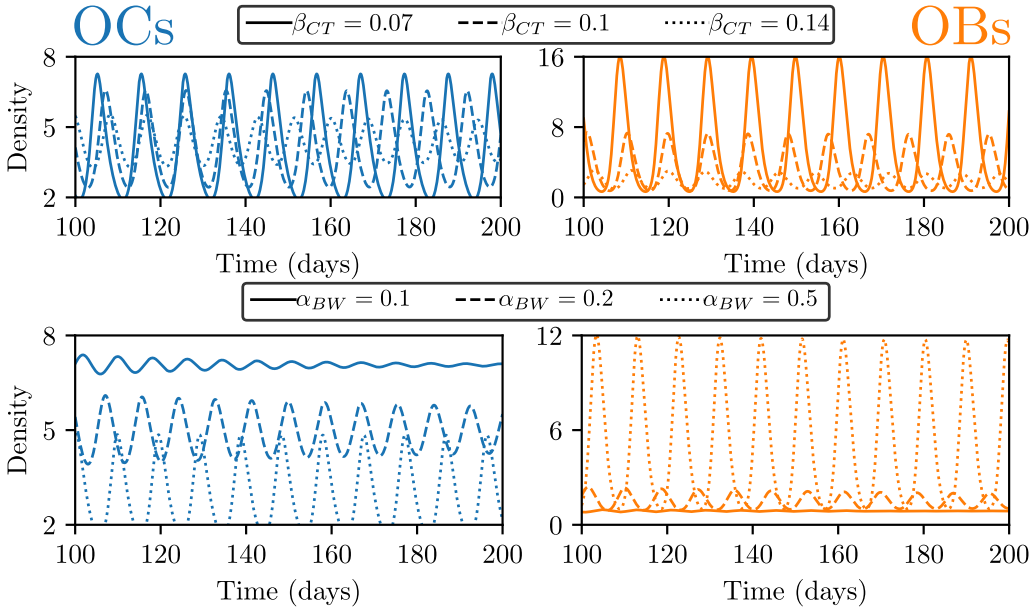

Figure 4.4: Sensitivity with respect to two main coupling elements: **Up:** β_{CT} and **Down:** α_{BW}. **Left:** Osteoclast density. **Right:** Osteoblast density.

parameters of the system. We identified elements from Table 4.2 that have antagonistic effects. For instance, the regulation parameter α_C antagonize with the elimination of osteoblasts β_B or with the elimination of Wnt β_W. Whereas Wnt and osteoblasts display regulatory effects on osteoclasts. From Table 4.2 we can infer that TGFβ have a potent coupling mechanism. If TGFβ liberation and activation α_T is increased, both osteoclast and osteoblast populations decrease.

In Figure 4.4 we gathered two important parameters. The first one is the apoptotic responsiveness to TGFβ from osteoclasts β_{CT}. The second parameter is the proliferation responsiveness to Wnt from osteoblasts α_{BW}. These parameters are of biological relevance because they can be linked to the corresponding cell receptors, which can be manipulated to test therapeutic possibilities (Wan et al., 2012). Also, they are relevant because they might be perturbed by unwelcome visitors like cancer cells, which may produce for instance antagonists to the Wnt signaling pathway. This is partially addressed in the next Section where we present a bone metastasis mathematical model that incorporates manipulation of the bone cell cross-talk due to cancer cells.

4.2 Bone metastasis

Having studied the bone remodeling process, now we ask how bone pathologies may arise by taking into account negative external forces like metastatic cancer cells. In this Section, we will introduce the biological assumptions for the bone metastasis dynamics.

During the vicious cycle of bone metastasis, osteoclast activity is up-regulated by cancer cells. Bone resorption causes embedded agents in the bone matrix to be released, being TGFβ one of them. Liberated in a latent form, TGFβ is then activated by active osteoclasts and subsequently promoting cancer cell proliferation (Mundy, 2002; Juárez & Guise, 2011). Osteoblast cell population may also be manipulated by cancer cell-produced

agents. For instance, some cancer cells produce Dkk1 which is a regulator that inhibits the Wnt signaling pathway (Suvannasankha & Chirgwin, 2014). In this way, osteoblast activity may be down- or up-regulated, depending on the balance of the cancer cell-produced osteoblast-promoting or -inhibiting agents (Chiechi & Guise, 2016). In general, depending on the balance in the osteoclast to osteoblast activity levels there are two types lesions: the osteolytic lesion (favors bone resorption) and the osteoblastic lesion (favors bone deposition) (Mundy, 2002; Krzeszinski & Wan, 2015).

As mentioned in the introduction, bone metastasis cells aim to create a vicious cycle in which osteoclastic activity is increased in order to release growth factors from the bone matrix. One of such factors is TGFβ that has important coupling effects in the bone remodeling process. Bone resorption causes embedded agents in the bone matrix to be released, being TGFβ one of them. Liberated in a latent form, TGFβ is then activated by active osteoclasts and subsequently promoting cancer cell proliferation (Mundy, 2002; Juárez & Guise, 2011). Osteoblast cell population may also be manipulated by cancer cell-produced agents. For instance, some cancer cells produce Dkk1 which is a regulator that inhibits the Wnt signaling pathway (Suvannasankha & Chirgwin, 2014). In this way, osteoblast activity may be down- or up-regulated, depending on the balance of the cancer cell-produced osteoblast-promoting or -inhibiting agents (Chiechi & Guise, 2016). In general, depending on the balance in the osteoclast to osteoblast activity levels there are two types lesions: the osteolytic lesion (favors bone resorption) and the osteoblastic lesion (favors bone deposition) (Mundy, 2002; Krzeszinski & Wan, 2015).

Besides assumptions *(H1)–(H8)* from Section 4.1, we incorporate the following ones to model bone metastasis:

(H9”’) Bone metastatic cells promote activation of osteoclasts by decreasing inhibition from osteoblasts (e.g. cancer-derived PTHrP increases the RANKL to OPG ratio) (Mundy, 2002; Coelho et al., 2016).

(H10”’) Bone metastatic cells produce factors to inhibition osteoblast activity (e.g. DKK1 inhibits Wnt pathway) (Florencio-Silva et al., 2015; Farhat et al., 2017).

(H11”’) Bone metastatic cells are affected positively by active TGFβ (Mundy, 2002; Farhat et al., 2017).

(H12”’) Bone metastatic cells follow an intrinsic logistic growth (Farhat et al., 2017).

Using these as building blocks, we incorporate bone metastasis into the bone remodeling dynamics.

4.2.1 Mathematical model

Similarly as in Section 4.1.1, we incorporate TGFβ and Wnt pathways (see Figure 4.1) in a modified version of previously proposed and studied model for bone metastasis (Chapters

Symbol	Description	Value
$x_M(0)$	Initial cancer cell proportion	0.01
K_C	OCs-OBs decoupling effect	0.5
K_B	Wnt production inhibition	0.2
α_{CM}	Promotion of active osteoclasts	0.01
α_M	Cancer cell growth rate	0.001
K_M	Carrying capacity	10.0
α_{MT}	Promotion due to TGFβ	0.1

Table 4.3: Bone metastasis parameter description of model (4.15)–(4.18). All the parameters are introduced in this Chapter.

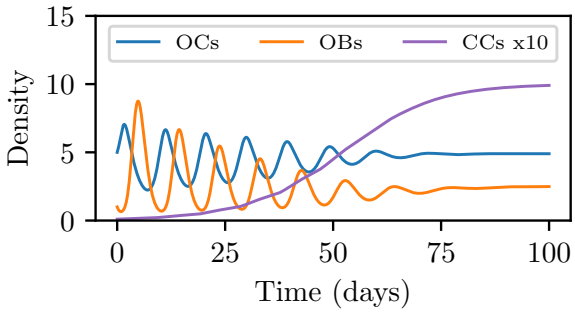

Figure 4.5: Bone metastasis evolution.

2 and 3):

$$\begin{cases} \dfrac{dx_C}{dt} = \alpha_C \underbrace{\left(1 - K_C \dfrac{x_M}{K_M}\right)}_{\textit{OCs-OBs decoup.}} x_B^{-1} - \beta_C x_C - \beta_{CT} x_C x_T + \underbrace{\alpha_{CM} x_M}_{\textit{Cancer prom.}}, & (4.15) \\ \dfrac{dx_B}{dt} = \alpha_{BW} x_B x_W - \beta_B x_B, & (4.16) \\ \dfrac{dx_T}{dt} = \alpha_T x_C - \beta_T x_T, & (4.17) \\ \dfrac{dx_W}{dt} = \alpha_W \underbrace{\left(1 - K_B \dfrac{x_M}{K_M}\right)}_{\textit{Wnt inhi.}} x_T x_C - \beta_W x_W, & (4.18) \\ \dfrac{dx_M}{dt} = \Big(\underbrace{\alpha_M}_{\textit{Cancer proli.}} + \underbrace{\alpha_{MT} x_T}_{\textit{TGFβ prom.}} \Big) \underbrace{x_M \left(1 - \dfrac{x_M}{K_M}\right)}_{\textit{logistic}}, & (4.19) \end{cases}$$

where $x_M(t)$ denotes metastatic cells residing within the BMU, α_M is the net proliferation rate of the cancer cells, K_M is the carrying capacity, and α_{MT} is the positive effect on cancer cell proliferation due to bone-derived TGFβ. The parameters K_C and K_B are the maximum effectivity of decoupling OCs-OBs signaling on OCs growth and of Wnt production inhibition by cancer cells, respectively. Note that $0 \leq K_C < 1$ and $0 \leq K_B < 1$. As before, this extended model is well-posed in the sense of positive solutions:

Theorem 4.3. *The set $\mathbb{R}^5_+$ is a positive-invariant set of the system (4.15)–(4.19).*

Proof. Similar as the one from Theorem 4.1. □

Now we search for the steady-states of the bone metastasis model. In this case we obtain to biologically relevant steady-states: the cancer-free equilibrium and the cancer-invasion equilibrium. This can be seen next:

Theorem 4.4. *The system (4.15)–(4.19) has two steady-states: a cancer-free equilibrium $\widehat{x}$ given by (4.11)–(4.14) together with $\widehat{x}_M = 0$, and a cancer-invasion equilibrium $\widetilde{x}$ that it is given by:*

$$\widetilde{x}_M = K_M, \tag{4.20}$$

$$\widetilde{x}_W = \widehat{x}_W = \frac{\beta_B}{\alpha_{BW}}, \tag{4.21}$$

$$\widetilde{x}_T = \sqrt{\frac{\beta_W}{\alpha_W(1-K_B)}\frac{\alpha_T}{\beta_T}\frac{\beta_B}{\alpha_{BW}}}, \tag{4.22}$$

$$\widetilde{x}_C = \sqrt{\frac{\beta_W}{\alpha_W(1-K_B)}\frac{\beta_T}{\alpha_T}\frac{\beta_B}{\alpha_{BW}}}, \tag{4.23}$$

$$\widetilde{x}_B = \frac{\alpha_C(1-K_C)}{\widetilde{x}_C(\beta_C + \beta_{CT}\widetilde{x}_T - \alpha_{CM}K_M)}. \tag{4.24}$$

Proof.

Straightforward from setting the left-hand side of the system equal to zero and solving. □

From Theorem 4.4 we can obtain the following observations:

1. At the cancer-invasion equilibrium, the presence of bone metastatic population does not change the levels of Wnt.

2. On the other hand, levels of TGFβ and osteoclasts increases as the Wnt production inhibition K_B increases.

3. Osteoblast levels at the cancer-invasion equilibrium decrease as the cancer-induced osteoclast-osteoblast decoupling K_C increases.

4. The direct osteoclast activation from cancer cells α_{CM} increases the osteoblast levels at the cancer-invasion equilibrium. This is due to the regulation from osteoblast to osteoclast. If α_{CM} is too high the system enters an unstable regime where solutions become unbounded.

These observations point out that control of bone metastasis is a complex process by direct inhibition of TGFβ. Yet again, it is difficult to gain more theoretical insight about this equilibrium state stability. However, we recur to this abstract result as a guideline for numerical simulations.

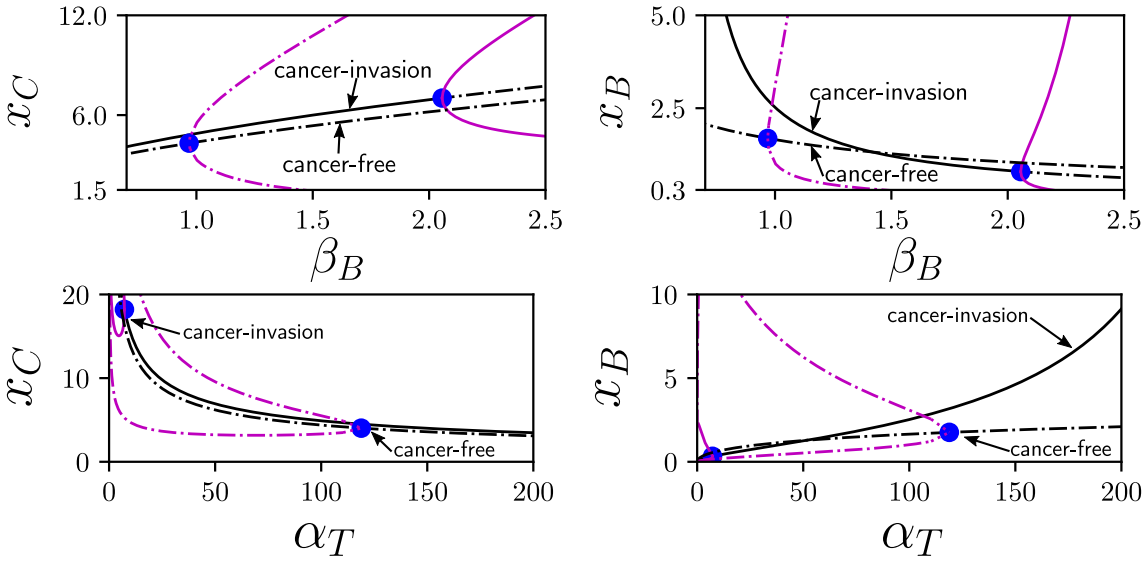

Figure 4.6: Bifurcation diagram for osteoclast (x_C) and osteoblast (x_B) equilibrium densities with respect to the parameters β_B (**up**) and α_T (**down**). The Hopf bifurcation is delayed in the presence of cancer for β_B, left for α_T). Solid lines represent stable equilibrium whereas dashed lines represent unstable equilibrium.

4.2.2 Numerical results

Baseline parameters

Together with parameters for the bone remodeling process (Table 4.1) we considered some baseline parameters to simulate metastatic bone disease. In Figure 4.5 we plotted the corresponding simulation. See Table 4.3.

For the cancer proliferation rate α_M we chose a comparable value from the literature (in Farhat et al. (2017) a value of 0.0023 is estimated for the case of prostate cancer bone metastasis). Additionally, we aimed to study a metastatic tumor with a low intrinsic growth rate (low α_M) that had a strong dependence on the TGFβ levels (high α_{MT}).

Oscillations

Analytical exploration of the equilibria stability of system (4.15)–(4.18) is now guided by the result found in C.2. We performed a numerical bifurcation diagram using the same homeostatic parameters as in Figure 4.3 and the cancer-associated baseline parameters 4.3. The resulting bifurcation diagrams are found in Figure 4.6. Observe in Figure 4.6 that the invasion equilibrium absorbed the local stability from the cancer-free equilibrium. In other words, the presence of cancer cells turns the cancer-invasion equilibrium state in a dominant, locally stable equilibrium. This means that solutions near the cancer-invasion equilibrium are going to approach or to oscillate with respect to this equilibrium point even if they start near the cancer-free equilibrium.

We can also observe in Figure 4.6 that a Hopf bifurcation point also appears in the cancer-invasion equilibrium. However, its appearance is delayed notoriously with respect to the bifurcation parameter β_B. This means that the presence of cancer cells may turn an oscillatory bone remodeling coupling into a transient dynamical behavior. If the levels

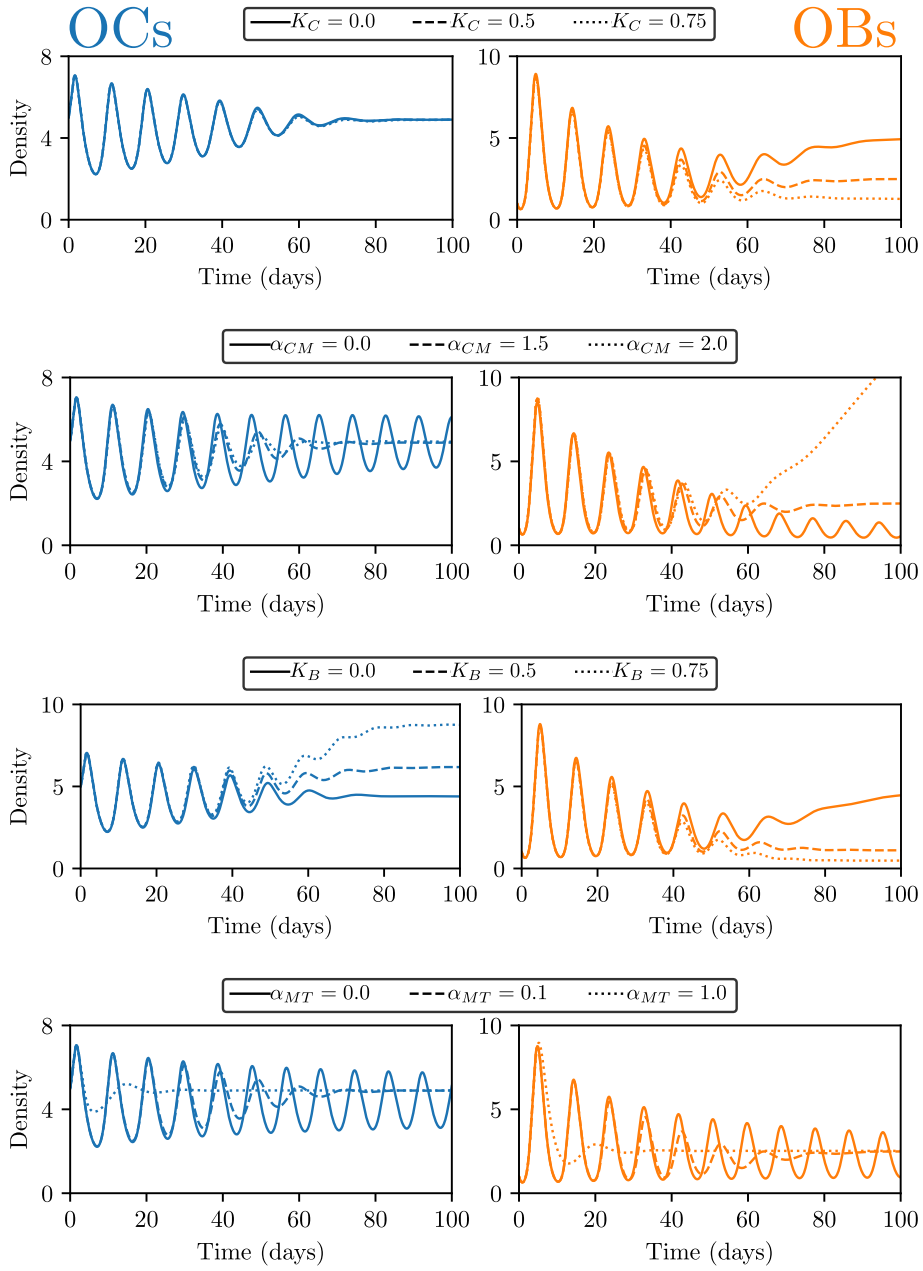

Figure 4.7: Parameter sensitivity for the bone metastasis model.

of osteoclast and osteoblast densities are far away in the transient regime then the bone mass is going to increase or decrease steadily, ending up rapidly in an osteolytic or an osteoblastic lesion.

Parameter sensitivity

Similar to the bone remodeling model, we proceeded to perform a qualitative parameter sensitivity analysis. In Figure 4.7 we gathered the results of increasing the cancer-associated parameters of the model.

As predicted by the steady-state analysis, the direct contribution from cancer to os-

teoclasts (α_{CM}) has an unstable effect of the osteoblast growth. The cancer-induced interference in the bone cells crosstalk has osteolytic effects. Increasing the parameter K_C decreases the osteoblast population to dramatic levels, leaving the osteoclast population at the same levels. On the other hand, the parameter K_B have both undesirable effects: increases osteoclasts and decreases osteoblasts. Finally, the contribution from TGFβ to the cancer growth (α_{MT}) does not change the equilibrium points. This parameter changes the oscillatory behavior and the rapidness of the cancer population growth.

4.3 Bone disease treatment modeling

In this Section, we explore a diversity of therapies for two bone diseases: osteoporosis (cancer-free) and an osteolytic lesion (cancer-invasion). In Skjødt et al. (2018) the authors present a discussion about the side-effects of the most relevant therapies associated with osteoporosis and bone metastasis. For instance, bisphosphonates conform anti-catabolic, osteoclast apoptosis promoter treatment that may imply osteonecrosis of the jaw and also gastrointestinal effects. On the other hand, intermittent parathyroid hormone is considered as an anabolic, osteoblast activity promoter treatment that may imply hypercalcemia (high levels of calcium) and thus abdominal and bone pain.

To model different treatment strategies while bearing in mind possible use limitation due to economical cost or side-effect burden we employ the optimal control framework. We propose objective functionals that aim to minimize undesirable quantities and also we incorporate into the dynamical system the corresponding effects of the treatments on the cell and molecular activities.

The theoretical approach to this and other types of optimal control problems has been long studied (Pontryagin et al., 1962). In this Chapter, we employ the computational tool BOCOP that finds approximations of optimal solutions through solving a nonlinear programming problem and an interior-point algorithm (Bonnans et al., 2017).

For the case of bone remodeling, we want to assess the optimal controllability of osteoporosis considering an anti-resorptive treatment (bisphosphonates) in combination with an anabolic treatment (Wnt introduction). For bone metastasis, we incorporate an anti-TGFβ therapy and also chemotherapy.

4.3.1 Osteoporosis therapy

Osteoporosis is a degradation of the bone. It is caused by higher levels of osteoclastic bone resorption. Several local and systemic factors are implicated as the culprits of osteoporosis. Two conventional treatments to deal with this pathology are denosumab bisphosphonates (Burkiewicz et al., 2009). Denosumab is a fully human monoclonal antibody that captures RANKL and thereby reduce osteoclast activation (Javed et al., 2018). Bisphosphonates, on the other hand, promote the apoptosis of osteoclasts (Coelho et al., 2016).

Recently, Wnt signaling has been proposed as a potential therapeutic opportunity for osteoporosis disease. Intense research is focusing to understand this anabolic approach for bone pathologies (Weivoda et al., 2016; Baron & Gori, 2018). Thus, here we focus on the standard bisphosphonates (anti-catabolic) and a novel, hypothetical Wnt protein injection (anabolic) treatments. Also, we incorporate a hypothetical TGFβ injection due to the pleiotropic effects of TGFβ in the bone remodeling process.

Let us consider the bone remodeling model (4.3)–(4.6) introduced in Section 4.1. We

associated the baseline parameters to osteoporosis due to the increased OCs level in comparison to the OBs level, see Section 4.1.1 and Figure 4.2. Let u_{bis}, u_{wnt} and u_{tg1} be control functions that model the impact of bisphosphonates, Wnt induction and TGFβ induction in the bone remodeling process, respectively. We propose the following modification to the original bone remodeling system (4.3)–(4.6):

$$\begin{cases} \dfrac{dx_C}{dt} = \alpha_C x_B^{-1} - \beta_C x_C - \beta_{CT} x_C x_T - \underbrace{u_{bis} x_C}_{Bisphos.}, & (4.25) \\ \dfrac{dx_B}{dt} = \alpha_{BW} x_B x_W - \beta_B x_B, & (4.26) \\ \dfrac{dx_T}{dt} = \alpha_T x_C - \beta_T x_T + \underbrace{u_{tg1}}_{TGF\beta\ ind.}, & (4.27) \\ \dfrac{dx_W}{dt} = \alpha_W x_T x_C - \beta_W x_W + \underbrace{u_{wnt}}_{Wnt\ ind.}, & (4.28) \end{cases}$$

The optimal control problem will have the following objectives:

1. Minimize the use of treatments u_{bis}, u_{tg1} and u_{wnt}.
2. Minimize the difference between osteoclast and osteoblast levels.
3. Keep low values of osteoclast levels.

Using the controlled system (4.25)–(4.28) and the proposed objectives we may introduce the following cost functional:

$$J(u) = \int_0^{t_f} C_1 u_{bis} + C_2 u_{wnt} + C_3 u_{tg1} + C_4 (x_C - x_B)^2 + C_5 (x_C - 1)^2 dt. \tag{4.29}$$

The coefficients C_i $(i = 1, \ldots, 5)$ are called weight parameters which balance the importance of each component to the total value of the cost functional J. For instance, if $C_i = 0$ then the corresponding quantity of the integral (4.29) does not imply an additional cost.

Applying an external input to a biological process usually implies having defined bounds for such input. Here, we assume the following bounds for the control functions u_{bis} and u_{wnt}:

$$0 \leq u_{bis}(t) \leq 0.5, \quad 0 \leq u_{tg1}(t) \leq 100, \quad 0 \leq u_{wnt}(t) \leq 2, \quad \text{for all } 0 \leq t \leq t_f. \tag{4.30}$$

The bounds in (4.30) are proposed for numerical exploration purposes while trying to equilibrate reasonable biological effects and variable magnitudes in the dynamical model.

Observe that in the cost functional (4.29) and in model (4.25)–(4.28) the control functions appear as linear terms. Thus, it is expected that the optimal solutions are of the so-called bang-bang type (Lenhart & Workman, 2007). In these type of solutions the control function switch from an 'off' state to an 'on' state. It is possible that singular arcs arise, giving intermediate values between the 'off' and 'on' states (Ledzewicz et al., 2019).

Here we consider three strategies for controlling osteoporosis:

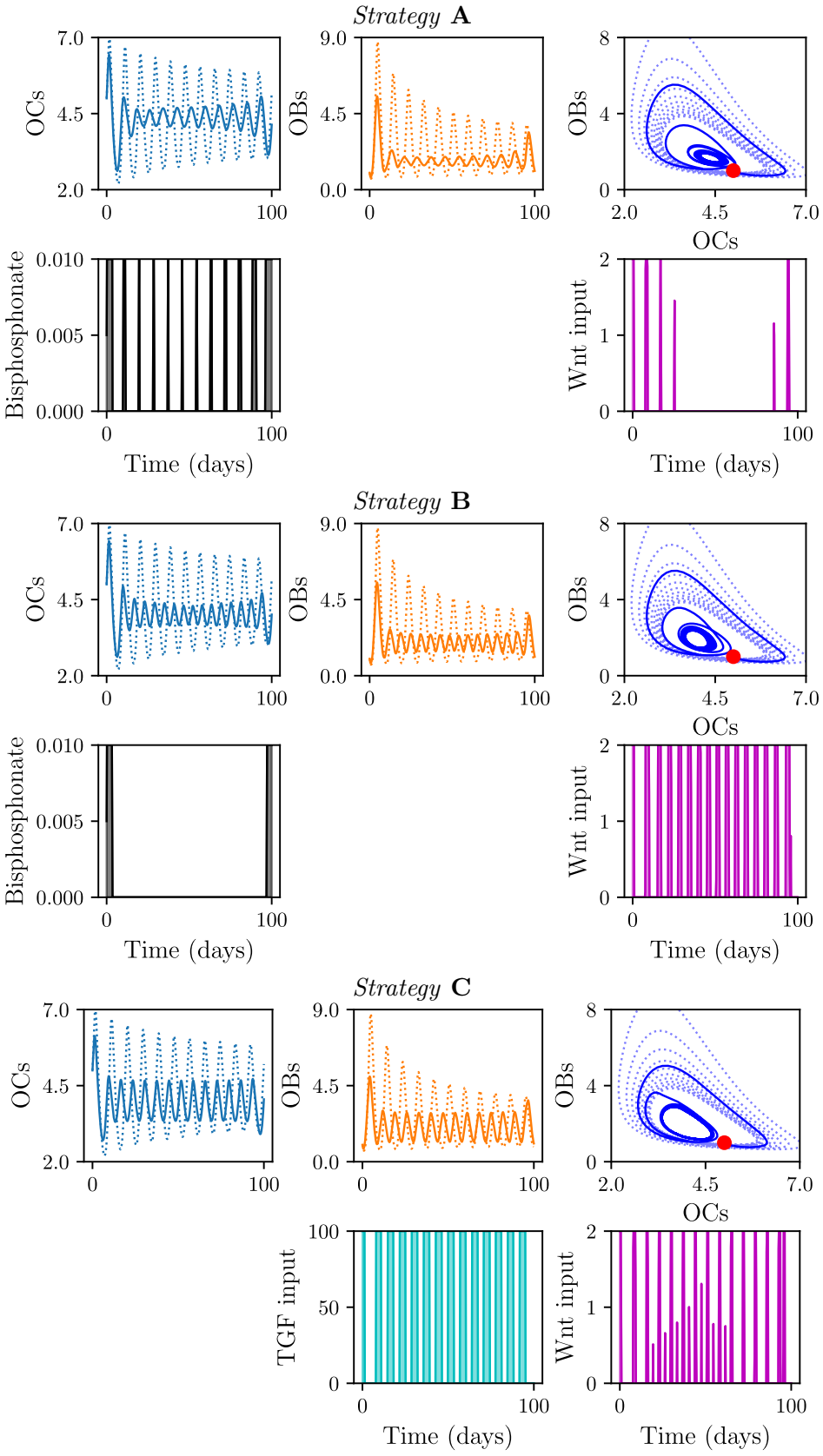

Figure 4.8: Bone remodeling model: Osteoporosis treatments. **Dashed lines** represent solutions without control. The **red dot** represents the initial condition $(x_C(0), x_B(0))$.

Strategy	u_{bis}?	C_1	u_{tgl}?	C_2	u_{wnt}?	C_3	C_4	C_5
A	✓	0			✓	15	1	2
B	✓	0			✓	12	2	1
C			✓	0.05	✓	7.2	1	1

Table 4.4: Summary of strategies explored for osteoporosis. Control functions without a check mark are regarded as zero functions.

- *Strategy* **A**. We consider the combination of bisphosphonates (u_{bis}) and Wnt input (u_{wnt}). We ask the cost functional to penalize high levels of OCs (C_5) more than the difference between OCs and OBs levels (C_4).

- *Strategy* **B**. We also consider bisphosphonates and Wnt input. We reduce slightly the cost of utilizing the u_{wnt} control. Also, we invert the roles of C_4 and C_5 putting emphasis on the difference between OCs and OBs levels.

- *Strategy* **C**. Finally, in this strategy, we focus on theoretical TGFβ and Wnt input therapies. In this strategy, we equalize the importance of the parameters C_4 and C_5.

Balancing the weight parameters C_i $(i = 1, \dots, 5)$ makes the optimal solution to focus on certain aspects of the model dynamics and the usage of the controls. In Table 4.4 we gathered these strategies and the corresponding numerical values used for the weight parameters C_i. We aimed to calibrate the weight parameters such that the optimal solutions were not in an 'on' state for prolonged periods of time.

In Figure 4.8 we gathered three different optimal control treatments for osteoporosis. In the first row, we put osteoclast and osteoblast evolution over time and in the second row the corresponding treatment schedule for bisphosphonate, TGFβ input, and Wnt input. In the third column of the first row, we put the phase plot to better appreciate the changes in the oscillatory behavior. We observe in Figure 4.8 that, for the three strategies, the ratio between osteoclasts and osteoblasts is close to 1 as imposed in the cost functional. This is more readily seen in the third column where the phase plot is presented, and it is important since we expect a balanced levels of OCs and OBs in order to get balanced bone resorption and bone formation. It is interesting to realize that the bisphosphonates and Wnt therapies complement each other –when one treatment is 'on' the other is 'off'– while minimizing the use of both treatments (*Strategies* **A** and **B**). In other words, in **A** there is a prolonged intermittent bisphosphonates application while Wnt input is reduced, and the opposite happens in **B**. On the other hand, TGFβ and Wnt therapies (*Strategy* **C**) have a synergy in relation to the optimal scheduling; they turn 'on' and 'off' together as intermittent therapies.

Comparing the effectiveness and deciding which of the optimal solutions between each other is difficult because changing the weight parameters C_i may change the behavior of the optimal controls. For the three *Strategies* presented here, we observe that each one has a different aim dictated by C_4 (the difference between OCs and OBs levels) and C_5 (OCs levels). More precisely, recall that the terms C_4 and C_5 in the cost functional (4.29) appear as $C_4(x_C - x_B)^2$ and $C_5(x_C - 1)^2$. Thus, higher values of C_4 and C_5 drive the optimal solution to (i) make x_C close to x_B and (ii) x_C close to 1. Baring this in mind, note that *Strategy* **A** focuses more on making x_C close to 1 because $C_5 > C_4$. On the other hand, *Strategy* **B** emphasizes the control over the ratio OCs/OBs, making x_C close

to x_B, because $C_4 > C_5$. Finally, *Strategy* **C** normalizes the relative importance of these elements by putting $C_4 = C_5 = 1$.

As observed in the OCs vs OBs plots, the three strategies have a reasonable performance in terms of controlling the amplitudes of the periodic solutions of OCs and OBs. It would be interesting to propose a more rigorous approach with experimental-derived weight parameters to perform a comparative cost-effectiveness analysis among different combination therapies.

4.3.2 Bone metastasis treatment

As mentioned in Section 4.2, the metastatic bone disease originates from cancer cells perturbing the bone remodeling process. In particular, cancer cells deceive bone cells through a vicious cycle in order to get cytokines such as TGFβ. As such, intense research has been focused on finding strategies to slow down the bone metastatic colonization. One of the proposed potential therapy to face metastatic bone disease is precisely the inhibition of TGFβ (Cook et al., 2016).

Like many other cancer diseases, the metastatic bone disease poses a huge multidisciplinary endeavor towards the quality of life of the patient (Mundy, 2002; Krzeszinski & Wan, 2015). Particularly, bone metastasis implies the undesirable increase of bone resorption or bone deposition. As such, anti-resorptive or anti-catabolic treatments are often recommended together with neoadjuvant chemotherapy (Coelho et al., 2016; Camacho & Pienta, 2014).

Here, we will incorporate TGFβ inhibition and chemotherapy to the previously introduced bisphosphonates and Wnt injection treatments. Consider now the bone metastasis model (4.15)–(4.19) introduced in Section 4.2. We associated the baseline parameters to a metastatic bone disease where the tumor has an inherent slow proliferation rate but TGFβ levels have an important positive effect on the tumor, see Section 4.2.1 and Figure 4.5. Let u_{bis} and u_{wnt} be two control functions that model the impact of bisphosphonates and Wnt induction in the bone remodeling process, respectively. We propose the following modification to the original bone remodeling system (4.3)–(4.6):

$$
\begin{cases}
\dfrac{dx_C}{dt} = \alpha_C \left(1 - K_C \dfrac{x_M}{K_M}\right) x_B^{-1} - \beta_C x_C - \beta_{CT} x_C x_T + \alpha_{CM} x_M \\
\qquad\qquad - u_{bis} x_C, & (4.31) \\
\dfrac{dx_B}{dt} = \alpha_{BW} x_B x_W - \beta_B x_B, & (4.32) \\
\dfrac{dx_T}{dt} = \alpha_T x_C - \beta_T x_T - \underbrace{u_{tg2} x_T}_{TGF\beta\ inhi.}, & (4.33) \\
\dfrac{dx_W}{dt} = \alpha_W \left(1 - K_B \dfrac{x_M}{K_M}\right) x_T x_C - \beta_W x_W + u_{wnt}, & (4.34) \\
\dfrac{dx_M}{dt} = (\alpha_M + \alpha_{MT} x_T) x_M \left(1 - \dfrac{x_M}{K_M}\right) - \underbrace{u_{chem} x_M}_{chemo.}, & (4.35)
\end{cases}
$$

The optimal control problem will have the following objectives:

1. Minimize the use of treatments u_{bis}, u_{tg2}, u_{wnt} and u_{chem}.

Strategy	u_{bis}?	C_1	u_{tg2}?	C_2	u_{wnt}?	C_3	u_{chem}?	C_4	C_5	C_6
A1	✓	50	✓	0.25					1000	5
B1	✓	50			✓	100			1000	5
C1			✓	0.25	✓	100			1000	5
A2			✓	0.25			✓	7000	1000	5
B2					✓	50	✓	7000	1000	5
C2	✓	50	✓	0.25	✓	100	✓	5000	1000	10

Table 4.5: Summary of strategies explored for cancer-induced disease. Control functions without a check mark are regarded as zero functions.

2. Minimize the difference between the osteoclast and osteoblast levels.

3. Keep low values of cancer cell levels.

The cost functional associated to the bone metastasis treatment model (4.31)–(4.35) is proposed as follows:

$$J(u) = \int_0^{t_f} C_1 u_{bis} + C_2 u_{tg2} + C_3 u_{wnt} + C_4 u_{chem} + C_5 x_M^2 + C_6 (x_C - x_B)^2 dt. \tag{4.36}$$

As in the bone remodeling model, in the bone metastasis model we also require the control functions u to satisfy the following bounds:

$$0 \leq u_{bis}(t) \leq 0.5, \quad 0 \leq u_{tg2}(t) \leq 200, \quad 0 \leq u_{wnt}(t) \leq 5, \quad \leq u_{chem}(t) \leq 0.1.$$

For cancer-induced bone disease, we consider six control strategies classified into two broad groups: without chemotherapy and with chemotherapy.

- Without chemotherapy.
  - *Strategy* **A1**. Bisphosphonates (u_{bis}) to control osteoclast activity and TGFβ inhibition (u_{tg2}) to control cancer cell proliferation.
  - *Strategy* **B1**. Bisphosphonates (u_{bis}) and Wnt input (u_{wnt}) to control bone resorption.
  - *Strategy* **C1**. TGFβ inhibition (u_{tg2}) to control cancer cell proliferation and Wnt input (u_{wnt}) to promote osteoblast activation.
- With chemotherapy (u_{chem}).
  - *Strategy* **A2**. TGFβ inhibition (u_{tg2}) to control cancer cell proliferation.
  - *Strategy* **B2**. Wnt input (u_{wnt}) to promote osteoblast activation.
  - *Strategy* **C2**. All the aforementioned control functions.

In Table 4.5 we gathered these strategies and the corresponding numerical values used for the weight parameters C_i. Analogously as with the bone remodeling model, we calibrated the weight parameters such that the optimal solutions were not in an 'on' state for prolonged periods of time. Additionally, we penalized strongly the usage of chemotherapy ($C_4 \in 5000, 7000$) and the presence of cancer cells ($C_5 = 1000$). For the bone metastasis model, the weight parameter calibration is more difficult than the bone remodeling model,

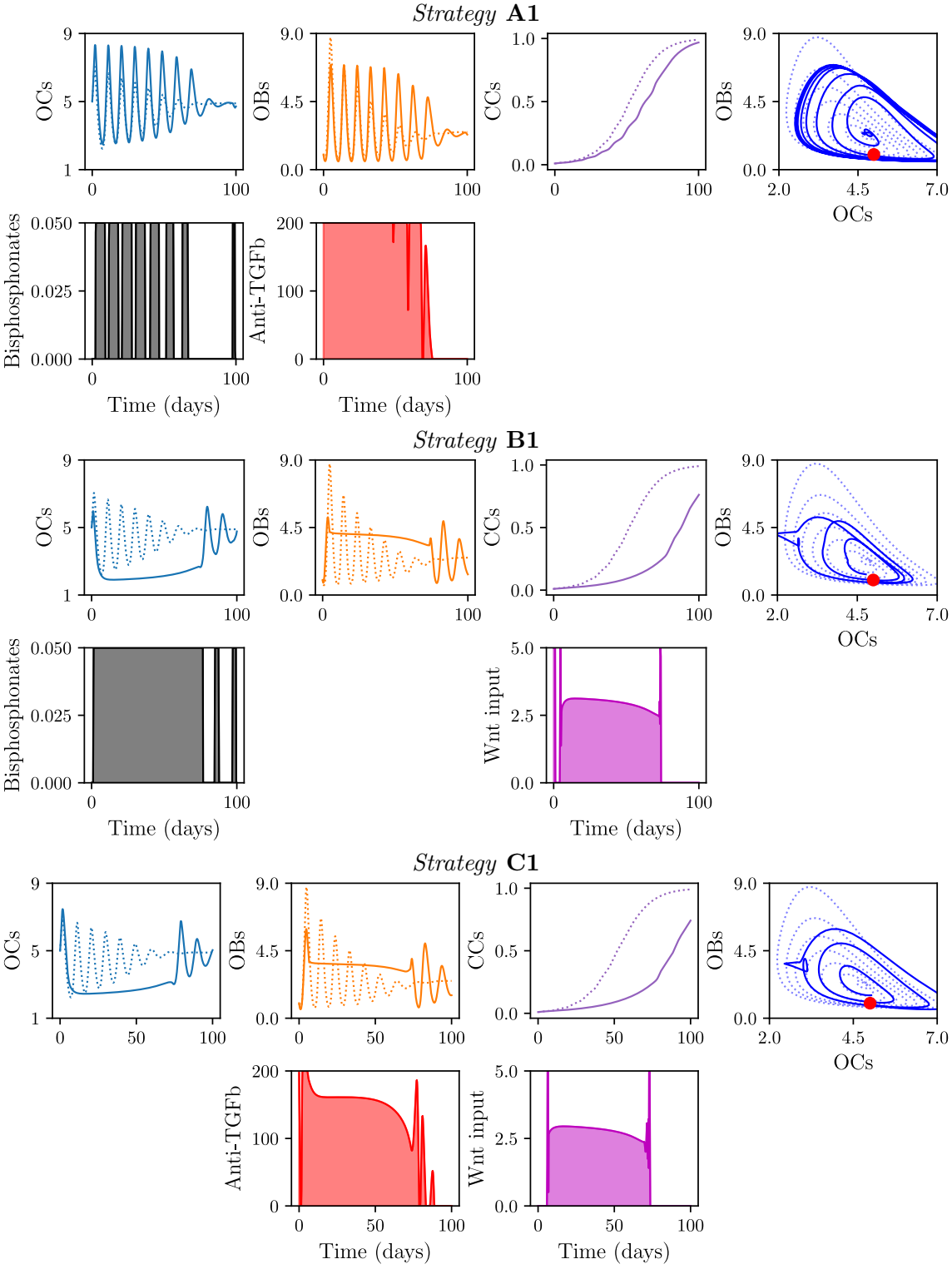

Figure 4.9: Bone metastasis treatments: strategies without chemotherapy. **Dashed lines** represent solutions without control. The **red dot** represents the initial condition $(x_C(0), x_B(0))$.

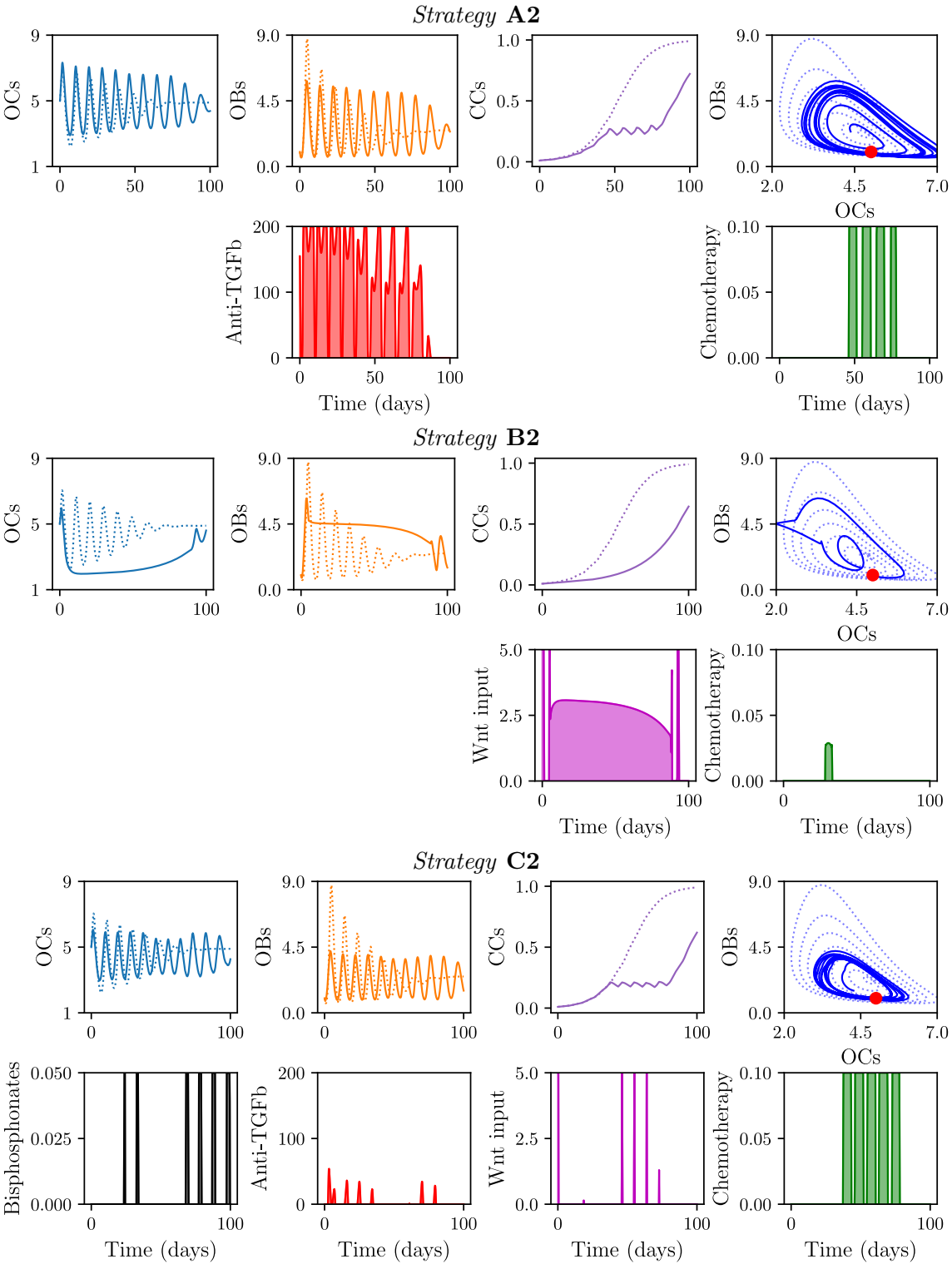

Figure 4.10: Bone metastasis treatments: strategies with chemotherapy. **Dashed lines** represent solutions without control. The **red dot** represents the initial condition $(x_C(0), x_B(0))$.

and so there are still some optimal solutions that remain in an 'on' state for a considerable amount of time.

As in the bone remodeling model, we expect bang-bang solutions with the possibility of singular arcs. We gathered some numerical simulations in Figure 4.9 (no-chemotherapy combination therapy) and in Figure 4.10 (chemotherapy included). It is interesting to observe in Figure 4.9 that some chemotherapy-free combined therapies may present a significant impact on cancer growth. In the case of *Strategy* **A1** (bisphosphonate + TGFβ inhibition), cancer progression is slowed down weakly but an oscillatory bone remodeling process is recovered. Next, in *Strategy* **B1** (bisphosphonate + Wnt input) we can observe a more significant decrease in cancer proliferation. Finally, *Strategy* **C1** (TGFβ inhibition + Wnt input) presents a similar behavior as the previous *Strategy*.

Combining chemotherapy with bone-related therapies may have a better performance than chemotherapy-free treatments, as seen in Figure 4.10. In *Strategy* **A2** (TGFβ inhibition + chemotherapy) the optimal solution allows a prolonged intermittent inhibition of TGFβ and also a brief intermittent use of chemotherapy. Besides the decrease of cancer proliferation, we can also observe a decrease in the amplitude of the oscillatory bone cell dynamics. In *Strategy* **B2** (Wnt input + chemotherapy) the optimal solution relies strongly upon the singular arc solution of Wnt application, leaving the chemotherapy use practically shut down except for a short time window. Finally, in *Strategy* **C2** we incorporated the four control functions. Note that we also increased C_6 from 5 to 10. Observe that the four control functions in this *Strategy* present an intermittent behavior. This *Strategy* presents a significant reduction in cancer proliferation and also a more controlled bone remodeling process.

In contrast to the bone remodeling-osteoporosis model, it is more feasible to compare the different *Strategies* for metastatic bone disease. This is due to the preservation of the weight parameters C_i across almost every *Strategy*, with differences in *Strategy* **B2** with C_3, and the all-in *Strategy* C_2 with C_4 and C_6. We noted that Wnt therapy has an important contribution in controlling the metastatic bone disease, suggesting further experimental research towards assessing the feasibility of combining Wnt therapy with conventional therapies. *Strategy* **C2** have the best qualitative performance in terms of controlling cancer cell proliferation while alleviating the osteolytic lesion as it is seen in the OCs vs OCs plot. Overall, these and the numerical simulations for osteoporosis point out that optimal timing and dose fraction are important but they are not easy to compute. Further experimental, theoretical and numerical analyses are needed in order to search for optimal and robust personalized combination therapies.

Discussions

In this Chapter, we presented two new mathematical models to study bone in health and in disease. The first mathematical model focused on the bone cells, osteoclasts and osteoblasts, and two remarkable molecular coupling agents, TGFβ and Wnt proteins. The model was further extended to consider bone metastatic cancer cells in a second mathematical model which was motivated by the observation that bone metastasis perturbs the bone remodeling crosstalk, favoring the cancer growth and bone cells unbalance.

For each corresponding mathematical model, we found the corresponding equilibrium points and performed a numerical local stability analysis. We identified the appearance of oscillatory coupling between osteoclasts and osteoblasts. This oscillatory behavior comes from the emergence of a Hopf bifurcation, which was found through numerical exploration. This discovery sheds some light in regards to the existence of oscillations in the bone remodeling process and the possible mechanisms responsible for them.

Analogously, we presented a brief steady-state analysis for the bone metastasis model. We found that parameters associated with the interference of bone cells crosstalk from cancer cells –corruption of the RANKL/OPG regulatory pathway, for instance– have strong effects on the solution dynamics. In particular, inhibition of the Wnt signaling from cancer cells have a dual negative effect on the bone: it increases osteoclasts and decreases osteoblasts. Also, we found that cancer invasion in the bone changes the qualitative behavior of the bone cell dynamics. Bone metastasis cells have the ability to delay the Hopf bifurcation appearance. This fact translates in expecting that bone metastasis returns back the osteoclast and osteoblast dynamics into a latent, non-oscillatory behavior.

Finally, we proposed an optimal control problem to each corresponding mathematical model. The aim of the optimal control framework is to minimize undesirable quantities of the system and maximize desirable ones while minimizing the use of external input. In the context of bone remodeling, we modeled bisphosphonates, TGFβ input and Wnt therapy as control functions to tackle osteoporosis disease. In the context of bone metastasis, we considered bisphosphonates and Wnt, and also TGFβ inhibition and chemotherapy. In both optimal control problems, one of the main objectives was to control the osteoclast to osteoblast ratio.

In the next and final Chapter, we motivate and propose spatial mathematical models. We present preliminary theoretical and numerical results and point out relevant questions to be addressed in the future.

Chapter 5

Spatial modeling of bone remodeling and bone metastasis

A basic multicellular unit (BMU) is a group of bone cells that acts temporarily on a certain region of the bone matrix to carry out the so-called remodeling process (Parfitt, 2002). BMUs couple two antagonistic mechanisms: remodeling starts with bone resorption due to osteoclasts and it is followed by osteoblasts-mediated bone formation. Complex biochemical and cell-cell interactions regulate the activity of the BMU (Chen et al., 2018). When some of the regulatory pathways fail, an imbalance between resorption and formation of bone matrix leads to fragile bone structures. Osteoporosis is an example of such failures.

In vivo experiments aimed to study bone metastasis are difficult to elaborate. Several mathematical models have been developed in order to understand more about the dynamics of the BMU in bone remodeling (Kroll, 2000; Komarova et al., 2003; Lemaire et al., 2004; Pivonka et al., 2008; Ji et al., 2012). Recently, some of those models have been extended to study a variety of phenomena that involves the dysfunction of the bone remodeling process. In particular, bone metastasis mathematical models have been constructed and analyzed (Ayati et al., 2010; Wang et al., 2011; Coelho et al., 2016; Farhat et al., 2017).

We will consider transforming growth factor-β (TGFβ) as a key agent in the bone metastasis dynamics. This factor is released from the bone matrix by osteoclast resorption. It is known that this factor has a multitude of effects on bone cell dynamics. In particular, the activation of TGFβ by osteoclasts stops osteoclastogenesis, thus diminishing osteoclast resorption, and also it has the potential to induce migration of osteoblast precursors to the resorbed area, stimulate their proliferation and promote their differentiation (Juárez & Guise, 2011). It is hypothesized that TGFβ induces the expression of Wnt1 from active osteoclasts, and Wnt1 is the major responsible for osteoblast differentiation at the resorbed area rather than TGFβ alone (Weivoda et al., 2016). Another important chemotactic factor is RANKL which it has been shown to promote osteoclasts and RANK-expressing cancer cells migration to resorbed areas at which they will try to establish a vicious cycle (Jones et al., 2006).

As pointed out in Ryser et al. (2010); Buenzli et al. (2011); Graham et al. (2012), the BMU dynamics is regulated not only by means of densities of the cytokines but also by the spatial distribution of these. The main approaches to tackle spatial modeling problems are partial differential equations (PDEs) and agent-based models (ABMs). Recently, in Araujo et al. (2014) and Cook et al. (2016) an ABM is developed with the objective of

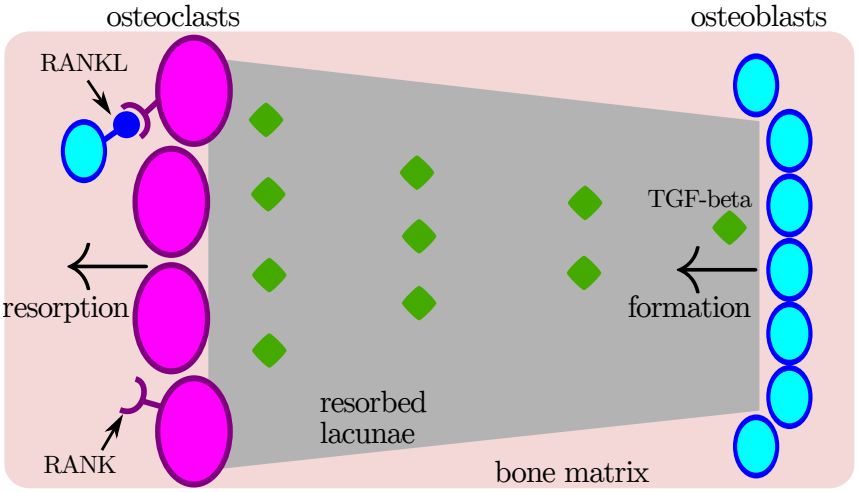

Figure 5.1: Schematic representation of spatial bone remodeling (up) and bone metastasis (down) processes.

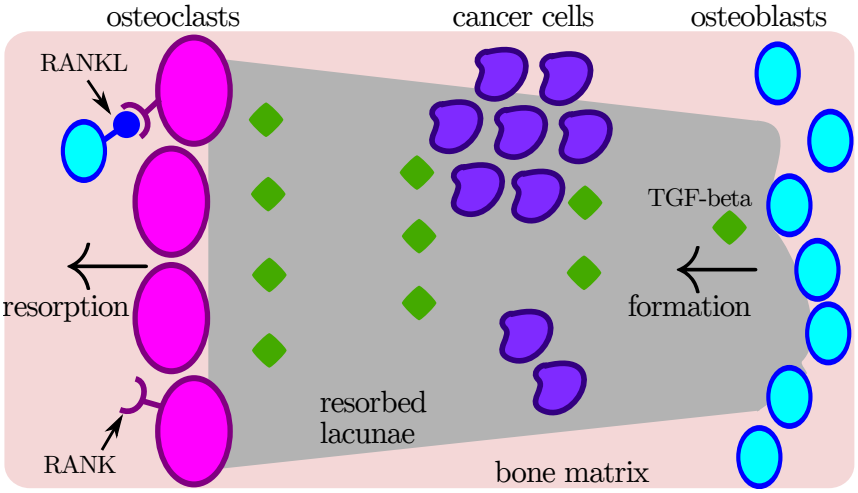

Figure 5.2: Schematic representation of spatial bone remodeling (up) and bone metastasis (down) processes.

studying prostate cancer bone metastasis. It is predicted that TGFβ inhibition helps in a preventive scenario more than in an invasion one. To our knowledge, only two works address the study of mathematical model bone cancer-mediated disease using PDEs: Ayati et al. (2010) in which multiple myeloma bone disease is studied through diffusion, and Ryser et al. (2012) in which RANKL and OPG are considered as explicit variables and the principal movement component is chemotaxis. Following Ryser et al. (2012), in this Chapter, we will study the spatial dynamics of bone metastases taking into consideration the main cells and the key biochemical agents. The main difference with Ryser et al. (2012) is that we are going to consider TGFβ concentrations as an important state variable.

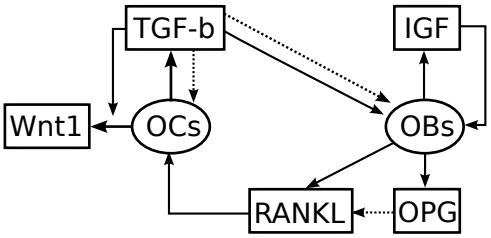

Figure 5.3: Key players in normal bone remodeling.

5.1 Spatial bone remodeling model: no cancer scenario

Let $u_1(t)$ denote the number of osteoclasts at time t and $u_2(t)$ the number of osteoblasts. Our model is based upon the base biochemical-simplified model showed in Section 1.1.2:

$$\frac{du_1}{dt} = \alpha_1 u_1^{g_{11}} u_2^{g_{21}} - \beta_1 u_1, \tag{5.1}$$

$$\frac{du_2}{dt} = \alpha_2 u_1^{g_{12}} u_2^{g_{22}} - \beta_2 u_2. \tag{5.2}$$

The exponent parameters try to codify the biochemical communication between cells. Specifically, g_{ij} represents the net effectiveness of the autocrine or paracrine signalings from cells of population u_j on the proliferation rate of population u_i. For instance, the major bone remodeling pathway, the RANK/RANKL/OPG pathway, is codified in the exponent g_{21} since RANKL and OPG are cytokines produced by osteoblasts that regulate osteoclasts promotion or inhibition (Komarova et al., 2003).

In Ryser et al. (2010), a spatial model for bone remodeling is presented. The authors follow a biochemical-simplified model extension with osteoclast and osteoblast densities. Further, they include concentrations of RANKL and OPG as state variables of their system. Because of that, they decide to drop out the exponent g_{21}, the paracrine effects of osteoblasts on osteoclasts. They also consider the exponent $g_{22} = 0$ under the assumption that autocrine effects of osteoblasts are negligible with respect g_{12}.

Here the proposed model is given by:

$$\text{(OCs)} \quad \frac{\partial u_1}{\partial t} = \underbrace{\alpha_1 u_1 u_2^{g_1}}_{\text{RANK/RANKL/OPG}} - \underbrace{\beta_1 u_1}_{\text{apoptosis}} - \underbrace{A_1 \frac{\partial u_1}{\partial x}}_{\text{advection}} - \underbrace{D_1 \frac{\partial^2 u_1}{\partial x^2}}_{\text{diffusion}}, \tag{5.3}$$

$$\text{(OBs)} \quad \frac{\partial u_2}{\partial t} = \underbrace{\alpha_2 u_1^{g_2} u_2}_{\text{TGF}\beta\text{, IGF}} - \underbrace{\beta_2 u_2}_{\text{apop. or osteo.}} - \underbrace{A_2 \frac{\partial u_2}{\partial x}}_{\text{advection}} - \underbrace{D_2 \frac{\partial^2 u_2}{\partial x^2}}_{\text{diffusion}}. \tag{5.4}$$

5.1.1 Existence of solutions

In Section 1.3, we presented the formulation of parabolic problems. In this Chapter, we restrict ourselves to one spatial dimension with $\Omega = (0, 1)$ and $T = 1000$. Note that this implies that $D_T = (0, 1000] \times (0, 1)$ and $S_T = (0, 1000] \times \{0, 1\}$ in (1.12)–(1.14). The advection-diffusion operator that we use here is

$$L = a \frac{\partial}{\partial x^2} + b \frac{\partial}{\partial x}$$

where a and b are fixed vectors. Additionally, we use only Dirichlet boundary conditions which are obtained by putting $\alpha_0 \equiv 0$ in (1.13).

Also, in Section 1.3 we presented theoretical results that guarantee the existence and uniqueness of solutions through upper and lower solutions. This is done by the Monotone Method. The reader is referred to Section 1.3 to recall the notation, and also to Theorem 1.6 to recall existence and uniqueness of coupled parabolic quasimonotone problems.

Theorem 5.1. *There exist solutions for model* (5.3)–(5.4).

Proof 1. The proof is based on the preliminary theory presented in Section 1.3.3. For model (5.3)–(5.4), the operator L is given by:

$$L(t,x) = \left(D_1 \frac{\partial^2}{\partial x^2} - A_1 \frac{\partial}{\partial x}, D_2 \frac{\partial^2}{\partial x^2} - A_2 \frac{\partial}{\partial x} \right) \tag{5.5}$$

with $D_1,\ D_2 > 0$. To assess the mixed quasimonotony of the reaction function (see Section 1.3.3) of model (5.3)–(5.4), we check the following relationships:

$$\begin{aligned} \frac{\partial}{\partial u_2} f_1(u_1,u_2) &= \alpha_1 g_1 u_1 u_2^{g_1-1} < 0 \quad \text{for fixed } u_1, \\ \frac{\partial}{\partial u_1} f_2(u_1,u_2) &= \alpha_2 g_2 u_1^{g_2-1} u_2 > 0 \quad \text{for fixed } u_2, \end{aligned}$$

where $f = (f_1, f_2)$ is the reaction function of the model (5.3)–(5.4).

In order to employ the Monotone Method Theorem, we must find coupled upper and lower solutions $\widetilde{u}_i$, $\widehat{u}_i$ for $i = 1, 2$ that satisfy the following relationships (see Section 1.3.3):

$$\frac{\partial}{\partial t}\widetilde{u}_1 - D_1 \frac{\partial^2}{\partial x^2}\widetilde{u}_1 + A_1 \frac{\partial}{\partial x}\widetilde{u}_1 \geq \alpha_1 \widetilde{u}_1 \widehat{u}_2^{g_1} - \beta_1 \widetilde{u}_1, \tag{5.6}$$

$$\frac{\partial}{\partial t}\widetilde{u}_2 - D_2 \frac{\partial^2}{\partial x^2}\widetilde{u}_2 + A_2 \frac{\partial}{\partial x}\widetilde{u}_2 \geq \alpha_2 \widetilde{u}_2 \widetilde{u}_1^{g_2} - \beta_2 \widetilde{u}_2, \tag{5.7}$$

$$\frac{\partial}{\partial t}\widehat{u}_1 - D_1 \frac{\partial^2}{\partial x^2}\widehat{u}_1 + A_1 \frac{\partial}{\partial x}\widehat{u}_1 \leq \alpha_1 \widehat{u}_1 \widetilde{u}_2^{g_1} - \beta_1 \widehat{u}_1, \tag{5.8}$$

$$\frac{\partial}{\partial t}\widehat{u}_2 - D_2 \frac{\partial^2}{\partial x^2}\widehat{u}_2 + A_2 \frac{\partial}{\partial x}\widehat{u}_2 \leq \alpha_2 \widehat{u}_2 \widehat{u}_1^{g_2} - \beta_2 \widehat{u}_2. \tag{5.9}$$

To find suitable functions $\widetilde{u}_i$, $\widehat{u}_i$, let us assume that $\widetilde{u}_1$, $\widehat{u}_1$, $\widetilde{u}_2$ and $\widehat{u}_2$ are constant functions. These two assumptions lead to the following system of inequalities:

$$0 \geq \alpha_1 \widetilde{u}_1 \widehat{u}_2^{g_1} - \beta_1 \widetilde{u}_1, \tag{5.10}$$

$$0 \geq \alpha_2 \widetilde{u}_2 \widetilde{u}_1^{g_2} - \beta_2 \widetilde{u}_2, \tag{5.11}$$

$$0 \leq \alpha_1 \widehat{u}_1 \widetilde{u}_2^{g_1} - \beta_1 \widehat{u}_1, \tag{5.12}$$

$$0 \leq \alpha_2 \widehat{u}_2 \widehat{u}_1^{g_2} - \beta_2 \widehat{u}_2. \tag{5.13}$$

From (5.10), if we propose:

$$\widehat{u}_2(t,x) \leq \left(\frac{\beta_1}{\alpha_1} \right)^{1/g_1}, \tag{5.14}$$

then (5.6) is satisfied.

From (5.13), if we propose:

$$\widehat{u}_1(t,x) \geq \left(\frac{\beta_2}{\alpha_2}\right)^{1/g_2} \tag{5.15}$$

then (5.9) is satisfied. Thus, we have found suitable lower solutions $\widehat{u}_i$.

From (5.12), if we propose:

$$\widetilde{u}_2(t,x) \geq \left(\frac{\beta_1}{\alpha_1}\right)^{1/g_1} \tag{5.16}$$

then (5.8) is satisfied.

Finally, from (5.11), if we propose:

$$\widetilde{u}_1(t,x) \leq \left(\frac{\beta_2}{\alpha_2}\right)^{1/g_2} \tag{5.17}$$

then (5.7) is satisfied. Thus, we have found suitable upper solutions $\widetilde{u}_i$. This finish the proof. However, notice from (5.15) and (5.17) that, since $\widehat{u}_1(t,x) \leq \widetilde{u}_1(t,x)$, then $\widehat{u}_1(t,x) = \widetilde{u}_1(t,x)$. □

Proof 2.

Following the same procedure as before, if we only assume that $\widehat{u}_1(t,x)$ and $\widetilde{u}_1(t,x)$ are constant functions, and further assume that the lower solution $\widehat{u}_1(t,x) \equiv 0$, then we may define implicitly the upper solution $\widetilde{u}_2$ and the lower solution $\widehat{u}_2$ as the solutions of the uncoupled system given by:

$$\frac{\partial}{\partial t}\widetilde{u}_2 - D_2\frac{\partial^2}{\partial x^2}\widetilde{u}_2 + A_2\frac{\partial}{\partial x}\widetilde{u}_2 = \alpha_2\widetilde{u}_2\widetilde{u}_1^{g_2} - \beta_2\widetilde{u}_2, \tag{5.18}$$

$$\frac{\partial}{\partial t}\widehat{u}_2 - D_2\frac{\partial^2}{\partial x^2}\widehat{u}_2 + A_2\frac{\partial}{\partial x}\widehat{u}_2 = -\beta_2\widehat{u}_2. \quad \square \tag{5.19}$$

5.1.2 Numerical simulations

In Figure 5.4 a normal remodeling simulation is shown. It is noteworthy to mention that osteoblasts were assumed to not have advection; however, the diffusion part makes them follow the path predefined by the osteoclasts wave that always goes first (that is, it appears before the osteoblast wave). This spatial section is remodeled three times, where a remodeling cycle is counted as the appearance of the OCs and the OBs waves. It can be noted that subsequent remodeling waves diminish progressively. Also, the second and third remodeling waves can be associated as two BMUs that make bone remodeling on the same location, where one of the BMUs comes from the left and the other from the right. This could be a mechanism of performing a more delicate bone remodeling in the section.

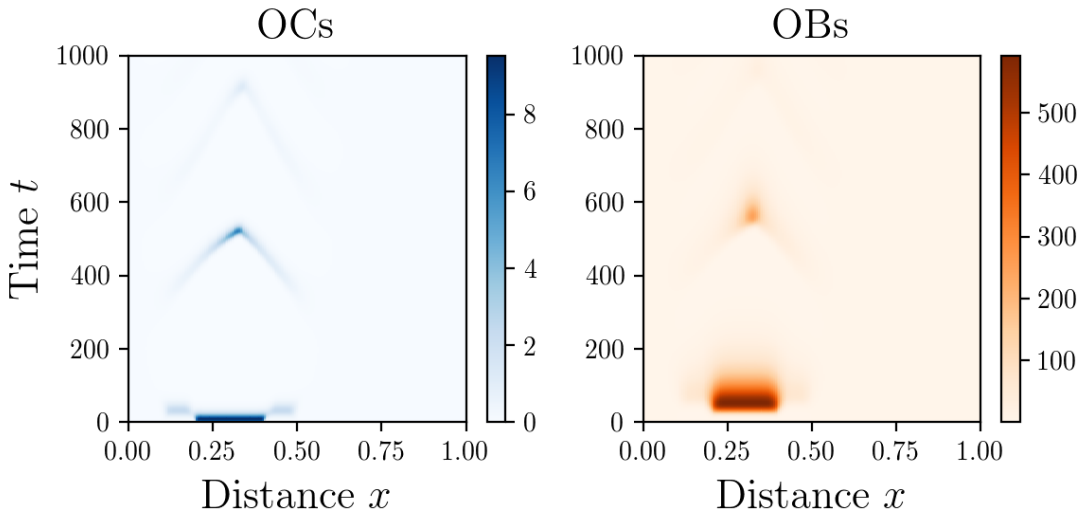

Figure 5.4: Spatial bone remodeling. BMU parameters are taken from Table 1.4. Spatial parameters are: $A_1 = 1.0 \times 10^{-4}$, $A_2 = 0$, $D_1 = 1.0 \times 10^{-6}$ and $D_2 = 2D_1$.

5.2 Spatial bone metastasis model

In this Chapter, we are concerned about including a spatial variable in a biochemical-simplified extension due to its importance to bone remodeling and bone metastasis dynamics, as pointed out in the introduction. We first focus on a model at a cellular level and then propose a cellular-molecular spatial model.

Due to its nature, TGFβ can be considered as an autocrine and paracrine factor produced by osteoclasts. That is, its effects are coded in the exponents g_{11} and g_{12}. As seen in the previous Chapter, TGFβ and Wnt have an important contribution to the coupling between osteoclasts and osteoblasts. Thus, we extend spatially the model presented in Chapter 4.

Let $u_3(t,x)$ the number of cancer cells, $u_{\mathrm{TG}}(t,x)$ the concentration of TGFβ and $u_{\mathrm{W}}(t,x)$ the concentration of Wnt at time t and location x. Let us extend also $u_1(t)$ and $u_2(t)$ to the spatial domain by $u_1(t,x)$ and $u_2(t,x)$.

5.2.1 Diffusion-reaction cellular level model

Following Ayati et al. (2010), we propose to extend the previous model from Chapter 2 spatially by adding diffusion:

$$\text{(OCs)}\quad \frac{\partial u_1}{\partial t} = \underbrace{\alpha_1 u_1 u_2^{g_1}}_{\text{RANK/RANKL/OPG}} - \underbrace{\beta_1 u_1}_{\text{apoptosis}} + \underbrace{\sigma_1 u_1 u_3}_{\text{promotion by cancer}} + \underbrace{D_1 \frac{\partial^2 u_1}{\partial x^2}}_{\text{diffusion}}, \tag{5.20}$$

$$\text{(OBs)}\quad \frac{\partial u_2}{\partial t} = \underbrace{\alpha_2 u_2 u_1^{g_2}}_{\text{TGF}\beta/\text{Eph}} - \underbrace{\beta_2 u_2}_{\text{apoptosis}} + \underbrace{\sigma_2 u_2 u_3}_{\text{effects of cancer}} + \underbrace{D_2 \frac{\partial^2 u_2}{\partial x^2}}_{\text{diffusion}}, \tag{5.21}$$

$$\text{(CCs)} \quad \frac{\partial u_3}{\partial t} = \underbrace{\alpha_3 u_3 \left(1 - \frac{u_3}{K}\right)}_{\text{logistic growth}} + \underbrace{\sigma_3 u_1 u_3}_{\text{TGF}\beta} + \underbrace{D_3 \frac{\partial^2 u_3}{\partial x^2}}_{\text{diffusion}}. \tag{5.22}$$

5.2.1.1 Numerical simulations

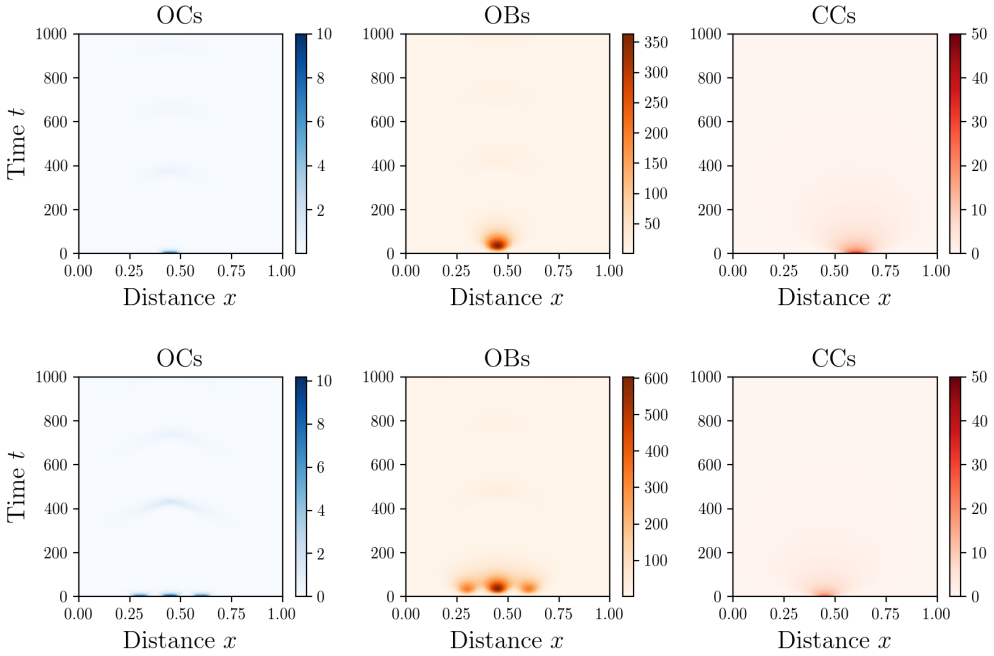

Figure 5.5: Spatial bone metastasis. BMU parameters are taken from Table 1.4. Bone metastasis parameters are taken from Table 2.1, *Periodicity 1.* Spatial parameters are: $A_1 = A_2 = 0$, $D_1 = 1.0 \times 10^{-5}$, $D_2 = 2D_1$ and $D_3 = 10D_1$.

For the sake of modeling different spatial initial configurations, we focus on two initial condition sets:

(*IC1*) Center $c = 0.3$, radius $r = c/8$,

$$u_1(0,x) = \begin{cases} 10, & x \in (c+3r, c+5r) \\ u_1^*, & \text{otherwise} \end{cases}$$

$$u_2(0,x) = \begin{cases} 5, & x \in (c+3r, c+5r) \cup (c+7r, c+9r) \\ u_2^*, & \text{otherwise} \end{cases}$$

$$u_3(0,x) = \begin{cases} 50, & x \in (c+7r, c+9r) \\ 0, & \text{otherwise} \end{cases}$$

(*IC2*) Center $c = 0.3$, radius $r = c/8$,

$$u_1(0,x) = \begin{cases} 10, & x \in (c-r, c+r) \cup (c+3r, c+5r) \cup (c+7r, c+9r) \\ u_1^*, & \text{otherwise} \end{cases}$$

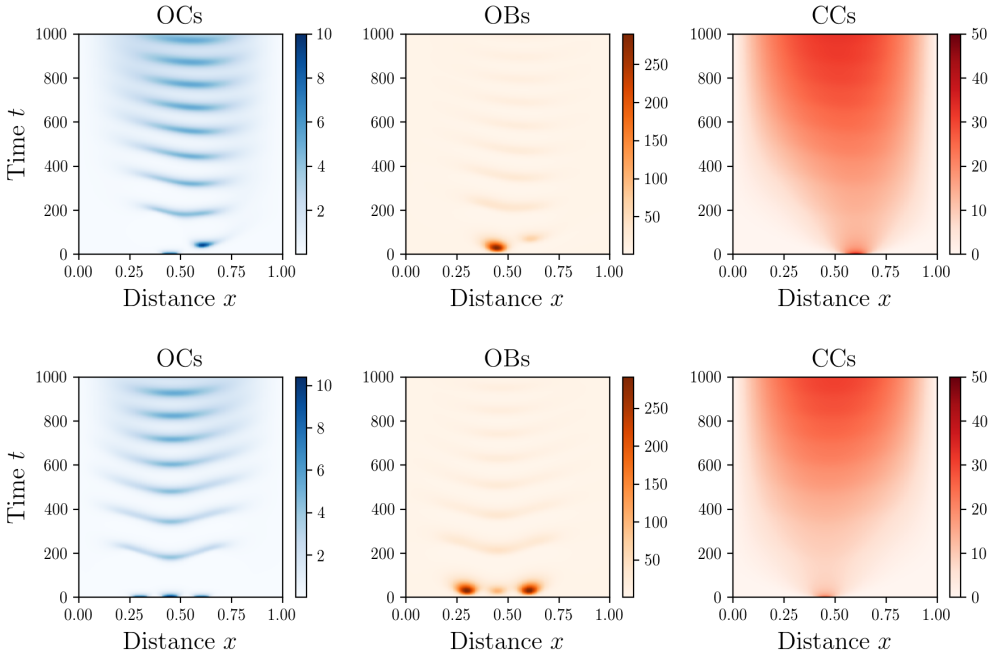

Figure 5.6: Spatial bone metastasis. BMU parameters are taken from Table 1.4. Bone metastasis parameters are taken from Table 2.1, *Mixed Lesion*. Spatial parameters are: $A_1 = A_2 = 0$, $D_1 = 1.0 \times 10^{-5}$, $D_2 = 2D_1$ and $D_3 = 10D_1$.

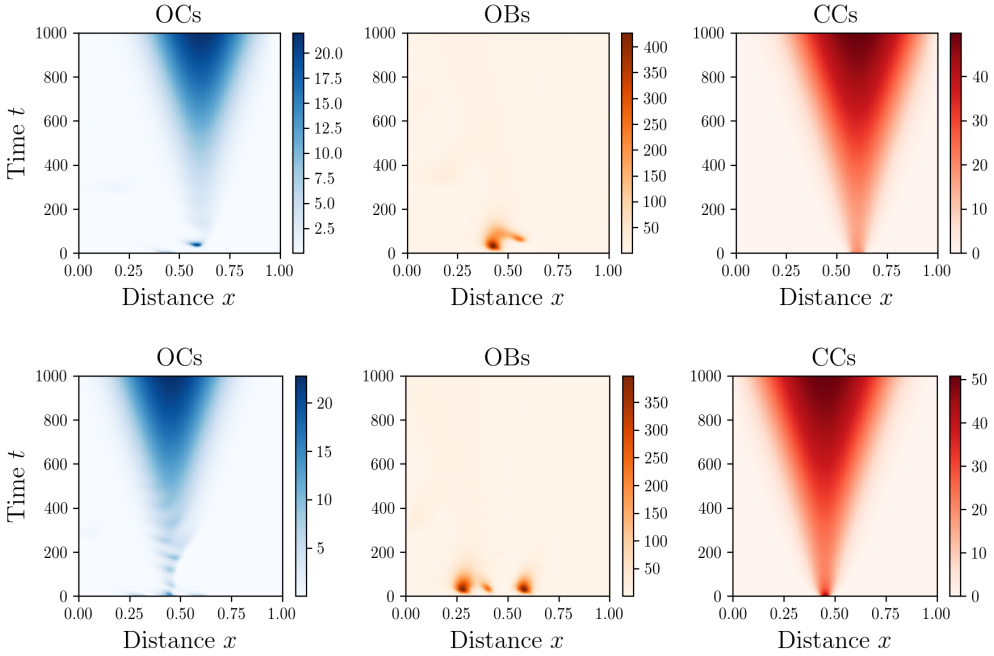

Figure 5.7: Spatial bone metastasis. BMU parameters are taken from Table 1.4. Bone metastasis parameters are taken from Table 2.1, *Osteolytic Lesion*. Spatial parameters are: $A_1 = -2.0 \times 10^{-3}$, $A_2 = 0$, $D_1 = 1.0 \times 10^{-6}$, $D_2 = 5D_1$ and $D_3 = 10D_1$.

Figure 5.8: QR code to watch the previous figures in video format.

$$u_2(0,x) = \begin{cases} 5, & x \in (c-r, c+r) \cup (c+3r, c+5r) \cup (c+7r, c+9r) \\ u_2^*, & \text{otherwise} \end{cases}$$

$$u_3(0,x) = \begin{cases} 50, & x \in (c+1.5r, c+2.5r) \\ 0, & \text{otherwise} \end{cases}$$

Recall that (u_1^*, u_2^*) refers to the steady-state of the bone remodeling base model presented in Section 1.1.2, see also (1.3).

In Figure 5.5 the *Periodicity 1* case (Chapter 2, Table 2.1) is showed. We obtain a similar qualitative behavior as with the temporal model. We observe that cancer cells are eliminated progressively, whereas the spatial bone remodeling shown previously in Figure 5.4 is recovered. this is seen in both initial condition sets *(IC1)* and *(IC2)* with differences in the amplitude of bone cell populations.

In Figures 5.6 and 5.7 we show the metastatic invasion scenarios *Mixed Lesion* and *Osteolytic Lesion* (Chapter 2, Table 2.1). In Figure 5.6 we note that the initial cancer cell population decreases at early progression stages, but then the osteoclast-mediated bone resorption is hijacked by the diffused cancer cells which aids cancer progression. Osteoblast population gets inhibited when cancer cell population increases. Osteoclast population presents a notorious increase in the appearance of successive resorption waves. In Figure 5.7 we observe a more adverse scenario. Osteoblast population is inhibited in a short time. Cancer cell population maintain at the beginning a steady population level and then show a sustained proliferation. Finally, in this case, the osteoclast population does not show an oscillatory behavior but rather a progressive increase in its population levels.

5.2.2 Advection-diffusion-reaction cellular-molecular model

As a first step to model the spatial dynamics of bone metastasis, we are going to consider the folowing simplest case. Osteoclasts an osteoblasts only move spatially by advection, that is, following a predefined direction. For example, we can consider an horizontal movement from right to left of these cell populations. Cancer cells and TGFβ will have a diffusive movement. We propose then the following model:

$$\text{(OCs)} \quad \frac{\partial u_1}{\partial t} = \alpha_C \underbrace{\left(1 - K_C \frac{u_3}{K_M}\right)}_{\textit{OCs-OBs decoup.}} u_2^{-1} - \beta_C u_1 - \beta_{CT} u_1 u_{TG} + \underbrace{\alpha_{CM} u_3,}_{\textit{Cancer prom.}} - \underbrace{A_1 \nabla u_1}_{\text{advection}}, \tag{5.23}$$

$$\text{(OBs)} \quad \frac{\partial u_2}{\partial t} = \alpha_{BW} u_2 u_W - \beta_B u_2 - \underbrace{A_2 \nabla u_2}_{\text{advection}}, \tag{5.24}$$

$$\text{(CCs)} \quad \frac{\partial u_3}{\partial t} = \Big(\underbrace{\alpha_M}_{\textit{Cancer proli.}} + \underbrace{\alpha_{MT} u_{TG}}_{\textit{TGF}\beta\textit{ prom.}} \Big) \underbrace{u_3 \left(1 - \frac{u_3}{K_M}\right)}_{\textit{logistic}} + \underbrace{D_3 \Delta u_3}_{\text{diffusion}}, \tag{5.25}$$

$$\text{(TGF}\beta\text{)} \quad \frac{\partial u_{TG}}{\partial t} = \alpha_T u_1 - \beta_T u_{TG} + \underbrace{D_{TG} \Delta u_{TG}}_{\text{diffusion}}, \tag{5.26}$$

$$\text{(Wnt)} \quad \frac{\partial u_W}{\partial t} = \alpha_W \underbrace{\left(1 - K_B \frac{u_3}{K_M}\right)}_{\textit{Wnt inhi.}} u_{TG} u_1 - \beta_W u_W + \underbrace{D_W \Delta u_W}_{\text{diffusion}}. \tag{5.27}$$

Discussions

In this Chapter, we developed spatial models to study bone remodeling and bone metastasis at a cellular and molecular level. Numerical experiments corroborate the importance of spatial dynamics on these two bone processes. Also, theoretical results of the temporal TGFβ model indicate that osteoblast recruitment and elimination rates are important to determine oscillatory behaviors; the equilibrium of TGFβ levels only depends on these two parameters. In other words, this temporal model predicts an important role of osteoblasts in the TGFβ dynamics. Further work is necessary to visualize numerical experiments for the TGFβ model and assess the relevance of its dynamics in a spatial context. Once the spatial dynamics is better understood, it would be interesting to assess if therapeutic strategies have different effects on the spatial models in comparison to the temporal models.

Conclusions and future work

The objective of this Thesis was to propose mathematical models that describe bone remodeling and the bone metastasis processes and identify key elements that originate bone diseases. Although several theoretical and numerical results were obtained, it is important to stress out that they should be contrasted with experimental data when they become readily available. This is a necessary feedback loop of paramount importance for every mathematical model to grasp the level of confidence in the descriptions given by the models proposed. Next, we condense the conclusions for each corresponding Chapter worked in this Thesis:

Chapter 2. In this chapter, we proposed a mathematical model based on a power-law approximations (S-Systems). The key feature is that we incorporate realistic hypotheses that couple cancer cell dynamics with the bone cell-related dynamics, filling a missing gap in the literature. Our base model is able to describe the different three types of bone diseases caused by bone metastasis: osteolytic lesion, osteoblastic lesion and mixed lesion. Numerical results validated and illustrated the cancer-free and cancer-invasion equilibrium solutions. We discovered with a numerical bifurcation analysis that there is a key coefficient for the change of stability of the equilibria and also for the existence of bifurcation points. As an important work for the future, we plan to make a parameter estimation based on quantitative experimental data rather than in qualitative data. Also, it may be interesting to check the prediction potential of the model with further experimental data.

Chapter 3. In this Chapter, we introduced control functions to model two treatments: denosumab and radiotherapy. The objective was to propose a modeling framework based on optimal control in which the use of control is not arbitrary. From the simulations, we found that inhibition of osteoclasts is not always the optimal answer, and it depends on the type of metastatic cancer residing in the bone microenvironment. As predicted, denosumab treatment poses a weak choice in terms of controlling the growth of the tumor in general. Radiation treatment has a higher potential than the previous one, but the effects on the bone cells still need to be analyzed, as well as the long-run side-effects and important economical cost that limit its applicability. A treatment that respects the natural microenvironment while attacking cancer cells would be more effective and desirable. It would be interesting to explore alternative treatment strategies by considering other potential control terms. For example, exploring a control function that halts interactions between cancer and osteoclasts and osteoblasts by inhibiting other key molecules rather than RANKL, like ILs or PTHrP. Whereas the optimal control framework is still used in numerous works, it prevails an urgent need to translate real quantitative data into the mathematical modeling language. The ultimate objective is to convert these types of models into predictive tools towards the development of patient-personalized treatments. Factors that need to be considered in extended works are, for instance, economic cost of

treatment, number of skeletal-related events and other side-effects of using the treatment, number of cells in a specific bone metastasis, and others. We visualize our results as a step forward to accomplish such objective.

Chapter 4. The base model, albeit its reduced number of parameters and mathematical tractability, is not able to answer questions related to particular biochemical agents. In this Chapter, we presented a new model that combines elements of biochemical-simplified and -detailed models. The emphasis is put in decoupling from the power-law approximation two key elements in bone remodeling: TGFβ and Wnt. These factors are not only important in bone remodeling but also they are suspect to have a relevant role in bone metastasis. Numerically, we identified the appearance of oscillatory coupling between osteoclasts and osteoblasts. However, the period of oscillation is different presented by the base model, and further experimental data must clarify which oscillatory behavior (if any) is more relevant. If the model is correct in describing bone remodeling process, the discovery of numerical oscillations sheds some light in regards to the existence of oscillations in the bone remodeling process and the possible mechanisms responsible for them. We also found that parameters associated with the interference of bone cells crosstalk from cancer cells have strong effects on the solution dynamics. In particular, inhibition of the Wnt signaling from cancer cells have a dual negative effect on the bone: it increases osteoclasts and decreases osteoblasts. This could be an interesting hypothesis to be tested in an experimental setting. We also found numerically that bone metastasis cells have the ability to delay the Hopf bifurcation appearance. On the other hand, TGFβ has pleiotropic effects on bone cells and our results point out that it is indeed a fragile element to be controlled when diseases like osteoporosis and bone metastasis start to develop. Wnt is an emerging pathway that had interesting regulatory effects on our numerical simulations of combination therapies, suggesting a strong positive effect towards reducing osteoporosis and bone metastasis osteolytic progression. Our numerical simulations also present relevant hypotheses related to theoretical optimal control of bone diseases. Emerging experimental data of these two important signaling pathways should be contrasted with and reincorporated into theoretical models to further our understanding of how to optimally control bone diseases. There are multiple opportunities for future work related to bone disease treatment strategies. One important aspect to consider in the future is one of off-targeting. In particular, TGFβ and Wnt signaling pathways are involved not only in bone remodeling but also in other cellular processes, in health and in disease. In this Chapter, we focused on the bone remodeling coupling the importance of these two signaling pathways. Improvements of the mathematical model should take into account more effects of these pathways in the bone and in cancer dynamics (Enders, 2009; Canalis, 2013; Marie, 2015). As such, other mathematical models have taken into account indirect control of these pathways, particularly of the Wnt signaling pathway. The indirect control in up-regulating Wnt levels has been done by inhibiting bone- or cancer-produced Wnt antagonists such as Dkk1 (Shah et al., 2015). Also, it could be interesting to find the mathematical conditions for the existence of Hopf bifurcation points, and further identify another important elements related to the genesis of oscillations. We plan to work on these relevant issues in the future.

Chapter 5. There is evidence that geometric distribution of bone cells is important for bone remodeling, and it also plays a relevant role in the distribution of bone metastasis

cancer cells. Baring this in mind, in this Chapter we proposed a modeling framework to explore the effects of a one-dimensional space variable. Through numerical experiments, we could assess that incorporating a spatial variable to bone remodeling and bone metastasis models may impact the qualitative behavior of the dynamical evolution. Experimental and computational data point that not only the distribution of cells but also the distribution of biochemical agents have to be considered for bone dynamics. Thus, we finished this Thesis by posing a mathematical model that have both spatial elements and the decoupling of TGFβ from the power-law approximation. To our knowledge, this is the first kind of mathematical model in the literature: other spatial mathematical models focus on RANKL/OPG. This Chapter offers the amplest window for future work. Numerical experiments for the TGFβ would be interesting for gaining some insight into the dynamical behavior of the model. Also, it would be more realistic to incorporate Wnt into the spatial model, as done in the previous Chapter. After introducing TGFβ and Wnt, an inviting problem to tackle would be the one of spatial control. There are similar theoretical and numerical approaches for studying optimal control problems in a spatial setting. Future work will also focus on this aspect.

APPENDICES

Appendix A

Routh-Hurwitz Criterion

The Routh-Hurwitz (R-H) criterion gives necessary and sufficient conditions so that all the roots of a polynomial have negative real part. In particular, we are interested in the case of a polynomial of order three:

$$Q(s) = c_3 s^3 + c_2 s^2 + c_1 s + c_0. \tag{A.1}$$

If the following conditions

(C1) $c_3 > 0$, $c_2 > 0$ and $c_0 > 0$,

(C2) $c_2 c_1 > c_0 c_3$,

are satisfied, then the roots of a polynomial (A.1) have negative real part. For more details of the R-H criterion, see (Gantmacher, 1959).

Appendix B

Uniqueness of optimal control solutions

We follow Fister et al. (1998) to show uniqueness of the optimal solution for the model (3.4) under certain conditions over the final time (Theorem 3.3). First, we prove some basic results.

Lemma 6. *Let $a, b, c, \bar{a}, \bar{b}, \bar{c}$ be real positive numbers such that they are bounded by some positive constant M. Then*

i) $ab - \bar{a}\bar{b} \leq M(|a-\bar{a}|+|b-\bar{b}|)$.

ii) $(ab - \bar{a}\bar{b})(c-\bar{c}) \leq M((a-\bar{a})^2 + (b-\bar{b})^2 + (c-\bar{c})^2)$.

Proof i) Notice that

$$\begin{aligned} ab - \bar{a}\bar{b} &\leq |ab - \bar{a}\bar{b}| \\ &\leq \frac{|a-\bar{a}|}{2} b + \frac{|b-\bar{b}|}{2} a + \frac{|a-\bar{a}|}{2} \bar{b} + \frac{|b-\bar{b}|}{2} \bar{a} \\ &\leq \frac{M}{2} \left(2|a-\bar{a}|+2|b-\bar{b}|\right) \\ &= M(|a-\bar{a}|+|b-\bar{b}|). \end{aligned}$$

ii) Multiplying by $(c-\bar{c})$ and using the Cauchy inequality (or the AM-GM inequality) we get

$$\begin{aligned} (ab - \bar{a}\bar{b})(c-\bar{c}) &\leq |ab - \bar{a}\bar{b}||c-\bar{c}| \\ &\leq M(|a-\bar{a}||c-\bar{c}|+|b-\bar{b}||c-\bar{c}|) \\ &\leq M\left(\frac{1}{2}\left((a-\bar{a})^2 + (c-\bar{c})^2\right) + \frac{1}{2}\left((b-\bar{b})^2 + (c-\bar{c})^2\right)\right) \\ &\leq M\left((a-\bar{a})^2 + (b-\bar{b})^2 + (c-\bar{c})^2\right). \end{aligned}$$

□

Lemma 7. *The function $f(x) = \max\{0, \min\{1, x\}\}$ is Lipschitz.*

Proof Notice that if $x \in (-\infty, 0) \cup (0, 1) \cup (1, +\infty)$ then there is nothing to prove: the function is of class C^1 in that set. So, we need to focus on $x = 0$ and $x = 1$. Suppose that

$x_1 < 0$ and $1 > x_2 > 0$, then:

$$|f(x_1) - f(x_2)| = |0 - x_2| = x_2 \leq x_2 - x_1 = |x_2 - x_1| = |x_1 - x_2|.$$

The other cases are analogous. We can conclude that $f(x)$ is Lipschitz. □

Now, we proceed to prove Theorem 2.

Proof Let suppose that there are two optimal pairs (x, λ, u) and $(\bar{x}, \bar{\lambda}, \bar{u})$ that solve the problem (3.4) and the adjoint system (3.12), where $x = (x_1, x_2, x_3)$ and $\lambda = (\lambda_1, \lambda_2, \lambda_3)$. Let $m > 0$ be fixed. Then there exist functions y_1, y_2, y_3 and μ_1, μ_2, μ_3 (also with bar) such that $x_i = y_i e^{mt}$, $\bar{x}_i = y_i e^{mt}$, $\lambda_i = \mu_i e^{-mt}$, $\bar{\lambda}_i = \bar{\mu}_i e^{-mt}$. Then:

$$u = \max\left\{0, \min\left\{1, \frac{\alpha_1 e^{mg_1 t} y_1 y_2^{g_1} \mu_1}{2B}\right\}\right\}, \quad \bar{u} = \max\left\{0, \min\left\{1, \frac{\alpha_1 e^{mg_1 t} \bar{y}_1 \bar{y}_2^{g_1} \bar{\mu}_1}{2B}\right\}\right\}.$$

Substituting into the optimality system (3.4b)-(3.4d) and (3.12) we get:

$$\begin{aligned}
y_1' e^{mt} + m y_1 e^{mt} &= \alpha_1 e^{mt} e^{mg_1 t} y_1 y_2^{g_1}(1-u) - \beta_1 e^{mt} y_1 + \sigma_1 e^{2mt} y_1 y_3,\\
y_2' e^{mt} + m y_2 e^{mt} &= \alpha_2 e^{mg_2 t} e^{mt} y_1^{g_2} y_2 - \beta_2 e^{mt} y_2 + \sigma_2 e^{2mt} y_2 y_3,\\
y_3' e^{mt} + m y_3 e^{mt} &= \alpha_3 e^{mt} y_3 \left(1 - e^{mt} y_3/K\right) - \beta_3 e^{mt} y_3 + \sigma_3 e^{mg_2 t} e^{mt} y_1^{g_2} y_3\\
&\quad + \sigma_4 e^{mg_1 t} e^{mt} y_2^{g_1} y_3,\\
\mu_1' e^{-mt} - m\mu_1 e^{-mt} &= -e^{-mt}\mu_1(\alpha_1 e^{mg_1 t} y_2^{g_1}(1-u) - \beta_1 + \sigma_1 e^{mt} y_3)\\
&\quad - e^{-mt}\mu_2(\alpha_2 g_2 e^{m(g_2-1)t} y_1^{g_2-1} e^{mt} y_2)\\
&\quad - e^{-mt}\mu_3(\sigma_3 g_2 e^{m(g_2-1)t} y_1^{g_2-1} e^{mt} y_3),\\
\mu_2' e^{-mt} - m\mu_2 e^{-mt} &= -e^{-mt}\mu_1(\alpha_1 g_1 e^{mt} e^{m(g_1-1)t} y_1 y_2^{g_1-1}(1-u))\\
&\quad - e^{-mt}\mu_2(\alpha_2 e^{mg_2 t} y_1^{g_2} - \beta_2 + \sigma_2 e^{mt} y_3)\\
&\quad - e^{-mt}\mu_3(\sigma_4 g_1 e^{m(g_1-1)t} y_2^{g_1-1} e^{mt} y_3),\\
\mu_3' e^{-mt} - m\mu_3 e^{-mt} &= -e^{-mt}\mu_1(\sigma_1 e^{mt} y_1) - e^{-mt}\mu_2(\sigma_2 e^{mt} y_2)\\
&\quad - e^{-mt}\mu_3(\alpha_3(1 - 2e^{mt} y_3/K) - \beta_3 + \sigma_3 e^{mg_2 t} y_1^{g_2} + \sigma_4 e^{mg_1 t} y_2^{g_1})\\
&\quad - 2e^{mt} y_3.
\end{aligned}$$

We can divide the first three equations by e^{mt} and the other three by e^{-mt}. Simplifying:

$$\begin{aligned}
y_1' + m y_1 &= \alpha_1 e^{mg_1 t} y_1 y_2^{g_1}(1-u) - \beta_1 y_1 + \sigma_1 e^{mt} y_1 y_3,\\
y_2' + m y_2 &= \alpha_2 e^{mg_2 t} y_1^{g_2} y_2 - \beta_2 y_2 + \sigma_2 e^{mt} y_2 y_3,\\
y_3' + m y_3 &= \alpha_3 y_3 \left(1 - e^{mt} y_3/K\right) - \beta_3 y_3 + \sigma_3 e^{mg_2 t} y_1^{g_2} y_3 + \sigma_4 e^{mg_1 t} y_2^{g_1} y_3,\\
\mu_1' - m\mu_1 &= -\mu_1(\alpha_1 e^{mg_1 t} y_2^{g_1}(1-u) - \beta_1 + \sigma_1 e^{mt} y_3) - \mu_2(\alpha_2 g_2 e^{mg_2 t} y_1^{g_2-1} y_2)\\
&\quad - \mu_3(\sigma_3 g_2 e^{mg_2 t} y_1^{g_2-1} y_3),\\
\mu_2' - m\mu_2 &= -\mu_1(\alpha_1 g_1 e^{mg_1 t} y_1 y_2^{g_1-1}(1-u)) - \mu_2(\alpha_2 e^{mg_2 t} y_1^{g_2} - \beta_2 + \sigma_2 e^{mt} y_3)\\
&\quad - \mu_3(\sigma_4 g_1 e^{mg_1 t} y_2^{g_1-1} y_3),\\
\mu_3' - m\mu_3 &= -\mu_1(\sigma_1 e^{mt} y_1) - \mu_2(\sigma_2 e^{mt} y_2)\\
&\quad - \mu_3(\alpha_3(1 - 2e^{mt} y_3/K) - \beta_3 + \sigma_3 e^{mg_2 t} y_1^{g_2} + \sigma_4 e^{mg_1 t} y_2^{g_1}) - 2e^{2mt} y_3.
\end{aligned}$$

The system related to the other optimal solution $(\bar{x}, \bar{\lambda}, \bar{u})$ is analogous. Subtracting the corresponding equations related to (x, λ, u) and $(\bar{x}, \bar{\lambda}, \bar{u})$ we get:

$$
\begin{aligned}
(y_1 - \bar{y_1})' + m(y_1 - \bar{y_1}) &= \alpha_1 e^{mg_1 t}(y_1 y_2^{g_1}(1-u) - \bar{y_1}\bar{y_2}^{g_1}(1-\bar{u})) \\
&\quad - \beta_1(y_1 - \bar{y_1}) + \sigma_1 e^{mt}(y_1 y_3 - \bar{y_1}\bar{y_3}), \\
(y_2 - \bar{y_2})' + m(y_2 - \bar{y_2}) &= \alpha_2 e^{mg_2 t}(y_1^{g_2} y_2 - \bar{y_1}^{g_2}\bar{y_2}) - \beta_2(y_2 - \bar{y_2}) \\
&\quad + \sigma_2 e^{mt}(y_2 y_3 - \bar{y_2}\bar{y_3}), \\
(y_3 - \bar{y_3})' + m(y_3 - \bar{y_3}) &= \alpha_3\left((y_3 - \bar{y_3}) - e^{mt}(y_3^2 - \bar{y_3}^2)/K\right) \\
&\quad - \beta_3(y_3 - \bar{y_3}) + \sigma_3 e^{mg_2 t}(y_1^{g_2} y_3 - \bar{y_1}^{g_2}\bar{y_3}) \\
&\quad + \sigma_4 e^{mg_1 t}(y_2^{g_1} y_3 - \bar{y_2}^{g_1}\bar{y_3}), \\
(\mu_1 - \bar{\mu_1})' - m(\mu_1 - \bar{\mu_1}) &= -\alpha_1 e^{mg_1 t}(\mu_1 y_2^{g_1} - \bar{\mu_1}\bar{y_2}^{g_1}) + \alpha_1 e^{mg_1 t}(\mu_1 y_2^{g_1} u - \bar{\mu_1}\bar{y_2}^{g_1}\bar{u}) \\
&\quad + \beta_1(\mu_1 - \bar{\mu_1}) - \sigma_1 e^{mt}(\mu_1 y_3 - \bar{\mu_1}\bar{y_3}) \\
&\quad - \alpha_2 g_2 e^{mg_2 t}(\mu_2 y_1^{g_2 - 1} y_2 - \bar{\mu_2}\bar{y_1}^{g_2 - 1}\bar{y_2}) \\
&\quad - \sigma_3 g_2 e^{mg_2 t}(\mu_3 y_1^{g_2 - 1} y_3 - \bar{\mu_3}\bar{y_1}^{g_2 - 1}\bar{y_3}), \\
(\mu_2 - \bar{\mu_2})' - m(\mu_2 - \bar{\mu_2}) &= -\alpha_1 g_1 e^{mg_1 t}(\mu_1 y_1 y_2^{g_1 - 1} - \bar{\mu_1}\bar{y_1}\bar{y_2}^{g_1 - 1}) \\
&\quad + \alpha_1 g_1 e^{mg_1 t}(\mu_1 y_1 y_2^{g_1 - 1} u - \bar{\mu_1}\bar{y_1}\bar{y_2}^{g_1 - 1}\bar{u}) \\
&\quad - \alpha_2 e^{mg_2 t}(\mu_2 y_1^{g_2} - \bar{\mu_2}\bar{y_1}^{g_2}) \\
&\quad + \beta_2(\mu_2 - \bar{\mu_2}) - \sigma_2 e^{mt}(\mu_2 y_3 - \bar{\mu_2}\bar{y_3}) \\
&\quad - \sigma_4 g_1 e^{mg_1 t}(\mu_3 y_2^{g_1 - 1} y_3 - \bar{\mu_3}\bar{y_2}^{g_1 - 1}\bar{y_3}), \\
(\mu_3 - \bar{\mu_3})' - m(\mu_3 - \bar{\mu_3}) &= -\sigma_1 e^{mt}(\mu_1 y_1 - \bar{\mu_1}\bar{y_1}) - \sigma_2 e^{mt}(\mu_2 y_2 - \bar{\mu_2}\bar{y_2}) \\
&\quad - \alpha_3(\mu_3 - \bar{\mu_3}) + \frac{2\alpha_3 e^{mt}}{K}(\mu_3 y_3 - \bar{\mu_3}\bar{y_3}) + \beta_3(\mu_3 - \bar{\mu_3}) \\
&\quad - \sigma_3 e^{mg_2 t}(y_1^{g_2} - \bar{y_1}^{g_2}) - \sigma_4 e^{mg_1 t}(y_2^{g_1} - \bar{y_2}^{g_1}) \\
&\quad - 2e^{2mt}(y_3 - \bar{y_3}).
\end{aligned}
$$

Now, we multiply each equation by the left-hand side without the derivative and then integrate from 0 to a time T:

$$
\begin{aligned}
&\frac{1}{2}(y_1 - \bar{y_1})^2\Big|_0^T + m\int_0^T (y_1 - \bar{y_1})^2 dt = \\
&\qquad \alpha_1 \int_0^T (y_1 - \bar{y_1}) e^{mg_1 t}(y_1 y_2^{g_1} - \bar{y_1}\bar{y_2}^{g_1}) dt \\
&\qquad - \alpha_1 \int_0^T (y_1 - \bar{y_1}) e^{mg_1 t}(y_1 y_2^{g_1} u - \bar{y_1}\bar{y_2}^{g_1}\bar{u}) dt \\
&\qquad - \beta_1 \int_0^T (y_1 - \bar{y_1})^2 dt + \sigma_1 \int_0^T (y_1 - \bar{y_1}) e^{mt}(y_1 y_3 - \bar{y_1}\bar{y_3}) dt, \\
&\frac{1}{2}(y_2 - \bar{y_2})^2\Big|_0^T + m\int_0^T (y_2 - \bar{y_2})^2 dt = \\
&\qquad \alpha_2 \int_0^T (y_2 - \bar{y_2}) e^{mg_2 t}(y_1^{g_2} y_2 - \bar{y_1}^{g_2}\bar{y_2}) dt - \beta_2 \int_0^T (y_2 - \bar{y_2})^2 dt
\end{aligned}
$$

$$
\begin{aligned}
&+\sigma_2\int_0^T(y_2-\bar{y_2})e^{mt}(y_2y_3-\bar{y_2}\bar{y_3})dt,\\
\frac{1}{2}(y_3-\bar{y_3})^2\Big|_0^T&+m\int_0^T(y_3-\bar{y_3})^2dt=\\
&\alpha_3\int_0^T(y_3-\bar{y_3})^2dt-\frac{\alpha_3}{K}\int_0^T(y_3-\bar{y_3})\left(e^{mt}(y_3^2-\bar{y_3}^2)\right)dt\\
&-\beta_3\int_0^T(y_3-\bar{y_3})^2dt+\sigma_3\int_0^T(y_3-\bar{y_3})e^{mg_2t}(y_1^{g_2}y_3-\bar{y_1}^{g_2}\bar{y_3})dt\\
&+\sigma_4\int_0^T(y_3-\bar{y_3})e^{mg_1t}(y_2^{g_1}y_3-\bar{y_2}^{g_1}\bar{y_3})dt,\\
-\frac{1}{2}(\mu_1-\bar{\mu_1})^2\Big|_0^T&+m\int_0^T(\mu_1-\bar{\mu_1})^2dt=\\
&\alpha_1\int_0^T(\mu_1-\bar{\mu_1})e^{mg_1t}(\mu_1y_2^{g_1}-\bar{\mu_1}\bar{y_2}^{g_1})dt\\
&-\alpha_1\int_0^T(\mu_1-\bar{\mu_1})e^{mg_1t}(\mu_1y_2^{g_1}u-\bar{\mu_1}\bar{y_2}^{g_1}\bar{u})dt\\
&-\beta_1\int_0^T(\mu_1-\bar{\mu_1})^2dt+\sigma_1\int_0^T(\mu_1-\bar{\mu_1})e^{mt}(\mu_1y_3-\bar{\mu_1}\bar{y_3})dt\\
&+\alpha_2g_2\int_0^T(\mu_1-\bar{\mu_1})e^{mg_2t}(\mu_2y_1^{g_2-1}y_2-\bar{\mu_2}\bar{y_1}^{g_2-1}\bar{y_2})dt\\
&+\sigma_3g_2\int_0^T(\mu_1-\bar{\mu_1})e^{mg_2t}(\mu_3y_1^{g_2-1}y_3-\bar{\mu_3}\bar{y_1}^{g_2-1}\bar{y_3})dt,\\
-\frac{1}{2}(\mu_2-\bar{\mu_2})^2\Big|_0^T&+m\int_0^T(\mu_2-\bar{\mu_2})^2dt=\\
&\alpha_1g_1\int_0^T(\mu_2-\bar{\mu_2})e^{mg_1t}(\mu_1y_1y_2^{g_1-1}-\bar{\mu_1}\bar{y_1}\bar{y_2}^{g_1-1})dt\\
&-\alpha_1g_1\int_0^T(\mu_2-\bar{\mu_2})e^{mg_1t}(\mu_1y_1y_2^{g_1-1}u-\bar{\mu_1}\bar{y_1}\bar{y_2}^{g_1-1}\bar{u})dt\\
&+\alpha_2\int_0^T(\mu_2-\bar{\mu_2})e^{mg_2t}(\mu_2y_1^{g_2}-\bar{\mu_2}\bar{y_1}^{g_2})dt-\beta_2\int_0^T(\mu_2-\bar{\mu_2})^2dt\\
&+\sigma_2\int_0^T(\mu_2-\bar{\mu_2})e^{mt}(\mu_2y_3-\bar{\mu_2}\bar{y_3})dt\\
&+\sigma_4g_1\int_0^T(\mu_2-\bar{\mu_2})e^{mg_1t}(\mu_3y_2^{g_1-1}y_3-\bar{\mu_3}\bar{y_2}^{g_1-1}\bar{y_3})dt,\\
-\frac{1}{2}(\mu_3-\bar{\mu_3})^2\Big|_0^T&+m\int_0^T(\mu_3-\bar{\mu_3})^2dt=\\
&\sigma_1\int_0^T(\mu_3-\bar{\mu_3})e^{mt}(\mu_1y_1-\bar{\mu_1}\bar{y_1})dt+\sigma_2\int_0^T(\mu_3-\bar{\mu_3})e^{mt}(\mu_2y_2-\bar{\mu_2}\bar{y_2})dt\\
&-(\beta_3-\alpha_3)\int_0^T(\mu_3-\bar{\mu_3})^2dt-\frac{2\alpha_3}{K}\int_0^T(\mu_3-\bar{\mu_3})e^{mt}(\mu_3y_3-\bar{\mu_3}\bar{y_3})dt
\end{aligned}
$$

$$+\sigma_3\int_0^T(\mu_3-\bar{\mu_3})e^{mg_2t}(y_1^{g_2}-\bar{y_1}^{g_2})dt$$
$$+\sigma_4\int_0^T(\mu_3-\bar{\mu_3})e^{mg_1t}(y_2^{g_1}-\bar{y_2}^{g_1})dt+2\int_0^T(\mu_3-\bar{\mu_3})e^{2mt}(y_3-\bar{y_3})dt.$$

Using the previous lemma with $x:=\frac{\alpha_1e^{mg_1t}y_1y_2^{g_1}\mu_1}{2B}$ we have:

$$\begin{aligned}\int_0^T(u-\bar{u})^2dt&=\int_0^T\left(\max\left\{0,\min\left\{1,\frac{\alpha_1e^{mg_1t}y_1y_2^{g_1}\mu_1}{2B}\right\}\right\}\right.\\&\quad\left.-\max\left\{0,\min\left\{1,\frac{\alpha_1e^{mg_1t}\bar{y}_1\bar{y}_2^{g_1}\bar{\mu}_1}{2B}\right\}\right\}\right)^2dt\\&\leq\int_0^T\left(\frac{\alpha_1e^{mg_1t}y_1y_2^{g_1}\mu_1}{2B}-\frac{\alpha_1e^{mg_1t}\bar{y}_1\bar{y}_2^{g_1}\bar{\mu}_1}{2B}\right)^2dt\\&\leq\frac{\alpha_1}{2B}\int_0^T\left(y_1y_2^{g_1}\mu_1-\bar{y_1}\bar{y_2}^{g_1}\bar{\mu_1}\right)^2dt.\end{aligned}$$

Now, using that the function $f(y_1,y_2,\mu_1)=y_1y_2^{g_1}\mu_1$ is locally Lipschitz, we can conclude that there exists a positive constant L such that:

$$\frac{\alpha_1}{2B}\int_0^T\left(y_1y_2^{g_1}\mu_1-\bar{y_1}\bar{y_2}^{g_1}\bar{\mu_1}\right)^2dt\leq\frac{\alpha_1L}{2B}\int_0^T\left((y_1-\bar{y_1})^2+(y_2-\bar{y_2})^2+(\mu_1-\bar{\mu_1})^2\right)dt.$$

Another useful inequality is derived from using Lemma 6 two times successively and the locally Lipschitz condition for $f(y_2)=y_2^{g_1}$. Hence we have:

$$|y_1-\bar{y_1}|(y_1y_2^{g_1}u-\bar{y_1}\bar{y_2}^{g_1}\bar{u})\leq M_5((y_1-\bar{y_1})^2+(u-\bar{u})^2+(y_2-\bar{y_2})^2)$$

for some constant $M_5>0$. Now, using the previous results we can get the desired bounds:

$$\begin{aligned}&\frac{1}{2}(y_1-\bar{y_1})^2\Big|_0^T+m\int_0^T(y_1-\bar{y_1})^2dt=\\&\alpha_1\int_0^T(y_1-\bar{y_1})e^{mg_1t}(y_1y_2^{g_1}-\bar{y_1}\bar{y_2}^{g_1})dt-\alpha_1\int_0^T(y_1-\bar{y_1})e^{mg_1t}(y_1y_2^{g_1}u-\bar{y_1}\bar{y_2}^{g_1}\bar{u})dt\\&-\beta_1\int_0^T(y_1-\bar{y_1})^2dt+\sigma_1\int_0^T(y_1-\bar{y_1})e^{mt}(y_1y_3-\bar{y_1}\bar{y_3})dt\\&\leq\alpha_1\int_0^T|y_1-\bar{y_1}||y_1y_2^{g_1}-\bar{y_1}\bar{y_2}^{g_1}|dt+\alpha_1\int_0^T|y_1-\bar{y_1}||y_1y_2^{g_1}u-\bar{y_1}\bar{y_2}^{g_1}\bar{u}|dt\\&+\sigma_1e^{mT}\int_0^T|y_1-\bar{y_1}||y_1y_3-\bar{y_1}\bar{y_3}|dt\\&\leq L_{11}\int_0^T\left((y_1-\bar{y_1})^2+(y_2-\bar{y_2})^2\right)dt+L_{12}e^{mT}\int_0^T\left((y_1-\bar{y_1})^2+(y_3-\bar{y_3})^2\right)dt\\&+\alpha_1\int_0^T|y_1-\bar{y_1}||y_1y_2^{g_1}u-\bar{y_1}\bar{y_2}^{g_1}\bar{u}|dt\end{aligned}$$

$$\leq L_{11}\int_0^T \left((y_1-\bar{y_1})^2+(y_2-\bar{y_2})^2\right)dt + L_{12}e^{mT}\int_0^T \left((y_1-\bar{y_1})^2+(y_3-\bar{y_3})^2\right)dt$$
$$+ M_{13}\int_0^T \left((y_1-\bar{y_1})^2+(u-\bar{u})^2+(y_2-\bar{y_2})^2\right)dt$$
$$\leq L_{11}\int_0^T \left((y_1-\bar{y_1})^2+(y_2-\bar{y_2})^2\right)dt + L_{12}e^{mT}\int_0^T \left((y_1-\bar{y_1})^2+(y_3-\bar{y_3})^2\right)dt$$
$$+ L_{13}\int_0^T \left((y_1-\bar{y_1})^2+(\mu_1-\bar{\mu_1})^2+(y_2-\bar{y_2})^2\right)dt.$$

Analogously, we get:

$$\frac{1}{2}(y_2-\bar{y_2})^2\Big|_0^T + m\int_0^T (y_2-\bar{y_2})^2 dt \leq$$
$$L_{21}e^{mg_2T}\int_0^T \left((y_1-\bar{y_1})^2+(y_2-\bar{y_2})^2\right)dt$$
$$+ L_{22}e^{mT}\int_0^T \left((y_2-\bar{y_2})^2+(y_3-\bar{y_3})^2\right)dt,$$
$$\frac{1}{2}(y_3-\bar{y_3})^2\Big|_0^T + m\int_0^T (y_3-\bar{y_3})^2 dt \leq$$
$$L_{31}\int_0^T (y_3-\bar{y_3})^2 dt + L_{32}e^{mT}\int_0^T (y_3-\bar{y_3})^2 dt$$
$$+ L_{33}e^{mg_2T}\int_0^T \left((y_1-\bar{y_1})^2+(y_3-\bar{y_3})^2\right)dt$$
$$+ L_{34}\int_0^T \left((y_2-\bar{y_2})^2+(y_3-\bar{y_3})^2\right)dt,$$
$$-\frac{1}{2}(\mu_1-\bar{\mu_1})^2\Big|_0^T + m\int_0^T (\mu_1-\bar{\mu_1})^2 dt \leq$$
$$L_{41}\int_0^T \left((\mu_1-\bar{\mu_1})^2+(y_2-\bar{y_2})^2\right)dt$$
$$+ L_{43}e^{mT}\int_0^T \left((\mu_1-\bar{\mu_1})^2+(y_3-\bar{y_3})^2\right)dt$$
$$+ L_{42}\int_0^T \left((\mu_1-\bar{\mu_1})^2+(y_2-\bar{y_2})^2+(y_1-\bar{y_1})^2\right)dt$$
$$+ L_{44}e^{mg_2T}\int_0^T \left((\mu_1-\bar{\mu_1})^2+(\mu_2-\bar{\mu_2})^2+(y_1-\bar{y_1})^2+(y_2-\bar{y_2})^2\right)dt$$
$$+ L_{45}e^{mg_2T}\int_0^T \left((\mu_1-\bar{\mu_1})^2+(\mu_3-\bar{\mu_3})^2+(y_1-\bar{y_1})^2+(y_3-\bar{y_3})^2\right)dt,$$
$$-\frac{1}{2}(\mu_2-\bar{\mu_2})^2\Big|_0^T + m\int_0^T (\mu_2-\bar{\mu_2})^2 dt$$
$$\leq L_{51}\int_0^T \left((\mu_2-\bar{\mu_2})^2+(\mu_1-\bar{\mu_1})^2\right)+(y_1-\bar{y_1})^2+(y_2-\bar{y_2})^2\right)dt$$

$$
\begin{aligned}
&+ L_{52}\int_0^T \left((\mu_2-\bar{\mu_2})^2+(\mu_1-\bar{\mu_1})^2+(y_1-\bar{y_1})^2+(y_2-\bar{y_2})^2\right)dt\\
&+ L_{53}e^{mg_2T}\int_0^T \left((\mu_2-\bar{\mu_2})^2+(y_1-\bar{y_1})^2\right)dt\\
&+ L_{54}e^{mT}\int_0^T \left((\mu_2-\bar{\mu_2})^2+(y_3-\bar{y_3})^2\right)dt\\
&+ L_{55}\int_0^T \left((\mu_2-\bar{\mu_2})^2+(\mu_3-\bar{\mu_3})^2)+(y_2-\bar{y_2})^2+(y_3-\bar{y_3})^2\right)dt,\\
-\frac{1}{2}(\mu_3-\bar{\mu_3})^2\Big|_0^T &+ m\int_0^T(\mu_3-\bar{\mu_3})^2dt\\
&\leq L_{61}e^{mT}\int_0^T \left((\mu_3-\bar{\mu_3})^2+(\mu_1-\bar{\mu_1})^2+(y_1-\bar{y_1})^2\right)dt\\
&+ L_{62}e^{mT}\int_0^T \left((\mu_3-\bar{\mu_3})^2+(\mu_2-\bar{\mu_2})^2+(y_2-\bar{y_2})^2\right)dt\\
&+ L_{63}\int_0^T \left((\mu_3-\bar{\mu_3})^2+(y_3-\bar{y_3})^2\right)dt\\
&+ L_{64}e^{mT}\int_0^T \left((\mu_3-\bar{\mu_3})^2+(y_3-\bar{y_3})^2\right)dt\\
&+ L_{65}e^{mg_2T}\int_0^T \left((\mu_3-\bar{\mu_3})^2+(y_1-\bar{y_1})^2\right)dt\\
&+ L_{66}e^{2mT}\int_0^T \left((\mu_3-\bar{\mu_3})^2+(y_3-\bar{y_3})^2\right)dt\\
&+ L_{67}\int_0^T \left((\mu_3-\bar{\mu_3})^2+(y_2-\bar{y_2})^2\right)dt.
\end{aligned}
$$

Summing the above six equations and grouping terms we get:

$$
\begin{aligned}
&\big(m - L_{11} - L_{12}e^{mT} - L_{13} - L_{21}e^{mg_2T} - L_{22}e^{mT} - L_{31} - L_{32}e^{mT} - L_{33}e^{mg_2T} - L_{34}\\
&-L_{41} - L_{42} - L_{43}e^{mT} - L_{44}e^{mg_2T} - L_{45}e^{mg_2T} - L_{51} - L_{52} - L_{53}e^{mg_2T} - L_{54}e^{mT} - L_{55}\\
&-L_{61}e^{mT} - L_{62}e^{mT} - L_{63} - L_{64}e^{mT} - L_{65}e^{mg_2T} - L_{66}e^{2mT} - L_{67}\big)\int_0^T \left((y_1-\bar{y_1})^2\right.\\
&\left.+(y_2-\bar{y_2})^2+(y_3-\bar{y_3})^2+(\mu_1-\bar{\mu_1})^2+(\mu_2-\bar{\mu_2})^2+(\mu_3-\bar{\mu_3})^2\right)dt \leq 0.
\end{aligned}
$$

This can be rewritten as:

$$
\begin{aligned}
&\big(m - C_1 - C_2e^{mT} - C_3e^{mg_2T} - C_4e^{2mT}\big)\int_0^T \left((y_1-\bar{y_1})^2+(y_2-\bar{y_2})^2+(y_3-\bar{y_3})^2\right.\\
&\left.+(\mu_1-\bar{\mu_1})^2+(\mu_2-\bar{\mu_2})^2+(\mu_3-\bar{\mu_3})^2\right)dt \leq 0.
\end{aligned}
$$

So if $m - C_1 - C_2e^{mT} - C_3e^{mg_2T} - C_4e^{2mT} > 0$ then $y_1 = \bar{y_1}$, $y_2 = \bar{y_2}$, $y_3 = \bar{y_3}$, $\mu_1 = \bar{\mu_1}$, $\mu_2 = \bar{\mu_2}$ and $\mu_3 = \bar{\mu_3}$, and therefore the OC solutions u and $\bar{u}$ are the same. □

Appendix C

Stability results for TGFβ and Wnt models

C.1 Local stability of the bone remodeling model

The characteristic polynomial of model (4.3)–(4.6) associated to its steady-state (4.11)–(4.14) is given by:

$$\begin{aligned} p(\lambda) =& \lambda^4 + \lambda^3 \left(\beta_C + \beta_{CT} C_1 + \beta_T + \beta_W\right) \\ &+ \lambda^2 \left(\beta_{CT}\beta_T C_1 + \beta_T\beta_W + \left(\beta_C + \beta_{CT} C_1\right)\left(\beta_T + \beta_W\right)\right) \\ &+ \lambda \frac{\beta_W}{C_2} \left(\alpha_{BW}\alpha_W \beta_1^2 \beta_B \beta_T C_1 + \alpha_{BW}\alpha_W \beta_C^2 \beta_T^2 C_1 + \alpha_T \beta_C \beta_{CT} \beta_B \beta_T \beta_W \right. \\ &\quad \left. - \alpha_T \beta_{CT}^2 \beta_B^2 \beta_W C_1 - 2\alpha_T \beta_{CT}^2 \beta_B \beta_T \beta_W C_1\right) \\ &+ \frac{2\beta_B \beta_T \beta_W C_1 \left(\alpha_{BW}\alpha_W \beta_C^2 \beta_T - \alpha_T \beta_{CT}^2 \beta_B \beta_W\right)}{C_2} \end{aligned} \tag{C.1}$$

where $C_1 = \widehat{x}_T$ and $C_2 = \alpha_{BW}\alpha_W \beta_C \beta_T C_1 - \alpha_T \beta_{CT} \beta_B \beta_W$.

We can state the following abstract result, which is a direct result of the Routh-Hurwitz criteria (Wiggers & Pedersen, 2018):

Theorem C.1. *Let $p(\lambda) = \lambda^4 + a_1\lambda^3 + a_2\lambda^2 + a_3\lambda + a_4$ be the characteristic polynomial (C.1) of model (4.3)–(4.6) with respect the steady-state (4.11)–(4.14), where a_i are the respective coefficients in terms of the model parameters. If the following inequalities hold:*

$$\begin{aligned} &a_i > 0 \quad (i = 1, 2, 3, 4), \\ &a_1 a_2 a_3 - a_1^2 a_4 - a_3^2 > 0, \end{aligned}$$

then the steady-state (4.11)–(4.14) is locally stable. □

C.2 Local stability of the bone metastasis model

The characteristic polynomial of model (4.15)–(4.19) associated to its cancer-invasion steady-state (4.20)–(4.24) is given by:

$$p(\lambda) =$$

$$
\begin{aligned}
&\lambda^5 + \lambda^4 \left(\alpha_M + \alpha_{MT} C_1 + \beta_C + \beta_{CT} C_1 + \beta_T + \beta_W\right) \\
&+ \lambda^3 \left(\beta_{CT}\beta_T C_1 + \beta_T \left(\beta_C + \beta_{CT} C_1\right) + \beta_W \left(\beta_C + \beta_{CT} C_1 + \beta_T\right)\right. \\
&\quad \left. + \left(\alpha_M + \alpha_{MT} C_1\right)\left(\beta_C + \beta_{CT} C_1 + \beta_T + \beta_W\right)\right) \\
&+ \frac{\lambda^2}{C_2}\left(-C_1 \left(1 - K_B\right)\left(1 - K_C\right) C_7 + \left(\beta_T \beta_W \left(\beta_C + 2\beta_{CT} C_1\right)\right.\right. \\
&\quad \left.\left. + \left(\alpha_M + \alpha_{MT} C_1\right)\left(\beta_{CT}\beta_T C_1 + \beta_T \left(\beta_C + \beta_{CT} C_1\right) + \beta_W \left(\beta_C + \beta_{CT} C_1 + \beta_T\right)\right)\right) C_2\right) \\
&+ \frac{\lambda}{C_2}\left(-\beta_T C_1 \left(1 - K_B\right)\left(1 - K_C\right) C_7 + C_1 \left(1 - K_B\right)\left(1 - K_C\right)\left(\beta_C + \beta_{CT} C_1\right) C_7\right. \\
&\quad - C_1 \left(1 - K_B\right)\left(1 - K_C\right)\left(\beta_C + \beta_{CT} C_1 + \beta_T\right) C_7 \\
&\quad \left. + \left(\alpha_M + \alpha_{MT} C_1\right)\left(\beta_T \beta_W \left(\beta_C + 2\beta_{CT} C_1\right) C_2 - C_1 \left(1 - K_B\right)\left(1 - K_C\right) C_7\right)\right) \\
&- \frac{2\beta_T C_1}{C_2}\left(1 - K_B\right)\left(1 - K_C\right)\left(\alpha_M + \alpha_{MT} C_1\right) C_7
\end{aligned}
\tag{C.2}
$$

where

$$
\begin{aligned}
C_1 &= \sqrt{\frac{\alpha_T \beta_B \beta_W}{\alpha_{BW}\alpha_W \beta_T}}, \\
C_2 &= K_M \alpha_{BW}\alpha_{CM}\alpha_T\alpha_W + \alpha_{BW}\alpha_W\beta_C\beta_T C_1 - \alpha_T\beta_B\beta_{CT}\beta_W, \\
C_3 &= K_M \alpha_{BW}\alpha_{CM}\alpha_T\alpha_W\beta_B\beta_{CT}\beta_W, \\
C_4 &= \alpha_{BW}\alpha_W\beta_B\beta_C^2\beta_T\beta_W, \\
C_5 &= K_M^2\alpha_{BW}^2\alpha_{CM}^2\alpha_T\alpha_W^2, \\
C_6 &= \alpha_T\beta_B^2\beta_{CT}^2\beta_W^2, \\
C_7 &= C_5 - 2C_3 - C_4 + C_6.
\end{aligned}
$$

For the bone metastasis model we have the following result for the local stability of the cancer-invasion steady-state (Wiggers & Pedersen, 2018):

Theorem C.2. *Let $p(\lambda) = \lambda^5 + a_1\lambda^4 + a_2\lambda^3 + a_3\lambda^2 + a_4\lambda + a_5$ be the characteristic polynomial (C.2) of model (4.15)–(4.19) with respect the cancer-invasion steady-state $\widetilde{x}$ (4.20)–(4.24), where a_i are the respective coefficients in terms of the model parameters. If the following inequalities hold:*

$$
\begin{aligned}
&a_i > 0 \quad (i = 1, 2, 3, 4), \\
&a_1 a_2 - a_3 > 0, \\
&(a_1 a_2 - a_3)(a_3 a_4 - a_2 a_5) - (a_1 a_4 - a_5)^2 > 0,
\end{aligned}
$$

then the cancer-invasion steady-state $\widetilde{x}$ is locally stable. □

Appendix D

Source code availability

The source code created for this Thesis may be found in the following link:

https://github.com/arielcam27/thesis2019

Bibliography

Alberts, B., Bray, D., Lewis, J., Raff, M., Roberts, K., & Watson, J. (2002). *Molecular Biology of the Cell* (4th ed.). Garland.

Araujo, A., Cook, L. M., Lynch, C. C., & Basanta, D. (2014). An integrated computational model of the bone microenvironment in bone-metastatic prostate cancer. *Cancer Research*, *74*(9), 2391–2401.

Araujo, A., Cook, L. M., Lynch, C. C., & Basanta, D. (2018). Size matters: Metastatic cluster size and stromal recruitment in the establishment of successful prostate cancer to bone metastases. *Bulletin of Mathematical Biology*, *80*(5), 1046–1058.

Ayati, B. P., Edwards, C. M., Webb, G. F., & Wikswo, J. P. (2010). A mathematical model of bone remodeling dynamics for normal bone cell populations and myeloma bone disease. *Biology Direct*, *5*(1), 28.

Bara, O., Djouadi, S., Day, J., & Lenhart, S. (2017). Immune therapeutic strategies using optimal controls with l 1 and l 2 type objectives. *Mathematical Biosciences*, *290*, 9–21.

Barker, H. E., Paget, J. T. E., Khan, A. A., & Harrington, K. J. (2015). The tumour microenvironment after radiotherapy: mechanisms of resistance and recurrence. *Nature Reviews Cancer*, *15*(7), 409–425.

Baron, R. & Gori, F. (2018). Targeting WNT signaling in the treatment of osteoporosis. *Current Opinion in Pharmacology*, *40*, 134–141.

Berkovitz, L. D. (2013). *Optimal control theory*, volume 12. Springer Science & Business Media.

Bonnans, Frederic, J., Giorgi, D., Grelard, V., Heymann, B., Maindrault, S., Martinon, P., Tissot, O., & Liu, J. (2017). Bocop – A collection of examples. Technical report, INRIA.

Brenner, D. J. (2008). The linear-quadratic model is an appropriate methodology for determining isoeffective doses at large doses per fraction. *Seminars in Radiation Oncology*, *18*(4), 234–239.

Buenzli, P., Pivonka, P., & Smith, D. (2011). Spatio-temporal structure of cell distribution in cortical bone multicellular units: A mathematical model. *Bone*, *48*(4), 918–926.

Buenzli, P. R. & Pivonka, P. (2017). Mathematical modelling of basic multicellular units: The functional units of bone remodeling. In Z. Guigen (Ed.), *Computational Bioengineering* chapter 9, (pp. 45–74). CRC Press.

Burkiewicz, J. S., Scarpace, S. L., & Bruce, S. P. (2009). Denosumab in osteoporosis and oncology. *Annals of Pharmacotherapy*, *43*(9), 1445–1455.

Camacho, A. & Jerez, S. (2018). Bone metastasis treatment modeling via optimal control. *Journal of Mathematical Biology*, *78*(1-2), 497–526.

Camacho, D. F. & Pienta, K. J. (2014). A multi-targeted approach to treating bone metastases. *Cancer and Metastasis Reviews*, *33*(2-3), 545–553.

Canalis, E. (2013). Wnt signalling in osteoporosis: mechanisms and novel therapeutic approaches. *Nature Reviews Endocrinology*, *9*(10), 575–583.

Carrère, C. (2017). Optimization of an in vitro chemotherapy to avoid resistant tumours. *Journal of Theoretical Biology*, *413*, 24–33.

Chappard, D., Bouvard, B., Baslé, M.-F., Legrand, E., & Audran, M. (2011). Bone metastasis: Histological changes and pathophysiological mechanisms in osteolytic or osteosclerotic localizations. a review. *Morphologie*, *95*(309), 65–75.

Chen, X., Wang, Z., Duan, N., Zhu, G., Schwarz, E. M., & Xie, C. (2018). Osteoblast–osteoclast interactions. *Connective Tissue Research*, *59*(2), 99–107.

Chen, Y.-C., Sosnoski, D. M., & Mastro, A. M. (2010). Breast cancer metastasis to the bone: mechanisms of bone loss. *Breast Cancer Research*, *12*(6).

Chiechi, A. & Guise, T. A. (2016). Pathobiology of osteolytic and osteoblastic bone metastases. In *Metastatic Bone Disease* (pp. 15–35). Springer New York.

Chow, E., van der Linden, Y. M., Roos, D., Hartsell, W. F., Hoskin, P., Wu, J. S. Y., et al. (2014). Single versus multiple fractions of repeat radiation for painful bone metastases: a randomised, controlled, non-inferiority trial. *The Lancet Oncology*, *15*(2), 164–171.

Clewley, R. H., Sherwood, W. E., LaMar, M. D., & Guckenheimer, J. M. (2007). PyDSTool, a software environment for dynamical systems modeling.

Coelho, R. M., Lemos, J. M., Alho, I., Valério, D., Ferreira, A. R., Costa, L., & Vinga, S. (2016). Dynamic modeling of bone metastasis, microenvironment and therapy. *Journal of Theoretical Biology*, *391*, 1–12.

Cook, L. M., Araujo, A., Pow-Sang, J. M., Budzevich, M. M., Basanta, D., & Lynch, C. C. (2016). Predictive computational modeling to define effective treatment strategies for bone metastatic prostate cancer. *Scientific Reports*, *6*(1).

Dingli, D., Chalub, F. A. C. C., Santos, F. C., Segbroeck, S. V., & Pacheco, J. M. (2009). Cancer phenotype as the outcome of an evolutionary game between normal and malignant cells. *British Journal of Cancer*, *101*(7), 1130–1136.

Enders, G. H. (2009). Wnt therapy for bone loss: golden goose or trojan horse? *Journal of Clinical Investigation*, *119*(4), 758–760.

Eriksen, E. F. (2010). Cellular mechanisms of bone remodeling. *Reviews in Endocrine and Metabolic Disorders*, *11*(4), 219–227.

Farhat, A., Jiang, D., Cui, D., Keller, E., & Jackson, T. (2017). An integrative model of prostate cancer interaction with the bone microenvironment. *Mathematical Biosciences*, *294*, 1–14.

Fister, K. R., Lenhart, S., & McNally, J. S. (1998). Optimizing chemotherapy in an hiv model. *Electronic Journal of Differential Equations*, *1998*, 1–12.

Fleming, W. & Rishel, R. (1975). *Deterministic and Stochastic Optimal Control*. Springer New York.

Florencio-Silva, R., da Silva Sasso, G. R., Sasso-Cerri, E., Simões, M. J., & Cerri, P. S. (2015). Biology of bone tissue: Structure, function, and factors that influence bone cells. *BioMed Research International*, *2015*, 1–17.

Frost, H. M. (1987). The mechanostat: a proposed pathogenic mechanism of osteoporoses and the bone mass effects of mechanical and nonmechanical agents. *Bone and mineral*, *2*(2), 73.

Ganesh, V., Chan, S., Raman, S., Chow, R., Hoskin, P., Lam, H., et al. (2017). A review of patterns of practice and clinical guidelines in the palliative radiation treatment of uncomplicated bone metastases. *Radiotherapy and Oncology*, *124*(1), 38–44.

Gantmacher, F. R. (1959). *Applications of the Theory of Matrices*. New York, NY, USA: Interscience Publishers, Inc.

Garzón-Alvarado, D. A. (2012). A mathematical model for describing the metastasis of cancer in bone tissue. *Computer Methods in Biomechanics and Biomedical Engineering*, *15*(4), 333–346.

Garzón-Alvarado, D. A., Ramírez-Martínez, A. M., & de Martínez, C. A. C. (2012). Numerical test concerning bone mass apposition under electrical and mechanical stimulus. *Theoretical Biology and Medical Modelling*, *9*(1), 14.

Graham, J. M., Ayati, B. P., Ramakrishnan, P. S., & Martin, J. A. (2012). Towards a new spatial representation of bone remodeling. *Mathematical Biosciences and Engineering*, *9*(2), 281–295.

Hanahan, D. & Weinberg, R. A. (2011). Hallmarks of cancer: The next generation. *Cell*, *144*(5), 646–674.

Janssens, K., ten Dijke, P., Janssens, S., & Hul, W. V. (2005). Transforming growth factor-β1 to the bone. *Endocrine Reviews*, *26*(6), 743–774.

Javed, S., Sohail, A., & Nutini, A. (2018). Integrative modeling of drug therapy and the bone turnover. *Clinical Biomechanics*, *60*, 141–148.

Javed, S., Younas, M., Bhatti, M. Y., Sohail, A., & Sattar, A. (2019). Analytic approach to explore dynamical osteoporotic bone turnover. *Advances in Difference Equations*, *2019*(1), 61.

Jerez, S. & Camacho, A. (2018). Bone metastasis modeling based on the interactions between the BMU and tumor cells. *Journal of Computational and Applied Mathematics*, *330*, 866–876.

Jerez, S. & Chen, B. (2015). Stability analysis of a Komarova type model for the interactions of osteoblast and osteoclast cells during bone remodeling. *Mathematical Biosciences*, *264*, 29–37.

Jerez, S., Díaz-Infante, S., & Chen, B. (2018). Fluctuating periodic solutions and moment boundedness of a stochastic model for the bone remodeling process. *Mathematical Biosciences*, *299*, 153–164.

Ji, B., Genever, P. G., Patton, R. J., & Fagan, M. J. (2014). Mathematical modelling of the pathogenesis of multiple myeloma-induced bone disease. *International Journal for Numerical Methods in Biomedical Engineering*, *30*(11), 1085–1102.

Ji, B., Genever, P. G., Patton, R. J., Putra, D., & Fagan, M. J. (2012). A novel mathematical model of bone remodelling cycles for trabecular bone at the cellular level. *Biomechanics and Modeling in Mechanobiology*, *11*(7), 973–982.

Jones, D. H., Nakashima, T., Sanchez, O. H., Kozieradzki, I., Komarova, S. V., Sarosi, I., et al. (2006). Regulation of cancer cell migration and bone metastasis by RANKL. *Nature*, *440*(7084), 692–696.

Juárez, P., Fournier, P. G., Mohammad, K. S., McKenna, R. C., Davis, H. W., Peng, X. H., et al. (2017). Halofuginone inhibits tgf-β/bmp signaling and in combination with zoledronic acid enhances inhibition of breast cancer bone metastasis. *Oncotarget*, *8*(49).

Juárez, P. & Guise, T. A. (2011). TGF-β in cancer and bone: Implications for treatment of bone metastases. *Bone*, *48*(1), 23–29.

Keller, E. T. & Brown, J. (2004). Prostate cancer bone metastases promote both osteolytic and osteoblastic activity. *Journal of Cellular Biochemistry*, *91*(4), 718–729.

Komarova, S. V., Smith, R. J., Dixon, S., Sims, S. M., & Wahl, L. M. (2003). Mathematical model predicts a critical role for osteoclast autocrine regulation in the control of bone remodeling. *Bone*, *33*(2), 206–215.

Kroll, M. H. (2000). Parathyroid hormone temporal effects on bone formation and resorption. *Bull Math Biol*, *62*(1), 163–188.

Krzeszinski, J. Y. & Wan, Y. (2015). New therapeutic targets for cancer bone metastasis. *Trends in Pharmacological Sciences*, *36*(6), 360–373.

Kuznetsov, Y. A. (2013). *Elements of applied bifurcation theory*, volume 112. Springer Science & Business Media.

Kwakwa, K. A., Vanderburgh, J. P., Guelcher, S. A., & Sterling, J. A. (2017). Engineering 3d models of tumors and bone to understand tumor-induced bone disease and improve treatments. *Current Osteoporosis Reports*, *15*(4), 247–254.

Kähkönen, T. E., Bernoulli, J., Halleen, J. M., & Suominen, M. I. (2019). Novel and conventional preclinical models to investigate bone metastasis. *Current Molecular Biology Reports*, *5*(1), 48–54.

Ledzewicz, U., , Schättler, H., Wang, S., , & and (2019). On the role of tumor heterogeneity for optimal cancer chemotherapy. *Networks & Heterogeneous Media*, *14*(1), 131–147.

Lemaire, V., Tobin, F. L., Greller, L. D., Cho, C. R., & Suva, L. J. (2004). Modeling the interactions between osteoblast and osteoclast activities in bone remodeling. *Journal of Theoretical Biology*, *229*(3), 293–309.

Lemos, J. M., Caiado, D. V., Coelho, R., & Vinga, S. (2016). Optimal and receding horizon control of tumor growth in myeloma bone disease. *Biomedical Signal Processing and Control*, *24*, 128–134.

Lenhart, S. & Workman, J. T. (2007). *Optimal Control Applied to Biological Models* (1st ed.). Boca Raton: CRC Press.

Lipton, A. (2004). Pathophysiology of bone metastases: how this knowledge may lead to therapeutic intervention. *The journal of supportive oncology*, *2*(3), 205–13.

Lipton, A., Fizazi, K., Stopeck, A., Henry, D., Smith, M., Shore, N., et al. (2016). Effect of denosumab versus zoledronic acid in preventing skeletal-related events in patients with bone metastases by baseline characteristics. *European Journal of Cancer*, *53*, 75–83.

Lukes, D. L. (1982). *Differential equations: classical to controlled*. New York: Academic Press.

Lutz, S., Balboni, T., Jones, J., Lo, S., Petit, J., Rich, S. E., Wong, R., & Hahn, C. (2017). Palliative radiation therapy for bone metastases: Update of an ASTRO evidence-based guideline. *Practical Radiation Oncology*, *7*(1), 4–12.

Madrasi, K., Li, F., Kim, M.-J., Samant, S., Voss, S., Kehoe, T., et al. (2018). Regulatory perspectives in pharmacometric models of osteoporosis. *The Journal of Clinical Pharmacology*, *58*(5), 572–585.

Manolagas, S. C. (2000). Birth and death of bone cells: Basic regulatory mechanisms and implications for the pathogenesis and treatment of osteoporosis. *Endocrine Reviews*, *21*(2), 115–137.

Marie, P. J. (2015). Osteoblast dysfunctions in bone diseases: from cellular and molecular mechanisms to therapeutic strategies. *Cellular and Molecular Life Sciences*, *72*(7), 1347–1361.

Massagué, J. & Obenauf, A. C. (2016). Metastatic colonization by circulating tumour cells. *Nature*, *529*(7586), 298–306.

Matsuo, K. & Irie, N. (2008). Osteoclast–osteoblast communication. *Archives of Biochemistry and Biophysics*, *473*(2), 201–209.

McAsey, M., Mou, L., & Han, W. (2012). Convergence of the forward-backward sweep method in optimal control. *Computational Optimization and Applications*, *53*(1), 207–226.

Mitlak, B. H., Burr, D. B., & Allen, M. R. (2014). Pharmaceutical Treatments of Osteoporosis. In *Basic and Applied Bone Biology* (pp. 345–363). Elsevier.

Moroz, A. (2012). The population model of bone remodelling employed the optimal control. *Molecular BioSystems*, *8*(11), 2974.

Mundy, G. R. (2002). Metastasis to bone: causes, consequences and therapeutic opportunities. *Nature Reviews Cancer*, *2*(8), 584–593.

Neto, J. P., Coelho, R. M., Valério, D., Vinga, S., Sierociuk, D., Malesza, W., Macias, M., & Dzieliński, A. (2018). Simplifying biochemical tumorous bone remodeling models through variable order derivatives. *Comput Math Appl*, *75*(9), 3147–3157.

Oest, M. E., Franken, V., Kuchera, T., Strauss, J., & Damron, T. A. (2015). Long-term loss of osteoclasts and unopposed cortical mineral apposition following limited field irradiation. *Journal of Orthopaedic Research*, *33*(3), 334–342.

Ota, K., Quint, P., Ruan, M., Pederson, L., Westendorf, J. J., Khosla, S., & Oursler, M. J. (2013). TGF-β induces wnt10b in osteoclasts from female mice to enhance coupling to osteoblasts. *Endocrinology*, *154*(10), 3745–3752.

Ottewell, P. D. (2016). The role of osteoblasts in bone metastasis. *Journal of Bone Oncology*, *5*(3), 124–127.

Paget, S. (1889). The distribution of secondary growths in cancer of the breast. *The Lancet*, *133*(3421), 571–573.

Pao, C. V. (1993). *Nonlinear Parabolic and Elliptic Equations*. Springer US.

Parfitt, A. (2002). Targeted and nontargeted bone remodeling: relationship to basic multicellular unit origination and progression. *Bone*, *30*(1), 5–7.

Parfitt, A. M. (1994). Osteonal and hemi-osteonal remodeling: The spatial and temporal framework for signal traffic in adult human bone. *Journal of Cellular Biochemistry*, *55*(3), 273–286.

Peterson, M. C. & Riggs, M. M. (2010). A physiologically based mathematical model of integrated calcium homeostasis and bone remodeling. *Bone*, *46*(1), 49–63.

Phan, T. C., Xu, J., & Zheng, M. H. (2004). Interaction between osteoblast and osteoclast: impact in bone disease. *Histology and histopathology*, *19*(4), 1325–1344.

Pillis, L. D. & Radunskaya, A. (2003). The dynamics of an optimally controlled tumor model: A case study. *Mathematical and Computer Modelling*, *37*(11), 1221–1244.

Pivonka, P. & Komarova, S. V. (2010a). Mathematical modeling in bone biology: From intracellular signaling to tissue mechanics. *Bone*, *47*(2), 181–189.

Pivonka, P. & Komarova, S. V. (2010b). Mathematical modeling in bone biology: From intracellular signaling to tissue mechanics. *Bone*, *47*(2), 181–189.

Pivonka, P., Zimak, J., Smith, D. W., Gardiner, B. S., Dunstan, C. R., Sims, N. A., Martin, T. J., & Mundy, G. R. (2008). Model structure and control of bone remodeling: A theoretical study. *Bone*, *43*(2), 249–263.

Pontryagin, L. S., Boltyanskii, V. G., Gamkrelidze, R. V., & Mishechenko, E. F. (1962). *The Mathematical Theory of Optimal Processes*. New York: John Wiley & Sons.

Raggatt, L. J. & Partridge, N. C. (2010). Cellular and molecular mechanisms of bone remodeling. *Journal of Biological Chemistry*, *285*(33), 25103–25108.

Randall, R. L. (2016). *Metastatic Bone Disease*. Springer-Verlag New York.

Ross, D. S., Mehta, K., & Cabal, A. (2017). Mathematical model of bone remodeling captures the antiresorptive and anabolic actions of various therapies. *Bulletin of Mathematical Biology*, *79*(1), 117–142.

Ryser, M. D. & Komarova, S. V. (2017). Mathematical modeling of cancer metastases. In Z. Guigen (Ed.), *Computational Bioengineering* chapter 9, (pp. 211–230). CRC Press.

Ryser, M. D., Komarova, S. V., & Nigam, N. (2010). The cellular dynamics of bone remodeling: A mathematical model. *SIAM Journal on Applied Mathematics*, *70*(6), 1899–1921.

Ryser, M. D. & Murgas, K. A. (2017). Bone remodeling as a spatial evolutionary game. *J Theor Biol*, *418*, 16–26.

Ryser, M. D., Nigam, N., & Komarova, S. V. (2009). Mathematical Modeling of Spatio-Temporal Dynamics of a Single Bone Multicellular Unit. *J Bone Miner Res*, *24*(5), 860–870.

Ryser, M. D., Qu, Y., & Komarova, S. V. (2012). Osteoprotegerin in bone metastases: Mathematical solution to the puzzle. *PLoS Computational Biology*, *8*(10), e1002703.

Savageau, M. A. (1988). Introduction to s-systems and the underlying power-law formalism. *Mathematical and Computer Modelling*, *11*, 546–551.

Schättler, H. & Ledzewicz, U. (2015). *Optimal control for mathematical models of cancer therapies*, volume 42. Springer.

Shah, A. D., Shoback, D., & Lewiecki, E. M. (2015). Sclerostin inhibition: a novel therapeutic approach in the treatment of osteoporosis. *International journal of women's health*, *7*, 565.

Shah, N. H., Shukla, N., Satia, M. H., & Thakkar, F. A. (2019). Optimal control of HCV transmission under liquoring. *Journal of Theoretical Biology*, *465*, 27–33.

Sharp, J. A., Browning, A. P., Mapder, T., Burrage, K., & Simpson, M. J. (2019). Optimal control of acute myeloid leukaemia. *Journal of Theoretical Biology*, *470*, 30–42.

Skjødt, M. K., Frost, M., & Abrahamsen, B. (2018). Side effects of drugs for osteoporosis and metastatic bone disease. *British Journal of Clinical Pharmacology*, *2018*.

Sousa, S. & Clézardin, P. (2018). Bone-targeted therapies in cancer-induced bone disease. *Calcified Tissue International*, *102*(2), 227–250.

Stephenson, B., Lanzas, C., Lenhart, S., & Day, J. (2017). Optimal control of vaccination rate in an epidemiological model of clostridium difficile transmission. *Journal of Mathematical Biology*, *75*(6-7), 1693–1713.

Stewart, B. W. & Wild, C. P. (2014). Iarc nonserial publication-world cancer report 2014. *Lyon/England: World Health Organization*, *630*.

Suvannasankha, A. & Chirgwin, J. M. (2014). Role of bone-anabolic agents in the treatment of breast cancer bone metastases. *Breast Cancer Research*, *16*(6).

Swan, G. W. (1990). Role of optimal control theory in cancer chemotherapy. *Mathematical Biosciences*, *101*(2), 237–284.

Takai, H., Kanematsu, M., Yano, K., Tsuda, E., Higashio, K., Ikeda, K., Watanabe, K., & Yamada, Y. (1998). Transforming growth factor-β stimulates the production of osteoprotegerin/osteoclastogenesis inhibitory factor by bone marrow stromal cells. *Journal of Biological Chemistry*, *273*(42), 27091–27096.

Theriault, R. L. & Theriault, R. L. (2012). Biology of bone metastases. *Cancer Control*, *19*(2), 92–101.

Vakaet, L. A.-L. & Boterberg, T. (2004). Pain control by ionizing radiation of bone metastasis. *The International Journal of Developmental Biology*, *48*(5-6), 599–606.

Wan, X., Li, Z.-G., Yingling, J. M., Yang, J., Starbuck, M. W., Ravoori, M. K., et al. (2012). Effect of transforming growth factor beta (TGF-β) receptor i kinase inhibitor on prostate cancer bone growth. *Bone*, *50*(3), 695–703.

Wang, Y., Pivonka, P., Buenzli, P. R., Smith, D. W., & Dunstan, C. R. (2011). Computational modeling of interactions between multiple myeloma and the bone microenvironment. *PLoS ONE*, *6*(11), e27494.

Warman, P., Kaznatcheev, A., Araujo, A., Lynch, C., & Basanta, D. (2018). Fractionated follow-up chemotherapy delays the onset of resistance in bone metastatic prostate cancer. *Games*, *9*(2), 19.

Weivoda, M. M., Ruan, M., Pederson, L., Hachfeld, C., Davey, R. A., Zajac, J. D., et al. (2016). Osteoclast TGF-β receptor signaling induces wnt1 secretion and couples bone resorption to bone formation. *Journal of Bone and Mineral Research*, *31*(1), 76–85.

Wiggers, S. L. & Pedersen, P. (2018). Routh–hurwitz-liénard–chipart criteria. In *Springer Tracts in Mechanical Engineering* (pp. 133–140). Springer International Publishing.

Zhang, J., Qiu, X., Xi, K., Hu, W., Pei, H., Nie, J., et al. (2018). Therapeutic ionizing radiation induced bone loss: a review of in vivo and in vitro findings. *Connective Tissue Research*, *59*(6), 509–522.